The Dynamics of Golgi Enzymes in Mammalian Cells Supports Cisternal Maturation

Thesis

The dynamics of Golgi enzymes in mammalian cells supports cisternal maturation

Riccardo Rizzo

MSc

Discipline: Life and Biomolecular Sciences

Affiliated Research Centre: Telethon Institute of Genetics and Medicine

Thesis submitted in accordance with the requirements of the Open University

for the degree of Doctor of Philosophy

September 2013

DATE of SUBMISSION: 30 SEPTEMBER 2013

DATE of AWARD: 14 APRIL 2014

Acknowledgments

During my Ph.D. several people have contributed to my growth not only from a scientific point of view. The first protagonist of my long and pleasant but sometimes stressful way of life is my boss Alberto Luini. I remember like it was yesterday my first interview with him before starting the doctoral studies. It ended with great joy because I was selected for the position and he helped me realize my dream of doing research. I feel fortunate to have met a person who has believed in me, a person who I respect very much from a human point of view and scientifically, that gave me all the tools to grow, learn and have training to tackle the difficult and competitive world of scientific research. My second fortune was to be entrusted to Parashuraman Seetharaman, who has represented for me a fundamental and indispensable scientific guide, as well as being a moral support that I consider him now as a brother. My third fortune was to be placed in a laboratory consisting of very helpful colleagues who made me feel very comfortable, welcoming me to the big family. They taught me the laboratory techniques and discussed the day-to-day scientific problems. For this reason, I have a moral duty to thank Jung Juan, Jorge Cancino, Ramanath Hedge, Giovanni D'Angelo, Anita Capalbo, Antonella Campli, Rosaria Di Martino, Serena Capasso, Advait Subramanian, and Altea Alfe. I also thank Antonella de Matteis, Roman Polishchuk, Gareth Griffiths, Gerry Dougherty and my external supervisor Martin Lowe for the many discussions and scientific advice. I thank Claudia Puri for help in immuno-EM experiments. I thank John Lucocq for help in EM quantitation and Peppino Mirabelli for sucrose gradient centrifugation experiment. Finally, I thank my family who has always supported me in everything, my father Rosario Rizzo, my mother Giovanna Mele and my brother Rizieri Rizzo. In the end I conclude by saying that in life each of us must be lucky to be in the right place at the right time and with the right people, and I consider myself one of those lucky few.

Abstract

The Golgi apparatus is organised as a 'ribbon' of interconnected stacks of membranous cisternae that have characteristic enzyme compositions that define where cargo proteins are glycosylated during their transport towards the plasma membrane in mammalian cells. There are two classes of Golgi transport schemes: one based on stable cisternae, and the other on 'maturing' cisternae. With the stable cisternae model, the Golgi resident proteins (e.g., glycosylating enzymes) always remain in the same cisterna and the secretory cargo is transported forwards in vesicles, to move progressively from one cisterna to the next. According to the maturation scheme, new cisternae form at the *cis*-Golgi face, and then 'move forward' through the stack; at the same time, the cisternae 'mature' by acquiring, and then losing, the glycosylating enzymes, which recycle backwards in step with cargo progression. Here, the cargo remains stable within the cisterna, and is transported forwards within the advancing cisternae. While the maturation mechanism has significant experimental support, the crucial evidence that Golgi enzymes recycle through the stack in mammalian cells remains missing. In the present study, I designed experiments based on the use of Golgi-resident enzyme constructs that can be reversibly polymerised to distinguish the maturing *versus* stable cisternae models. The data strongly fit with the predictions of the cisternal maturation model.

Table of Contents

List of figures

List of Tables

Abbreviations

3D	Three-dimensional
ARF	ADP-ribosylation factor
BCA	Bicinchoninic acid
BFA	Brefeldin A
BSA	Bovine serum albumin
CD8	Cluster of differentiation 8
GFP	Green fluorescence protein
CGN	*Cis*-Golgi network
CHX	Cycloheximide
COG	Conserved oligomeric Golgi
CS	Calf serum
DMEM	Dulbecco's modified Eagle's medium
EDTA	Ethylenediaminetetraacetic acid
EM	Electron microscopy
$EndoH^r$	EndoH resistant
$EndoH^s$	EndoH sensitive
EPON	Epoxy resin
ER	Endoplasmic reticulum
ERES	ER exit sites
ERGIC	ER-Golgi intermediate compartment
EXT	Extosin
FCS	Foetal calf serum
FM	Mutant FK506 binding protein (FKBP-Phe36Met)
GAlNacT2	N-acetylgalactosaminyltransferase 2
GALT	β-1,4-galactosyltransferase

GAPs	GTPase-activating proteins
GDP	Guanosine diphosphate
GEFs	Guanine nucleotide-exchange factors
GFP	Green fluorescence protein
GOLPH3	Golgi phosphoprotein 3
GOLPH3L	Golgi phosphoprotein 3-like
GTP	Guanosine triphosphate
HEPES	4-(2-Hydroxy-ethyl)-piperazine-1-ethane-sulfonic acid
hGH	Human growth hormone
HRP	Horseradish peroxidase
LB	Luria-Bertani broth
hMANI	human α-1,2-Mannosidase IB
MANI-FM	mouse α-1,2-mannosidase IB fused to three tandem mutant FK506 binding protein (FKBP-Phe36Met) domains (-FM) and an HA tag
MTOC	Microtubule organising centre
NA	Numerical aperture
NSF	N-ethylmaleimide-sensitive factor
O/N	Overnight
PBS	Phosphate-buffered saline
PLA2	Phospholipase A_2
PM	Plasma membrane
RT	Room temperature
SDS	Sodium dodecyl sulphate
SDS-PAGE	Sodium dodecyl sulphate-polyacrylamide gel electrophoresis
SEM	Standard error of the mean

SNARE	Soluble N-ethylmaleimide sensitive factor attachment protein receptor
TEM	Transmission electron microscopy
TEMED	N,N,N',N'-tetramethylethylenediamine
TGN	*Trans*-Golgi network
TMD	Transmembrane domain
Tris	Tris[hydroxymethyl]aminomethane
Tween-20	Polyoxyethylenesorbitan monolaurate
VSVG	Vesicular stomatitis virus glycoprotein
VTCs	Vesicular-tubular clusters
α-SNAPs	α-soluble NSF-attachment proteins

CHAPTER 1

Introduction

1.1 From the *cis* to the *trans* face of the Golgi apparatus: structure and function

More than a century ago, the anatomist Camillo Golgi discovered a new organelle using the "black reaction" in neuronal cells, which causes the deposition of silver on histological sections. Initially defined as "apparato reticolare interno" (Golgi 1989), the Golgi apparatus was first considered to be an artefact of fixation, and only with the introduction of electron microscopy (EM) into the field of biology was it possible to establish the structure and the preserved nature of the Golgi apparatus as an organelle that is conserved in almost all cell types (Farquhar and Rinehart 1954; Sjostrand and Hanzon 1954; Dalton and Felix 1954).

In mammalian cells, the Golgi apparatus is composed of 70-100 Golgi stacks that are connected to each other by networks of tubules, called the non-compact zones, that form a ribbon-like structure that localises in the peri-nuclear region of the cell, near to the microtubule organising centre (MTOC). Each Golgi stack can be divided into three morphologically and functionally different regions, called the *cis*-, medial- and *trans*-Golgi, where specific Golgi resident proteins are located that provide the identity of each of these compartments (Dunphy and Rothman 1985; Mellman and Simons 1992). Every stack intercalates between two networks of membranes that represent the entrance face of the Golgi, named the *cis*-Golgi network (CGN), and the exit face of the Golgi, named the *trans*-Golgi network (TGN). The flux of membranes and proteins that reach and leave the Golgi apparatus must be accurately tuned to maintain the homeostasis and the correct

function of the Golgi (Wieland, Gleason et al. 1987), and both the CGN and the TGN have important roles in this process.

1.1.1 Endoplasmic reticulum exit sites

Proteins that follow the secretory pathway are first synthesised by the endoplasmic reticulum (ER)-associated ribosomes, and then can be co-translationally inserted into the ER membranes. Alternatively, the proteins can be post-translationally translocated across the ER membrane and, after folding, they usually concentrate at the level of the ER exit sites (ERES). These are ribosome-free portions of the ER membranes that form Ω-shape profiles or 'buds' when seen by EM; these are coated with the COPII coatomer (see **Fig. 1.1**; Palade 1975; Sesso, de Faria et al. 1994; Bannykh, Rowe et al. 1996). The budding process at the ERES starts when Sec12 activates the Sar1 GTPase through the exchange of GDP for GTP. Sar1-GTP induces deformation of the ER membrane by insertion of a hydrophobic N-terminal helix into the membrane bilayer. Sar1-GTP then drives the initial recruitment of Sec23-24, a heterodimer that represents the inner layer of the COPII coat, in contact with the forming vesicle membrane. Subsequently, a second heterodimer, composed of Sec13-31, which represents the outer layer of the COPII coat, recognizes the premature complex composed of Sar1-GTP, Sec23-24, and the cargo. This interaction supports membrane bending, leading finally to vesicle formation and fission from the ER membrane (Barlowe, Orci et al. 1994; Barlowe 2003). The newly generated COPII-coated carriers then lose their coat, and can homotypically fuse with each other or with the network of membranes known as vesicular-tubular clusters (VTCs) (Bannykh, Rowe et al. 1996).

1.1.2 Vesicular-tubular clusters

The VTCs are also known as the ER-Golgi intermediate compartment (ERGIC) (Hauri, Kappeler et al. 2000), and this represents the cross-roads of the early secretory pathway for the exchange of membranes with the ER from one side and with the Golgi apparatus on the other. From a morphological point of view, the VTCs appear as a network of membranes that is composed of vesicles and/or tubules that, when branched, appear with a typical triangular shape (see **Fig. 1.1**). Rarely, the ER can be connected with the VTCs (Bannykh, Nishimura et al. 1998), but frequently tubules that connect the VTCs with the first *cis*-Golgi cisterna can be seen (Krijnse-Locker, Ericsson et al. 1994). The main function of the VTCs is to allow the recycling of ER components, like chaperones, cargo receptors, and other ER-resident proteins, so that they can return to the ER to start a new cycle of transport (Breuza, Halbeisen et al. 2004). This function is mediated by a heptameric protein complex that constitutes a different coatomer, called COPI (Lewis and Pelham 1990; Letourneur, Gaynor et al. 1994). Additional functions of the VTCs include glycosylation (Krijnse-Locker, Ericsson et al. 1994), concentration of cargo proteins that have to proceed through the secretory pathway (Martinez-Menarguez, Geuze et al. 1999), and an additional control of protein folding (Zuber, Fan et al. 2001; Anelli, Ceppi et al. 2007). The most specific marker of the VTCs is the protein ERGIC53, which shows a tight segregation between VTCs and the Golgi membranes (see review by Klumperman 2011).

How the cargo reaches the Golgi apparatus is still under debate (reviewed in (Polishchuk and Mironov 2004). From the one hand, it is proposed that VTC-derived carriers fuse with a pre-existing *cis*-Golgi cisterna. This concept implies that there is a specific subset of COPI-coated carriers that contain anterograde cargoes to transport them to the *cis*-Golgi. On the other hand, VTCs can be seen as anterograde carriers in their own right. According to this model, VTCs can fuse with each other to generate a *cis*-Golgi cisterna that will then mature, to allow cargo transport from the *cis*- to the *trans*-Golgi sub-regions.

1.1.3 The Golgi stack

The Golgi stack represents the basic structural unit of the mammalian Golgi ribbon. The Golgi ribbon is composed of about 100 stacks that are laterally connected to each other through a network of tubules and vesicles that extends for a length that can vary from 200 nm to 800 nm, known as the non-compact zone (Thorne-Tjomsland, Dumontier et al. 1998; Ladinsky, Mastronarde et al. 1999). Morphologically, each Golgi stack appears as a series of cisternae that vary from 3 to 11 in number, and range from 0.7 μm to 1.1 μm in length (Rabouille, Misteli et al. 1995). These are juxtaposed and aligned, and they are held together by the Golgi matrix proteins (see **Fig. 1.1**) (Franke, Kartenbeck et al. 1972; Cluett and Brown 1992; Slusarewicz, Nilsson et al. 1994; Sinka, Gillingham et al. 2008; Ramirez and Lowe 2009). The cisternae are typically tight in the central part (10-20 nm) and dilated at the periphery; moreover, they have holes of varied diameters from <65 nm to up to 100 nm. There are called perforated zones, and they decrease in number and size going from the *cis*- to medial Golgi, and increase again along the medial to *trans* axis (Ladinsky, Mastronarde et al. 1999). The *cis*- and *trans*-sides of the Golgi stacks share similar morphological characteristics, like the presence of fenestrae, and small round profiles and tubules that are projected into the cytosol to form a network of interconnected membranes.

Another important characteristic of the Golgi stack is the presence of COPI-coated vesicles that under EM appear as round electron-dense profiles of 50 nm to 80 nm in diameter, and are present within a 200-nm distance from the rims of the cisternae. Rarely, tubules connecting heterologous cisternae can be seen, which have the same diameter as a normal cisterna (20 nm). In certain specific cell types, these tubules can increase in number, which probably reflects an increase in the cell secretory needs (Vivero-Salmeron, Ballesta et al. 2008). It is also known that intercisternal connections can form during the arrival of cargo at the Golgi apparatus, a process in which cytosolic phospholipase $(PLA)_2$ has a key role (San Pietro, Capestrano et al. 2009). Whether vesicles and tubules represent a shuttle

for the anterograde *cis* to *trans* movement of proteins in the Golgi apparatus or whether they have a role in the recycling of the Golgi enzymes is still under debate.

Glycosylation is the main, but not the only, function of the Golgi apparatus (Mellman and Simons 1992; Rabouille, Misteli et al. 1995; Varki 1998). Indeed, the Golgi apparatus is also a signalling platform that participates in the partitioning and integration of many signalling molecules, in addition to being a site for lipid biosynthesis including many sphingolipids (van Meer 1998). At the ultrastructural level, ER membranes that do not have ribosomes (i.e., smooth ER) can be found in tight contact (<10 nm) with the *trans*-cisterna of the Golgi stack, which forms a region defined as "ER-Golgi membrane contact sites", which have a key role in the regulation of the amount and homeostasis of the sphingolipids (Ladinsky, Wu et al. 2002).

1.1.4 The trans-Golgi network

The TGN is the main interchange station of the endocytic and exocytic pathways, and it represents a platform where proteins and lipids coming from the Golgi apparatus are sorted to their final destination (see review by De Matteis and Luini 2008). Structurally, the TGN appears as a network of membranes that is composed of tubules, vesicles and pleiomorphic carriers that can vary in size and shape (see **Fig. 1.1**) between cell types and depending on the level of protein synthesis (Hand and Oliver 1984; Griffiths, Fuller et al. 1989).

Besides the presence of COPI coated buds, a peculiar feature of the TGN is the presence of a different coat protein, named clathrin (see **Fig. 1.1**), which gives an identity to this compartment and provides functional discrimination from the other Golgi cisternae (Pearse and Robinson 1990). The diameter of clathrin-coated membrane buds is about 100 nm (Peden, Oorschot et al. 2004) and a typical spiky pattern can also be revealed on TGN tubules (Ladinsky, Wu et al. 2002, Mogelsvang, Marsh et al. 2004). However, not all post-Golgi carriers show this coat or a regular shape, as in the case of large pleiomorphic

carriers containing vesicular stomatitis virus glycoprotein (VSVG) (Polishchuk, Polishchuk et al. 2000).

The *trans*-most cisterna of each Golgi stack also appears to be part of the TGN (Clermont, Rambourg et al. 1995; Griffiths, Pfeiffer et al. 1985). This consideration is, however, in contrast to many observations that have highlighted the different identity of the TGN, which is considered to be an independent organelle (Geuze and Morre 1991). For example, the composition of membrane lipids, proteins and enzymes is different comparing Golgi stacks and the TGN (Novikoff 1976); Moreover, the pH of the TGN is particularly low, and more similar to that of the late endosomal compartment. In agreement with these experimental observations, the use of brefeldin A (BFA), an inhibitor of Arf1 (Fujiwara, Oda et al. 1988), induces the fusion of the Golgi apparatus with the ER, while the TGN appears to mix with the recycling endosomal system (Lippincott-Schwartz, Yuan et al. 1991).

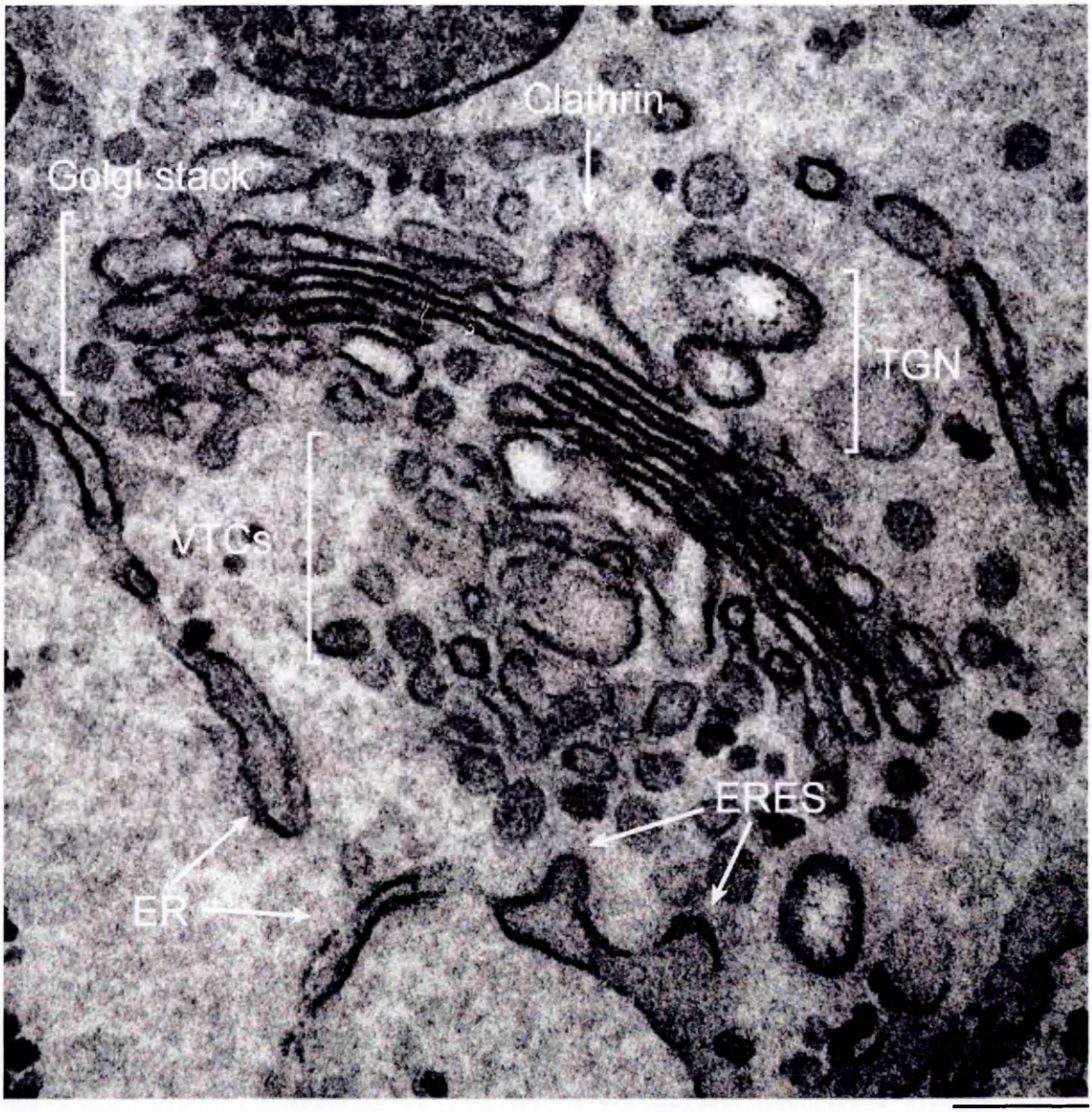

Figure 1.1 Electron microscopy micrograph depicting the secretory pathway.

HeLa cells were plated, and after 24 h they were fixed and processed for regular EPON embedding (see Materials and Methods, Electron microscopy tomography, section **3.16**). After sample embedding, thin sections (60-70 nm) were obtained and examined under EM (Tecnai-12; FEI). Each compartment of the secretory pathway is indicated. See text for abbreviations. Bar: 150 nm.

1.2 Intracellular membrane-transport regulators

One of the main classes of molecular regulators of intracellular membrane transport is the superfamily of small GTP-binding proteins that includes the Ypt/Rab, Arf and Rho families. These molecules can switch between an active membrane-associated GTP-bound state to a cytosolic inactive GDP-bound state. This reversible GDP-GTP switching is regulated by two family of proteins - guanine nucleotide-exchange factors (GEFs) catalyse the replacement of GDP with GTP, whereas GTPase activating proteins (GAPs) trigger GTP hydrolysis to GDP (Bos, Rehmann et al. 2007).

The Arf proteins can be grouped into three classes: the Golgi-localised Class I (Arf1, 2 and 3) and II (Arf4 and 5) proteins, and the class III protein that includes only Arf6, which has a role at the plasma membrane (PM). One of the best characterised Arfs, Arf1, has been implicated in the biogenesis of COPI vesicles. Indeed, soon after the activation of Arf1 by nucleotide exchange, Arf1-GTP recruits the coatomer onto the Golgi membrane (Donaldson, Cassel et al. 1992; Serafini, Orci et al. 1991). Then, Arf1 GAPs (ArfGAPs) catalyse the GTP hydrolysis (Tanigawa, Orci et al. 1993), thus promoting the uncoating of COPI carriers, which are then free to fuse with their target membrane.

The Rab proteins share a similar structure, with the exception of the hypervariable C-terminal region that appears to be an important determinant for Rab localisation (Stenmark, Valencia et al. 1994; Ali, Wasmeier et al. 2004). Each step of the intracellular transport process requires specific Rab proteins (Bonifacino and Glick 2004). Within the Golgi, Rab1 and Rab43 have been suggested to promote anterograde transport (see reviews by Barr 2009, Dejgaard, Murshid et al. 2008), while Rab6 and Rab33b have been shown to be crucial for retrograde transport within the Golgi apparatus and from the Golgi to the ER (Martinez, Schmidt et al. 1994; White, Johannes et al. 1999; Valsdottir, Hashimoto et al. 2001; Jiang and Storrie 2005; Starr, Sun et al. 2010). The Rab proteins can also bind many Golgi matrix proteins, including GM130, p115, golgin-84, golgin-45, golgin-245 and

golgin-97, and these interactions can allow the formation of a tentacular matrix that surrounds the Golgi apparatus to capture Rab-coated membranes, which thus contributes to the coordination of the intra-Golgi transport process (Munro 2011).

Another class of key molecules involved in the regulation of membrane transport within the cell is represented by the soluble N-ethylmaleimide-sensitive factor (NSF) attachment protein receptor (SNARE) family of proteins. The SNAREs have roles in the final docking and fusion events between transport intermediates and their respective target compartment (Sollner, Bennett et al. 1993; McNew, Parlati et al. 2000). Different SNAREs have been found in distinct compartments along the secretory and endocytic pathways (Jahn and Scheller 2006; Malsam, Kreye et al. 2008). From a functional and topological point of view, the SNAREs, which are associated with the vesicle/carrier intermediate, are classified as v-SNAREs, and t-SNAREs, which are associated with the cognate target compartment. The formation of a *trans*-SNARE complex, as a result of v-SNARE and t-SNARE interactions, catalyses the fusion of the two opposite membranes in a zipper-like fashion (Melia, Weber et al. 2002; Pobbati, Stein et al. 2006). The new *cis*-SNARE complex is formed in the target compartment and will then be disassembled by the combined actions of α-soluble NSF attachment proteins (α-SNAPs) and NSF (Block, Glick et al. 1988; Whiteheart, Griff et al. 1993). NSF is an ATPase that functions as an hexamer and uses the energy released by the hydrolysis of ATP to dissociate the SNARE complex, which liberates the SNAREs for a new cycle of docking and fusion events (Sollner, Whiteheart et al. 1993; Mayer, Wickner et al. 1996).

Concerning the vesicles that provide transport within the Golgi apparatus, there are two SNARE complexes that have been well characterised and implicated in this process: the syntaxin5-Bet1-Sec22-membrin complex, and syntaxin5-GS15-GOS28-Ykt6 complex. While the t-SNAREs syntaxin5 and GOS28 are homogeneously distributed in the Golgi, the v-SNARE Bet1, the t-SNAREs Sec22 and membrin show *cis*-Golgi concentration,

compared to the v-SNARE GS15, which shows a more *trans*-Golgi distribution. The differential intra-Golgi compartmentalisation of these SNAREs might be responsible for the vesicle targeting specificity within the Golgi (Volchuk, Ravazzola et al. 2004).

1.3 Mechanisms of localisation of Golgi resident enzymes within the Golgi stack

Within the cell there is a huge flux of membranes along the secretory pathway. However, despite the enormous amounts of protein and lipid that cross the Golgi apparatus, the overall ultrastructural shape and polarity of the Golgi remains unaffected. At the EM level, the *cis*-Golgi cisternae usually appear fenestrated, whereas the *trans*-side of the Golgi can be morphologically identified by the presence of clathrin-coated vesicles. The sub-compartmentalisation of the stack into *cis*, medial and *trans* is not only a classification based on the morphological features of the Golgi cisternae, but also a functional classification based on the localisation of the Golgi enzymes. There are more than 200 glycosyltransferases localised to the Golgi, and their localisation within the Golgi stack reflects their order of action on their glycolipid and glycoprotein substrates (Mellman and Simons 1992; Dunphy and Rothman 1985). For example, α-mannosidase I (MANI) is an early acting enzyme that is located at the *cis* side of the Golgi stack, while α-2,6-sialyltransferase is a late-acting enzyme that is enriched at the *trans* side of the Golgi stack (Kornfeld and Kornfeld 1985; Roth, Taatjes et al. 1985).

Each enzyme has a gradient distribution across the Golgi stack, with a peak in one or two cisternae, which implies that the Golgi residents should contain some characteristics that contribute to their specific localisation within the stack. Mutations of regions of the enzymes that are critical for their intra-Golgi localisation, or perturbation of a machinery involved in the retention/recycling process, can strongly impact on the general glycosylation process, giving rise to many different diseases (Hu, Eggers et al. 2011; Freeze 2013; Reynders, Foulquier et al. 2011).

Most of the glycosyltransferases are type II membrane proteins that are composed of four domains: a short cytosolic tail, a single transmembrane domain, a stem region, and a large luminal catalytic domain. Different mechanisms have been proposed to explain how Golgi enzymes are retained/recycled within the Golgi stack, but what is clear is that the cytosolic, transmembrane and stem domains are sufficient to localise the residents to a particular Golgi subcompartment, possibly through the cooperation of different processes, like protein-protein interactions, binding affinity of the enzymes for COPI, and their preference for certain lipid subdomains (Harris and Waters 1996); Todorow, Spang et al. 2000; Sato, Sato et al. 2001; Abe, Noda et al. 2004; Saint-Jore-Dupas, Gomord et al. 2004; Glick and Nakano 2009; Jackson 2009).

1.3.1 The kin-recognition model

The kin-recognition model is based on the observation that different Golgi enzymes can homo- or hetero-oligomerise (Nilsson, Hoe et al. 1994; Nilsson, Rabouille et al. 1996) with other enzymes that are present in the same compartment (see **Fig. 1.3, 1**). The formation of these aggregates not only prevents the complex from entering the budding COPI vesicles, but also appears to be important for the correct functioning of the interacting glycosyltransferases (McCormick, Duncan et al. 2000; Giraudo, Daniotti et al. 2001; de Graffenried and Bertozzi 2004). For the kin-recognition property of the enzymes, the transmembrane and stem regions of the glycosyltransferases is known to be essential (Weisz, Swift et al. 1993; Nilsson, Rabouille et al. 1996; Opat, Houghton et al. 2000; Qian, Chen et al. 2001; Fenteany and Colley 2005).

1.3.2 The bilayer-thickness model

The correlation between the length of the transmembrane domain (TMD) of a Golgi glycosyltransferase and the thickness of the membrane bilayer (Bretscher and Munro 1993;

Munro 1998) has led to the postulation of the "bilayer-thickness model". According to this model, the length of the TMD of the Golgi glycosyltransferases is sufficient signal to localise these enzymes to a particular lipid bilayer, such that the length of the TMD matches with the thickness of the lipid bilayer (see **Fig. 1.3, 2**). Different concentrations of cholesterol and other sterols are known to influence the thickness of the bilayer. Indeed, in the early secretory pathway, where the concentration of these lipids is low, the membrane is thinner compared with the PM, which is thicker due to an elevated amount of sterols (see review by Bretscher and Munro 1993). Indeed, a gradient of concentration of cholesterol has been shown to be present in the Golgi apparatus, with the TGN being a cholesterol-rich compartment compared with the *cis*-Golgi (Orci, Montesano et al. 1981). The compartmentalisation of the Golgi resident enzymes in sterol-depleted membrane domains might then prevent the incorporation of these enzymes into transport vesicles destined for the cell surface, providing in this way a mechanism for their retention in the Golgi apparatus. An apparent discrepancy does arise however: some enzymes that localise to the late-Golgi compartment, like β-1,4-galactosyltransferase (GALT), have a shorter transmembrane domain when compared to that of the resident enzymes in the early Golgi compartment, like MANI (Becker, Haggarty et al. 2000). This situation can still be explained if the length of the TMD is not the only determinant for the correct localisation in certain lipid environments, and thus if other biophysical properties have important roles in this context. The amino acid composition, the shape of the TMD, and the presence of positively charged residues in the cytosolic flanking regions of the TMDs can cooperate together as a way to reflect the physical properties of the bilayers in which they reside (Sharpe, Stevens et al. 2010).

1.3.3 Golgi glycosyltransferase recycling by the conserved oligomeric Golgi complex

A molecular machinery known to have a role in maintaining the correct distribution of the Golgi glycosyltransferases within the Golgi cisternae is known as the conserved oligomeric Golgi (COG) complex.

The COG complex includes eight subunits that form two lobes: lobe A that includes subunits 1-4, and lobe B that is formed by subunits 5-8 (Ungar, Oka et al. 2002). Deletion of the lobe A subunits in mammalian cells causes severe glycosylation defects and affects cell growth in yeast, whereas a less prominent phenotype appears in both yeast and mammals in the absence of the lobe B subunits (Kingsley, Kozarsky et al. 1986; Whyte and Munro 2001). The common phenotype for COG complex mutants is alteration of glycosylation homeostasis (Miller and Ungar 2012) due to mislocalisation of these Golgi resident enzymes (Kingsley, Kozarsky et al. 1986; Oka, Ungar et al. 2004; Zolov and Lupashin 2005).

Protein interaction studies have further improved our knowledge at the molecular level of the function of the COG complex. Indeed, it is well established that this hetero-octameric complex interacts with SNAREs, Rab GTPases, and the COPI coat coatomer (Suvorova, Duden et al. 2002, Zolov and Lupashin 2005) to carry out its function. It is also known that the COG complex interacts with two golgin proteins, known as p115 and golgin-84, and in particular, the binding of the COG complex with p115 is mediated by the Cog2 subunit, a process that has been shown to be essential for maintaining Golgi structure (Sohda, Misumi et al. 2007). In the case of golgin-84, this interaction occurs through Cog7, and this has been shown to be required for intra-Golgi retrograde transport, through the formation of a SNARE complex (Sohda, Misumi et al. 2010).

The role of the COG complex in retrograde transport of vesicles at the Golgi apparatus appears to be well accepted (Miller and Ungar 2012). In support of this, depletion of Cog3 led to the accumulation of COG-complex-dependent vesicles that

contained Golgi glycosyltransferases as cargo (Zolov and Lupashin 2005). Molecular and functional experimental details allowed the proposal of a possible model for COG complex function in the mechanisms of retention of Golgi glycosyltransferases. In particular, through multiple interactions with SNAREs and tethering proteins like golgins and Rab GTPases, the COG complex can bind and direct the fusion of COPI vesicles to specific sites within the Golgi apparatus, thus promoting the retention of the Golgi resident enzymes (see **Fig. 1.3, 3**) through a recycling mechanism (Miller and Ungar 2012).

1.3.4 Golgi glycosyltransferase recycling by VPS74/GOLPH3

A mechanism for the recycling of glycosyltransferases from the Golgi to the ER and within the Golgi itself is a well-known process that happens for several glycosyltransferases (Harris and Waters 1996; Storrie, White et al. 1998; Todorow, Spang et al. 2000). Perturbation of COPI function, or of COPI-interacting proteins like the COG complex and/or VPS74/GOLPH3, results in mislocalisation of the Golgi enzymes, which highlights the importance of the COPI coat and/or the COPI-related machinery in the context of Golgi glycosyltransferase retention (Tu, Tai et al. 2008; Miller and Ungar 2012). Whether COPI vesicles and/or tubules (which might be dissociated or connected with adjacent cisternae) are involved in this recycling is still under debate (Orci, Amherdt et al. 2000; Lanoix, Ouwendijk et al. 2001; Martinez-Menarguez, Prekeris et al. 2001; Kweon, Beznoussenko et al. 2004; Trucco, Polishchuk et al. 2004), but recently new evidence came from the study of the molecular mechanisms of COPI-mediated retention of Golgi glycosyltransferases.

VPS74, the yeast homologue of GOLPH3, has been shown to have an essential role in the correct localisation of the Golgi enzymes. The dual interactions of VPS74 with COPI and with a conserved sequence (F/L)-(L/V)-(S/T) in the cytosolic tail of many glycosyltransferases is necessary for its function in the localisation of the Golgi enzymes,

probably via the recycling of COPI-coated vesicles (see **Fig. 1.3, 4**). Depletion of VPS74 results in mislocalisation and degradation of a subset of glycosyltransferases in yeast, which includes Mnn2, Mnn9 and Ktr6CT, and VPS74 overexpression induces a relocation of Kre2CT from the Golgi apparatus to the ER. The many similarities between GOLPH3 and VPS74, including structural ones, suggest that the functions of GOLPH3 and VPS74 are likely to have been preserved. Indeed, GOLPH3 and its paralogue GOLPH3L can partially substitute for VPS74 when they are expressed in mutant yeast cells that lack the endogenous VPS74 (Tu, Tai et al. 2008). Whether GOLPH3 and GOLPH3L indeed have similar roles in the localisation of the Golgi enzymes in mammals remains to be better defined.

Recently, it has been shown that similar to yeast VPS74, the *Drosophila* homologue of GOLPH3, known as Rotini, mediates the intra-Golgi recycling of Extosin (EXTs), a cis-medial Golgi glycosyltransferase that mislocalises to the TGN after Rotini knock-down and to the transitional ER upon Rotini overexpression (Chang, Chang et al. 2013). Unlike in yeast or *Drosophila*, the reduction in GOLPH3 levels in mammalian cells leads to relocalisation of core 2 N-acetylglucosaminyltransferase 1 to the ER, rather than to the TGN or to post-Golgi compartments (Ali, Chachadi et al. 2012).

Golgi glycosyltransferase retention/recycling mechanisms are not mutually exclusive, so it is likely that many signals that involve distinct regions of these molecules act together to mediate the efficient targeting of these enzymes to the Golgi apparatus.

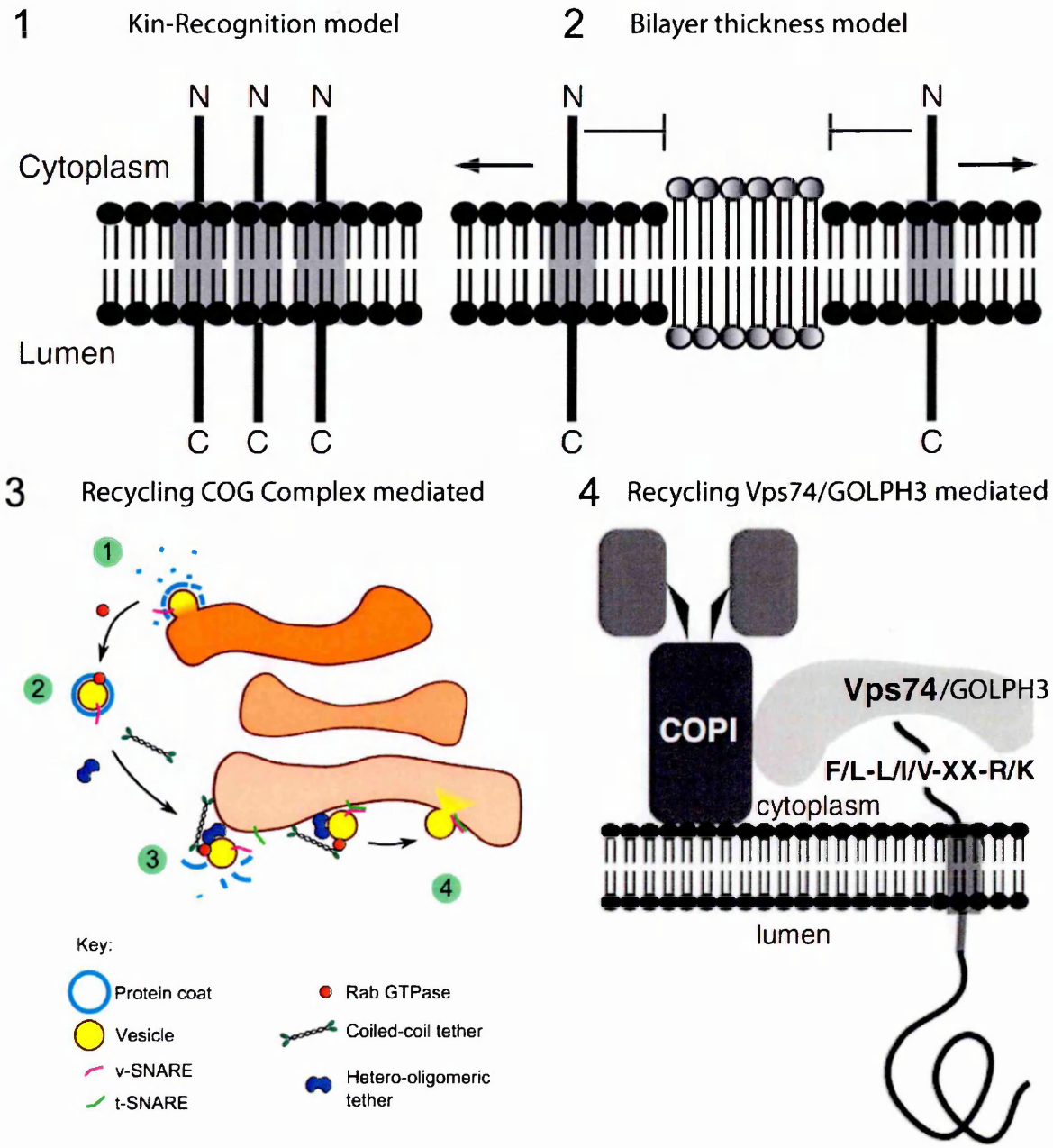

Figure 1.3 Models of glycosyltransferase retention within the Golgi apparatus

Mechanisms of protein-protein interactions (**1**, adapted from Banfield 2011), or based on lipid exclusion (**2**, adapted from Banfield 2011), as well as molecular machinery based on COGs (**3**, adapted from Cottam and Ungar 2012) and Vps74/GOLPH3 (**4**, adapted from Tu and Banfield 2010), might cooperate together to promote the correct localisation of glycosyltransferases within the Golgi apparatus.

1.4 Mechanisms of intra-Golgi transport

After synthesis in the ER, cargo proteins move to and traverse the Golgi complex, an organelle that is composed of stacks of membranous cisternae where cargo is modified by glycosylating enzymes during transport. The mechanism of intra-Golgi transport has been studied for decades, and most, if not all, of the possible avenues of investigation have been documented or hypothesised. It is fair to say, however, that transport through the Golgi remains one of the main unsettled questions in membrane biology (Pfeffer 2007). Different models have been proposed to explain how proteins move from the *cis*- to *trans*-Golgi, and below I summarise the main experimental observations that argue in favour or against each model.

1.4.1 Cisternal-progression model

This model was the first to be proposed to explain the mechanisms of intra-Golgi transport. Based on morphological evidence, it indicates that proteins that leave the ER by carriers reach the *cis* side of the Golgi apparatus, where they fuse with each other to form the first *cis* cisterna. The entire cisternae then progress in the *cis*-to-*trans* direction, changing their position over time and acting in this way as a shuttle for cargo proteins. During this process, a new cisterna forms at the *cis*-Golgi face, and the last *trans* cisterna is consumed at the *trans* face. The main evidence supporting this model is based on the observation that large algal scales were exclusively present in the lumen of the Golgi cisternae (Becker, Bolinger et al. 1995) and absent from peri-Golgi vesicles.

1.4.2 Vesicular-transport model

The discovery that the composition of each cisterna in a given Golgi stack has a specific biochemical identity pointed to the inability of the cisternal-progression model to explain such a distribution. A reformulation of the intra-Golgi transport models to reconcile these

observations led to the vesicular-transport model. The view of the Golgi complex as a stable compartment in which the cisternae are static and the cargo is moved forward by shuttling COPI transport vesicles (see **Fig. 1.4, 2**) represents the basic concept of this model (Farquhar and Palade 1981).

Strong evidence in favour of this hypothesis came from *in vitro* experiments, in which cells lacking N-acetylglucosaminyl transferase I and expressing VSVG were fused with wild-type cells, and surprisingly VSVG with incomplete glycosylation achieved the normal glycosylation profile after this fusion event (Rothman 1987). This evidence, coupled with the identification and characterisation of the machinery involved in vesicle formation and fusion (Rothman and Wieland 1996), gave further support to the vesicular-transport model.

Further *in vitro* studies showed that VSVG can enter 50-60-nm diameter COPI-coated vesicles (Ostermann, Orci et al. 1993), and moreover, other cargoes, like proinsulin, were detected in a subset of vesicles (Orci, Stamnes et al. 1997). In contrast, COPI vesicles were also reported to be depleted of other cargoes, like apolipoproteins E and B (Dahan, Ahluwalia et al. 1994), casein submicelles (Clermont, Xia et al. 1993), and the polymeric immunoglobulin receptor (Malsam, Satoh et al. 2005; Gilchrist, Au et al. 2006). The most striking evidence that cannot be explained by the vesicular-transport model concerned the transport of alga scales and procollagen, because they are too large to enter the 50-60-nm diameter COPI vesicles.

1.4.3 Cisternal-progression/ maturation model

The cisternal-progression/ maturation model stems from a re-evaluation of the old cisternal-progression model to accommodate the well-established differential compositions of the Golgi cisternae. This thus includes the concept of recycling of the Golgi resident enzymes, which move from the distal to proximal cisternae via retrograde COPI-coated

carriers, in synchrony with cisternal progression (see **Fig. 1.4, 1**). A key experiment specifically designed to test the hypothesis of cisternal-maturation model came from the study of the trafficking of procollagen, which was shown to progress from the *cis*- to the *trans*-Golgi in 10 min to 15 min without ever leaving the lumen of the cisternae (Bonfanti, Mironov et al. 1998). Later, using a reversibly polymerisable system, it was suggested that "megavesicles" might be involved in the intra-Golgi transport of such large cargoes. (Volchuk, Amherdt et al. 2000).

Nevertheless, other evidence supporting the cisternal-progression/maturation model was obtained when EM experiments showed that small transmembrane proteins (VSVG) and a large polymer (procollagen) traverse the Golgi apparatus at similar rates, without entering into COPI vesicles or "megavesicles" (Mironov, Beznoussenko et al. 2001), and the identification of Golgi resident enzymes in COPI vesicles (Martinez-Menarguez, Prekeris et al. 2001) (although this finding remains controversial; see Orci, Amherdt et al. 2000).

Due to the peculiar characteristics of yeast Golgi, in which the cisternae are not arranged in stacks, two different laboratories visualised cisternal maturation *in vivo* through live-cell imaging. Using different fluorescence markers for early and late Golgi, it was possible to follow the change in composition of a Golgi cisterna over time due to the recycling of the Golgi residents (Losev, Reinke et al. 2006; Matsuura-Tokita, Takeuchi et al. 2006). Compartment maturation has also been reported to exist in other transport steps of the cell, and specifically in the endocytic pathway, where early endosomes acquire the characteristics of late endosomes through the loss of Rab5 and the subsequent acquisition of the Rab7 marker (Rink, Ghigo et al. 2005).

The relatively recent discovery of Golgi heterotypic tubular connections by EM and tomography studies (Marsh, Volkmann et al. 2004; Trucco, Polishchuk et al. 2004), and their implication for the recycling of Golgi enzymes, have suggested a possible integration

of the progression/maturation models (see review of Glick and Luini 2011). The identification of the enzyme responsible for the formation of intercisternal tubular continuities and their implication in transport through the Golgi apparatus (San Pietro, Capestrano et al. 2009) highlighted the importance of these carriers in the context of intra-Golgi transport. Nevertheless, if heterotypic tubular connections are responsible for the recycling of Golgi enzymes or for anterograde transport of small secretory cargos, or for both, still needs to be fully defined (see review by Glick and Luini 2011).

1.4.4 Rapid partitioning within a two-phase membrane system

According to the rapid-partitioning model, the Golgi apparatus is viewed as a single compartment that contains two lipid sub-domains: the processing domain that is responsible for the glycosylation reactions, and the export domain where cargo proteins are exported out of the Golgi (see **Fig. 1.4, 4**; Patterson, Hirschberg et al. 2008). This relatively recent model changed the mainstream prospective of the Golgi apparatus drastically. This formulation of a new model for intra-Golgi transport was suggested by fluorescence microscopy experiments in which membrane cargoes, soluble cargoes, and large cargoes exited the Golgi apparatus with exponential kinetics, which means that the cargoes can exit the Golgi at every level of the Golgi stack. This study also presented evidence that cargo proteins and Golgi resident enzymes occupy different regions of the same compartment, similar to an earlier published observation (Pelhaman et al 2001). Many other key observations cannot be easily explained by the rapid-partitioning model, like the order of the glycosylation reactions on glycolipids and glycoproteins, which reflects their *cis*-to-*trans* distribution in the Golgi (Emr, Glick et al. 2009), or the progressive condensation of procollagen and secretory granules observed in the Golgi. Moreover, the exit of cargoes from the *cis* side of the Golgi that is predicted by this rapid-partitioning model has never been observed. Notwithstanding the weaknesses of this

model, a plausible way to explain the mono-exponential kinetics of the cargo exit comes from the observation that most cargoes are concentrated in the post-Golgi compartment, the TGN, at steady-state and the observed exit of cargoes from the Golgi actually reflects the exit from the TGN (see review by Glick and Luini 2011).

1.4.5 Cisternal-progenitor model

This recent model was proposed by (Pfeffer 2010) and it represents an evolution of the old vesicular-transport concept in which the Golgi apparatus is still viewed as a static compartment with anterograde *cis*-to-*trans* movement of the cargoes resulting from a process known as the Rab cascade. There are two main premises for the cisternal-progenitor model: first of all, it is known that the Golgi ribbon undergoes continuous lateral fission and fusion events, and thus it is a metastable structure. Nocodazole treatment fragments the Golgi ribbon into ministacks, and its wash-out leads to rapid ribbon reformation (see review by Thyberg and Moskalewski 1985), thus demonstrating the metastable nature of the mammalian Golgi ribbon. The second premise is based on a mechanism named Rab conversion, in which the sequential recruitment of active Rab GTPases appears to be important during cargo progression between early and late endosomes (Rink, Ghigo et al. 2005). Moreover, this cascade has been shown to exist in the yeast Golgi apparatus, where a Rab GTPase recruits a GEF for the subsequent-acting Rab, thus providing vectoriality to the transport that occurs in the Golgi apparatus (Ortiz and Novick 2006). Based on these premises, the progenitor model explained the *cis*-to-*trans* movement of cargo proteins in the mammalian Golgi apparatus through sequential steps, the first being a segregation mechanism of a specific Rab into each cisternae, followed by the fission and homotypic fusion events that are responsible for the directionality of anterograde intra-Golgi transport (see **Fig. 1.4, 3**; Pfeffer 2010).

This progenitor model, however, has several weaknesses; indeed, the presence of a specific Rab in each mammalian Golgi cisterna still requires experimental evidence, and furthermore, the fission and fusion events have never been visualised during the maturation of the yeast Golgi (Losev, Reinke et al. 2006; Matsuura-Tokita, Takeuchi et al. 2006).

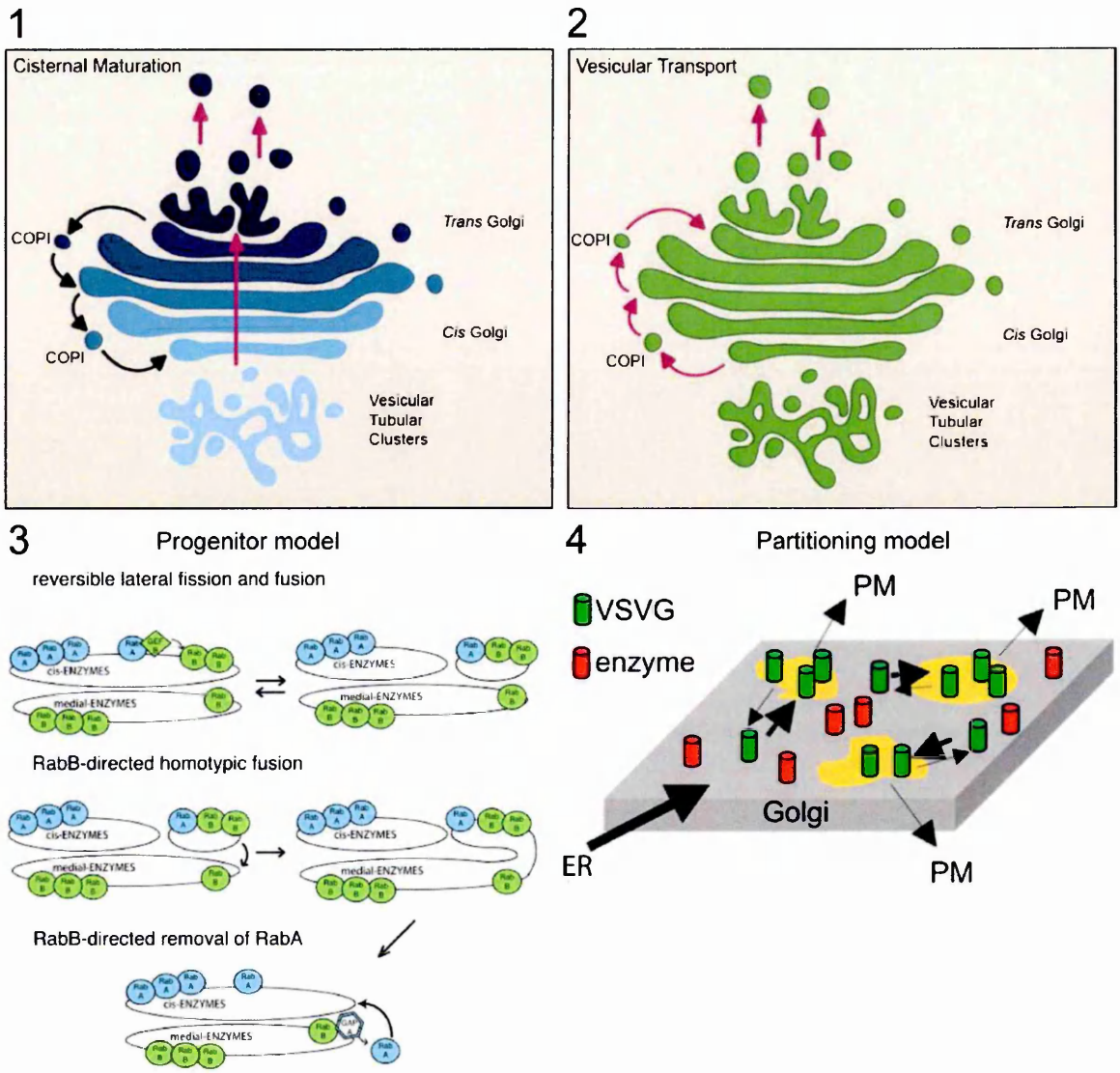

Figure 1.4 Models of intra-Golgi transport.

1, **2** (from Nilsson, Au et al. 2009); **3** (from Pfeffer 2010); **4** (from Patterson, Hirschberg et al. 2008).

CHAPTER 2

Objectives

Despite the development of new technologies in the scientific field in the last few years, the mechanisms of intra-Golgi transport are still an important and unresolved issue in cell biology. Different models have been proposed to explain how secretory proteins cross this complex organelle, but still none of them have gained a consensus among the scientific community. All of the models described above can be mainly grouped into two types: one based on stable cisternae, and the other on 'maturing' cisternae. One of the main differences between them is the behaviour of the Golgi resident enzymes that are supposed to remain fixed within static cisternae. In the case of stable cisternal models (Rothman and Wieland 1996; Patterson, Hirschberg et al. 2008; Pfeffer 2010), the Golgi enzymes are considered to be stably localised to the cisternae, while they are thought to be dynamic in the case of the cisternal-progression/maturation model. In this latter case, to maintain their intra-Golgi distribution, the Golgi enzymes need to be recycled back during the progression of the cisternae (see reviews Nakano and Luini 2010; Glick and Luini 2011). This mechanism enjoys a degree of experimental support (Bonfanti, Mironov et al. 1998); (Matsuura-Tokita, Takeuchi et al. 2006), but crucial evidence that Golgi enzymes maintain their position in the stack by recycling in step with transport is still missing in mammalian cells (Emr, Glick et al. 2009).

Here, I have studied the dynamics of the Golgi-resident proteins, and in particular the glycosylation enzymes, to determine how their dynamics are coupled to those of the cargoes that are transported through the Golgi apparatus. To this end, I have engineered Golgi resident constructs that can be reversibly polymerised to prevent their entry into

carriers, and examined the transport behaviour of these constructs in monomeric and polymeric states. Under these conditions, the stable and maturing cisternae models predict very different behaviour. The Golgi progression/maturation model predicts that, if a suitably modified *cis*-Golgi resident protein is prevented from recycling, it will remain within the lumen of a cisterna and hence move to the *trans*-side of the stack at the rate of cisternal progression (see **Fig. 2.1**; Bonfanti, Mironov et al. 1998). This condition might be achieved by reversibly polymerising a suitable *cis*-resident construct, as polymers might be too large to enter recycling vesicles or tubules, and/or incompatible with the vesicular membrane curvature. If then, once at the *trans*-Golgi, such a polymer were depolymerised, the resulting monomers might re-enter vesicles and recycle back to the *cis*-Golgi. In contrast, according to the stable cisternae models, a Golgi resident, such as an enzyme, should localise in the stack independently of its ability to enter Golgi carriers (see **Fig. 2.1**).

Thus, in this study, I used an assay to manipulate the aggregation state of the Golgi resident enzymes, and I studied their behaviour through the combination of confocal and EM microscopy techniques.

The objectives of this study were:

- Engineering and characterisation of Golgi resident enzymes in terms of their localisation and reversible polymerisation properties;
- Examination of the entry of the engineered Golgi resident enzymes into vesicular/tubular carriers under aggregation/disaggregation conditions;
- Study of the fate of a *cis*-Golgi resident after its polymerisation in the Golgi apparatus;
- Study of the Golgi functions under polymerisation conditions of the engineered Golgi resident enzyme.

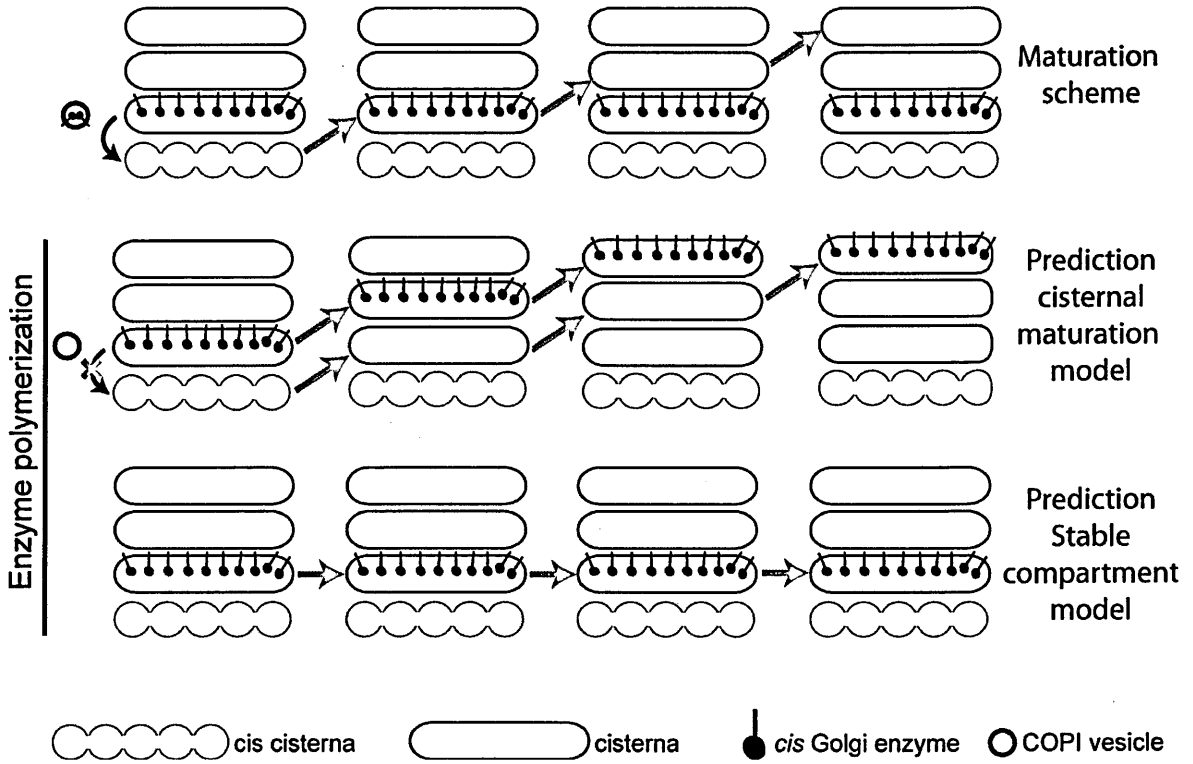

Figure 2.1 Experimental strategy.

Polymerisation of a *cis*-Golgi enzyme as a tool to discriminate between the stable *versus* maturation models of intra-Golgi transport. Each model predicts very different behaviour for a polymerised *cis*-Golgi resident enzyme. The red arrow indicates the fate of the same cisterna over time.

CHAPTER 3

Materials and methods

3.1. Cell culture.

3.1.1 Materials.

Dulbecco's modified Eagle's medium (DMEM) and calf serum (CS) were from Nitrogen (UK). Foetal calf serum (FCS), penicillin, streptomycin, trypsin-EDTA and L-glutamine were from Biochrom KG (Berlin, Germany). All of these reagents were as 10× stock solutions. All of the plastic-ware was from Corning (NY, USA) or Falcon (NJ, USA). Filters (0.45 and 0.2 μm) were from Albet (USA).

3.1.2 Growth media.

HeLa cells were cultured in RPMI supplemented with 4.5 g/l glucose, 2 mM glutamine, 100 U/ml penicillin, 100 μg/ml streptomycin and 10% foetal calf serum (FCS). Normal rat kidney (NRK) cells were grown in DMEM supplemented with 4.5 g/l glucose, 2 mM glutamine, 100 U/ml penicillin, 100 μg/ml streptomycin, and 10% FCS.

3.1.3 Growth conditions.

All of the cell lines were grown in a controlled atmosphere in the presence of 5% CO_2 at 37 °C. The cells were grown in flasks until 90% confluence. To detach the cells from the surface of the flasks, the medium was removed and 0.25% trypsin-EDTA in normal saline solution was added for 2-5 min at room temperature (RT). Complete medium was then

added back to block the protease action, and the cells were collected in a plastic test-tube and centrifuged at 300× *g* for 5 min. The pellet of cells was resuspended in fresh medium and seeded into new plastic flasks.

3.2 Transformation of bacteria using heat shock

3.2.1 Materials

Bacto™ tryptone, Bacto™ yeast extract, and agar were from Becton, Dickinson and Company (USA). NaCl was from Carlo Erba (Italy). Glycerol was from Merck (Germany).

3.2.2 Procedures

The plasmid DNA (1 μg/μl) was diluted in 10 mM Tris-HCl/ EDTA to a final concentration of 50 ng/μl. One microliter of the DNA (50 ng/μl) was added to 200 μl competent bacteria previously thawed on ice. After gentle mixing, the bacteria were incubated on ice for 20 min, heat shocked for 90 s at 42 °C, and after addition of 800 μl LB broth, incubated under shaking (200 rpm) at 37 °C for 45 min. The bacteria were plated on LB agar containing the appropriate selective antibiotic, and incubated overnight (O/N) at 37 °C. The following day, an isolated bacterial colony was picked and inoculated into 2 ml LB broth containing the appropriate antibiotic. The culture was incubated at 37 °C O/N, and 700 μl 50% sterile glycerol was added to 700 μl bacterial culture, which was then stored at –80 °C.

3.3 Cell transfection

3.3.1 Constructs preparation

(i)The pcDNA4B-FM3-HA construct (FM-HA) was prepared as follows:

Three copies of tandem FM (mutant FK506 binding protein (FKBP-Phe36Met)) domains, with an HA tag at the C-terminal region was amplified using polymerase chain reaction from $pC_4EN\text{-}FM_3$ (from Ariad Pharmaceuticals www.ariad.com; (Rivera, Wang et al. 2000) vector using the forward primer: 5'-cgggatccagaaaggtgtctagaggagtgcaggtg-3' and reverse primer: 5'-cggaattcttatgcgtagtctggtacgtcgtacggataagatccgtaataactagtttc-3'. The product was digested with *BamH*I and *EcoR*I and subcloned into *BamH*I/*EcoR*I digested pcDNA4B (Invitrogen).

(ii)The GALT-FM construct was prepared as follows:

The cytosolic, transmembrane, and luminal stem domains of β-1,4-galactosyltransferase (GALT) was amplified using polymerase chain reaction from GALT-GFP construct (Cole, Smith et al. 1996) using the forward primer: 5'-cccaagcttatgccgggcgcg-3' and reverse primer 5'-cggggtaccagaaaggtgtctagaggagtg-3'. The product was digested with *Hind*III and *Kpn*I and subcloned into the *Hind*III/*Kpn*I-digested FM-HA to obtain GALT-FM.

(iii) The MANI-FM construct was prepared as follows:

The cytosolic, transmembrane, and luminal stem domains of mouse Golgi alpha1,2-mannosidase IB was amplified using polymerase chain reaction from pEYFP-N1-MannosidaseI construct (Marra et al., 2001) using the forward primer: 5'-ccaagcttatgcccgtgggggggcctg -3' and reverse primer 5'- ggggtaccaaacagatccttgtcacgcag -3'. The product was digested with *Hind*III and *Kpn*I and subcloned into the *Hind*III/*Kpn*I-digested FM-HA to obtain MANI-FM.

3.3.2 Materials

TrisHCl and EDTA were from SIGMA (USA). The Qiagen plasmid kits for large-scale plasmid DNA preparation was from Qiagen (USA).

3.3.3 Large scale preparation of plasmid DNA

A single colony of XL-1 Blue *Escherichia coli* bacteria (Stratagene, USA) transformed with the plasmid of interest was inoculated into 500 ml LB broth plus the appropriate selective antibiotic. After 15 h to 20 h of incubation, the bacteria were collected by centrifugation at 6000 rpm (4000 x *g*) in a JA10 rotor for 10 min at 4 °C, and processed according to the manufacturer instructions (Quiagen plasmid kits). The DNA obtained was resuspended in TE buffer (10 mM TrisHCl, 1 mM EDTA, pH 7.5) to a final concentration of 1 mg/ml, and stored at -20 °C.

3.3.4 TransIT-LT1-reagent-based cell transfection

The cells were plated onto glass coverslips in 24-well plates, or into 3.5-cm glass-bottomed petri dishes or 10-cm petri dishes, in normal culture medium at a concentration suitable to have 50% to 70% confluence for transfection. The day after, a transfection mixture was prepared by diluting the TransIT-LT1 reagent in OptiMEM culture medium, which was incubated at RT for 5 min. The DNA was then added to the transfection mixture, which was gently shaken, and kept at RT for another 20 min, to allow the DNA-TransIT-LT1 reagent complex to form. The cells were then incubated prior to the assays with the transfection mixture for 24 h at 37 °C, in complete medium without antibiotics, as reported for each experiment.

3.4 Radioactive labelling

The method used was essentially as described previously (Bonifacino 2001), with small modifications as described below. HeLa cells transfected with the construct for MANI linked to the FK506 binding protein (FKBP)-domain mutant (FM) (MANI-FM) were cultured in the presence of AP12998 for 12 h, and then the media was substituted with one containing 0.05 mCi/ml radiolabelled ([^{35}S]) cysteine and methionine, and further cultured

for 24 h in the presence of AP12998. The cells were then lysed in RIPA buffer (150 mM NaCl, 20 mM Tris, pH 8.0, 0.1% [w/v] sodium dodecyl sulphate [SDS], 0.5% sodium deoxycholate, 1% [v/v] Triton X-100) and centrifuged at 14,000 rpm (20000 x *g*)for 5min, and the supernatant was used for immunoprecipitation.

3.5 Immunoprecipitation procedures

3.5.1 Materials

Lysis buffer: RIPA buffer (150 mM NaCl, 20 mM Tris, pH 8.0, 0.1% [w/v] SDS, 0.5% [w/v] sodium deoxycholate, and 1% [v/v] Triton X-100), and protease inhibitor cocktail (Complete Mini EDTA free; Roche)

3.5.2 Procedures

After the radioactive labelling experiment, the cells were washed with phosphate-buffered saline (PBS), lysed with RIPA buffer, and then centrifuged at 13,000x *g* for 10 min at 4 °C. Then 500 µg lysate was incubated O/N with 5 µg mouse anti-HA antibody or 5 µg anti-hMANI antibody. Then 30 µl Protein-G Sepharose beads (Amersham) were added and incubated for an additional 1 h at 4 °C. After washing 3 times with lysis buffer and twice with lysis buffer without Triton X-100, the bound protein was eluted by boiling the samples for 10 min in 100 µl Laemmli buffer. The immunoprecipitate was resolved by SDS-PAGE followed by autoradiography. The intensity of the bands was quantitated using ImageJ.

3.6 General biochemical procedures

3.6.1 Materials

SDS, glycine, Trizma base, Ponceau red, polyoxyethylenesorbitan monolaurate (Tween-20), ammonium persulphate, and N,N,N',N'-tetramethylethylenediamine (TEMED) were from Sigma-Aldrich (WI, USA). Acrylamide stock solution, at 40% (w/v) acrylamide:bis-acrylamide (37.5:1), was from Eurobio (France). Acetic acid was from Carlo Erba (Italy). Secondary antibodies conjugated with horse radish peroxidase (HRP) and directed against mouse or rabbit IgGs were from Calbiochem (CA, USA). The ECL reagents were from Amersham Pharmacia Biotech (NJ, USA).

3.6.2 Solutions

Running buffer: 25 mM Trizma base, 200 mM glycine, 0.1% (w/v) SDS.

SDS sample buffer: 62.5 mM Tris-HCl, pH 6.8, 2% (w/v) SDS, 10% (v/v) glycerol, 5% (v/v) C-mercaptoethanol and 0.1% (w/v) bromophenol blue.

Transfer buffer: 25 mM Trizma base, 200 mM glycine, 20% (v/v) methanol.

TBS: 150 mM NaCl, 20 mM Tris-HCl, pH 7.5.

TTBS (TBS plus Tween 20): 0.05% (w/v) Tween 20, 150 mM NaCl, 20 mM Tris-HCl, pH 7.5.

Blocking solution for Western blotting: 1% (w/v) bovine serum albumin (BSA) in TTBS; 5% skimmed milk in TTBS.

3.6.3 Assembly of polyacrylamide gels

Two 16 cm × 18 cm plates were used for standard gels. The plates were assembled to form a chamber using two 1.5-mm plastic spacers aligned along the lateral edges of the plates. The plates were then fixed using two clamps and mounted into a plastic base which sealed the bottom. All of the materials were from Hoefer Scientific Instruments (Germany). The 'running' polyacrylamide gel was prepared by mixing water, 40% (w/v)

acrylamide:bisacrylamide solution, 1.5 M Tris-HCl, pH 8.8, 10% (w/v) SDS, to have the selected concentration of acrylamide in 375 mM Tris-HCl, 0.1% (w/v) SDS. Then, 0.06% (w/v) ammonium persulphate and 0.06% (v/v) TEMED were added, and the solution was mixed and poured into the gap between the plates, leaving ~5 cm for the stacking gel. Soon after pouring, the gel was covered with a layer of water and left at RT for ~2 h. The water layer was then removed. The 'stacking' polyacrylamide gel was prepared by mixing water, 40% (w/v) acrylamide:bisacrylamide solution, 500 mM Tris-HCl, pH 6.8, 10% (w/v) SDS, to have 4% (w/v) acrylamide, 125 mM Tris-HCl, 0.1% (w/v) SDS. Then, 0.1% (w/v) ammonium persulphate and 0.07% (v/v) TEMED were added, and the solution was mixed and poured onto the 'running' gel. Immediately, a 15-well or 10-well comb was inserted between the glass sheets and the apparatus was left for 1 h at RT.

3.6.4 Evaluation of protein concentrations

Protein concentrations were evaluated using a commercially available bicinchoninic acid (BCA) protein assay kit (Bio-Rad Laboratories, UK), according to the manufacturer instructions.

3.6.5 SDS-PAGE sample preparation and running

Samples were prepared by adding SDS sample buffer, incubating at 100 °C for 5-10 min in a multi-block heater (Lab-Line, IL, USA), cooling to RT, briefly centrifuging and finally loading onto an SDS gel. One well was loaded with 5 µl Rainbow recombinant protein molecular weight markers (Amersham Pharmacia Biotech, NJ, USA) or with 5 µg Low Molecular Weight Standards (Bio-Rad Laboratories, UK). The gel was then transferred into the electrophoresis apparatus (Hoefer Scientific Instruments, NJ, USA), and the electrophoresis was carried out under constant current of 8 mA (for O/N runs) or 40 mA (for ~4-h runs).

3.7 Western blotting

3.7.1 Protein transfer onto nitrocellulose

The polyacrylamide gels were soaked for 15 min in transfer buffer, placed on a sheet of 3MM paper (Whatman, NJ, USA) and covered with a nitrocellulose filter (Schleicher & Schuell, Germany). The filter was covered with a second sheet of 3MM paper, to form a 'sandwich', which was subsequently assembled into the blotting apparatus (Hoefer Scientific Instruments, NJ, USA). The protein transfer was carried out at 500 mA for 4 h, or at 125 mA O/N. At the end of the run, the sandwich was disassembled, and the nitrocellulose filter was soaked in 0.2% Ponceau red (Sigma-Aldrich, WI, USA) and 5% (v/v) acetic acid for 5 min to appropriately visualise the protein bands, and then rinsed with 5% acetic acid to remove excess unbound dye.

3.7.2 Probing the nitrocellulose with specific antibodies

The nitrocellulose filters were cut into strips with a razor blade. The strips containing the proteins of interest were incubated in the blocking solution for Western blotting plus 1% (v/v) BSA or 5% (w/v) milk powder (for ECL-based detection) for 1 h at RT, and then with the primary antibody diluted to its working concentration in the blocking solution for Western blotting (see Table 2.1, for the list of antibodies used in the Western blotting experiments). After a 2-3-h incubation at RT, or an O/N incubation at 4 °C, the antibody was removed and the strips were washed twice in TTBS, for 10 min each. The strips were next incubated for 1 h with the appropriate HRP-conjugated secondary antibody diluted in the blocking solution for Western blotting (anti-rabbit: 1:10,000; anti-mouse: 1:10,000) and washed twice in TTBS, for 10 min each, and once in TBS for 3 min. After washing,

the strips were incubated with the ECL reagents, according to the manufacturer instructions for ECL-based detection.

3.8 Experimental conditions for MANI-FM polymerisation

HeLa cells were transfected with the MANI-FM construct (see section **3.3.1)** using Mirus transfection reagent, following the manufacturer instructions. After 24 h transfection in the presence of 1 μM AP12998 at 37 °C, the media was changed and 1 μM fresh AP12998 was added for 30 min at 37 °C. The cells were then treated with 33 μM nocodazole for 3 h in the presence of 1 μM AP12998, and 50 μM cycloheximide (CHX) was added for the last 30 min at 37 °C. Importantly, the MANI-FM levels at the Golgi remained constant throughout this period. The AP12998 was then washed out of a subset of samples for the indicated times in the presence of CHX and nocodazole. All of the experiments were carried out in the presence of nocodazole and CHX, unless otherwise indicated.

3.9 MANI-FM sedimentation/ polymerisation assay

The sedimentation assay to reveal the polymerisation status of MANI-FM was performed as described previously (Volchuk, Amherdt et al. 2000). In brief, after treatment, the cells were lysed in lysis buffer (1% [v/v] Triton X-100, 20 mM Hepes, pH 7.4, 100 mM KCl, 2 mM EDTA, 1 mM dithiothreitol, and protease inhibitor cocktail [Roche]) at 4 °C for 30 min. The lysate was then centrifuged at 20,000× *g* for 10 min, and the pellet and supernatant fractions were separated and analysed by SDS-PAGE and immunoblotting.

3.10 Sucrose gradient centrifugation

Sucrose gradients (5%-20% sucrose) in lysis buffer (1% [v/v] Triton X-100, 20 mM Hepes, pH 7.4, 100 mM KCl, 2 mM EDTA, 1 mM dithiothreitol, and protease inhibitor cocktail [Roche]) were prepared and cooled to 4 °C. The cells were treated and lysed as described

in section 3.9, and a volume of 500 µl of clarified lysate was layered on the top of the gradient. The gradients were centrifuged at 36,000 rpm in a SW-41 rotor (Beckman Coulter) for 20 h at 4 °C. The sucrose gradients were fractionated, and each fraction was precipitated with trichloroacetic acid. The trichloroacetic-acid-precipitated proteins were analysed by SDS-PAGE (Section **3.6.5**).

3.11 Infection of cells with vesicular stomatitis virus

The infectious stocks of the temperature-sensitive (ts-0-45) mutant strain of VSV were prepared by Antonella Di Campli (Instituto di Biochimica delle Proteine, Consiglio Nazionale delle Richerche, Naples, Italy) according to (Bergmann 1989). For each infectious stock, the optimal working concentration was experimentally defined as the lowest concentration causing 100% infection of HeLa cells, judged by staining of the viral membrane glycoprotein (VSVG).

The system of VSV is often used in membrane-traffic studies (Bergmann 1989), as the virus has a very small genome and does not have the machinery for protein translation, post-translational processing, or transport of its membrane proteins. Indeed, the VSV genome codes for only five proteins, among which there is an integral membrane glycoprotein (VSVG). As the virus inhibits the synthesis of host cell proteins, the total translational capacity of the cell is devoted to the synthesis of the viral proteins. In the ts-0-45 strain, VSVG bears a point mutation that causes its misfolding at temperatures higher than 39.5 °C. The misfolded protein is retained in the ER and excluded from transport carriers involved in ER-to-Golgi transport (Rose and Bergmann 1983; Schnitzer, Dickson et al. 1979).

The cells were washed twice in serum-free culture medium and incubated with the diluted VSV infectious stock for 1 h at 32 °C. For HeLa-cell infection, VSV was diluted 1:40 in serum-free medium. After infection, the cells were washed with PBS to remove

extracellular viral particles, and then they were subjected to different transport protocols as described in Chapter 4 (Section 4.4.1).

3.11.1 Acquisition of endoH resistance

VSVG has been used extensively as a marker to study the biochemical and molecular basis for transport along the exocytic pathway both *in vivo* (Tisdale, Bourne et al. 1992) and *in vitro* (Davidson and Balch 1993). VSVG is a type I transmembrane protein that has two N-linked carbohydrate chains and is transported from the ER to the Golgi apparatus and then sequentially through the *cis*-, medial and *trans*-Golgi compartments. Its transport through the Golgi can be followed by the processing of two oligosaccaride chains from the high mannose endoH-sensitive form (which is found in the ER and in the pre-Golgi compartments) to the endoH-resistant form (which is found in the Golgi stack). The processing intermediates can be easily distinguished by SDS-PAGE (Davidson and Balch 1993). The first endoH-resistant form corresponds to the transport of VSVG from the ER to the early Golgi compartment (endoH-resistance develops after its transport to the medial Golgi), where one or both of the oligosaccaride chains becomes endoH resistant by the action of the resident 1,2-mannosidases and glycosyltransferases (Davidson and Balch 1993; Tisdale, Bourne et al. 1992). The subsequent transport of VSVG to the TGN results in the appearance of the fully processed form, which contains two complex endoH-resistant oligosaccarides (Davidson and Balch 1993, Tisdale, Bourne et al. 1992). The appearance of sequential processing intermediates allows the direct examination of the effects of drug treatments on both ER-to-Golgi and intra-Golgi transport in the same experiment (Davidson and Balch 1993; Tisdale, Bourne et al. 1992).

3.11.2 Materials

RIPA buffer (150 mM NaCl, 20 mM Tris, pH 8.0, 0.1% [w/v] SDS, 0.5% [w/v] sodium deoxycholate, and 1% [v/v] Triton X-100), sodium citrate, β-mercaptoethanol, and protease inhibitors were from SIGMA (USA). EndoH was from New England BioLabs (USA). 4-(2-hydroxyethyl)-monosodium salt (Hepes) was from Merck (Germany).

3.11.3 VSVG transport assay

HeLa cells transfected with MANI-FM (see Experimental conditions for MANI-FM polymerisation; Section **3.8**) were seeded in Multiwell^{TM} 6-well tissue culture plates in normal culture medium, at a concentration suitable to have 50% to 70% confluence on the day of the experiment. The cells were washed twice with medium containing 20 mM Hepes without serum, and then incubated for 1 h at 32 °C with VSV diluted in the same medium. The cells were washed and incubated for 2 h with complete medium containing 20 mM Hepes at 32 °C to allow the synthesis of VSVG to proceed. The cells were subsequently washed, incubated with complete medium at 40 °C for 3 h, then washed twice, incubated with complete medium containing 20 mM Hepes and shifted to 32 °C for 0, 30, 60, 120, 180 min. At each time point, the cells were washed twice with PBS on ice and then lysed in RIPA buffer (150 mM NaCl, 20 mM Tris, pH 8.0, 0.1% [w/v] SDS, 0.5% [w/v] sodium deoxycholate, and 1% [v/v] Triton X-100) at 4 °C for 30 min. The lysates were clarified by centrifugation at 20000x *g* for 10 min. The supernatants were treated with endoglycosidase H in the endoH buffer (0.05 M sodium citrate, pH 5.5) at 37 °C O/N. The treated samples were then resolved by SDS-PAGE, and then Western blotting was carried out using an anti-VSVG antibody.

3.12 Immunofluorescence microscopy

3.12.1 Materials

Glass coverslips were from Carlo Erba (Italy). Mowiol was from Calbiochem (Germany). Paraformaldehyde was from Electron Microscopy Sciences (EMS, USA). Saponin and NH_4Cl were from Fluka (Sigma, USA). 4-(2-Hydroxyethyl)-monosodium salt (Hepes) was from Merck (Germany).

3.12.2 Sample preparation

The cells were grown on coverslips and fixed with 4% paraformaldehyde for 10 min at RT, and then permeabilised with 0.2% saponin in blocking solution (PBS containing 1% BSA, 50 mM NH_4Cl) followed by incubation with the antibodies to the antigen of interest in the same solution at 4 °C overnight, followed by second antibodies labelled with Alexa Fluor dyes (Invitrogen). The coverslips were then mounted in the mounting media (16% [w/v] Mowiol 4–24 [EMD Millipore] and 30% [v/v] glycerol in PBS) and examined under a confocal microscope (LSM710; Carl Zeiss)

3.12.3 Confocal microscopy and line scanning

The images were acquired with a pinhole set to 1 and under non-saturation conditions using a 63× objective (1.4 NA). The images were acquired using the Zen software system (Carl Zeiss). The line scan analysis was performed as described previously (Dejgaard, Murshid et al. 2007). In brief, images of stacks stained for GM130, TGN46, and MANI-FM were acquired as described earlier. Only cells with a moderate level of expression were considered for the analysis. Cells that expressed high levels of the MANI-FM construct were avoided, as this leads to the localisation of the protein at the PM (~20% of the cells). Golgi stacks with clearly separated GM130-stained and TGN46-stained zones were

identified and used for the analysis. A line was drawn in the middle of the stacks along the *cis-trans* direction, and the fluorescence intensity of each stained marker along this line was plotted. The images obtained were then processed using Metamorph 7.7.3.0 (Universal Imaging), with the "Image with Zoom" function for presentation. At least 30 stacks were examined per treatment, and a representative image is shown. For the computational coalescence of line scans, the normalised line scans to be coalesced were plotted together and coalesced using the Gaussian curve fitting option of GraphPad Prism version 5.0 software. The normalisation of the distances was carried out by considering the start of the GM130 peak as 0, and the end of the TGN peak as 1.

3.13 Pre-embedding techniques

The name of these techniques arises because the labelling is performed before the sample embedding. Briefly, the samples are chemically fixed and the antigen is labelled using a specific primary antibody that is recognized by a secondary antibody conjugated with ultra-small gold particles (Section **3.13.2**). The detection of the gold particles is almost unequivocal, and they can be exactly quantitated; however, one limitation of the use of colloidal gold conjugates (5, 10, 15 nm gold particles) has been that generally they do not penetrate cells, even after permeabilisation. Therefore, their use in pre-embedding immuno-staining has up to now been restricted both to the labelling of cell-surface antigens, either for scanning or transmission EM, and for tracing endocytic pathways in living cells. Recently, 1.4-nm gold conjugates that can penetrate cells and tissues much more readily have been used successfully to immunolabel intracellular structures. Ultra-small immuno-gold probes label more efficiently than do the larger colloidal gold particles (1.4> 5> 10> 15 nm). The only drawback of this approach is that to detect 1.4-nm gold probes by conventional transmission EM, the gold enhancement (see Section **3.13.2**) reaction has to be developed and this procedure typically produces particles of variable

diameters, unlike the 5, 10, and 15 nm particles that instead are uniform in diameter. Another advantage of this approach is the possibility to cut serial consecutive sections of the specimen, which can be used for three-dimensional (3D) reconstruction of organelles using electron tomography (see Section **3.16**).

3.13.1 Materials

Fab' fragments conjugated with nanogold (1.4-nm gold particles) were from Nanoprobes (USA). Goldenhance™ –EM was from Nanoprobes. Multiwell™ (6 well) tissue-culture plates were from Becton Dickinson (France). Grids, osmium tetraoxide, paraformaldehyde and glutaraldehyde were from Electron Microscopy Sciences (EMS, USA). Sodium cacodylate, saponin, NH_4Cl and the epoxy resin kits were from Fluka (Sigma, USA). BSA was from Sigma (USA). Potassium ferrocyanide, ethanol and acetone were from Carlo Erba (Italy). Tris-HCl was from Merck (Germany).

3.13.2 Gold enhancement

The cells were grown in 6-well plates, and were fixed with a mixture of 4% paraformaldehyde and 0.05% glutaraldehyde in 0.15 M Hepes for 5 min at RT, and then placed in 4% paraformaldehyde in 0.15 M Hepes for 30 min at RT. Afterwards, the cells were washed 6 times in PBS at RT, and incubated with blocking solution for 30 min at RT. Finally, the cells were incubated with the primary antibody diluted in blocking solution (see **Tab 3.1**) overnight at 4 °C. On the following day, the cells were washed 6 times with PBS at RT, and incubated with goat anti-mouse Fab' fragments coupled to 1.4-nm gold particles (diluted in blocking solution, 1:100) for 2 h and finally washed six times with PBS at RT. Meanwhile, the activated Goldenhance™-EM was prepared according to the manufacturer instructions, and 300 µl was added into each of the wells. The reaction was monitored by conventional light microscope, and was stopped after 5 min to 10 min when

the cells had turned "dark enough", by washing several times with PBS. Osmification followed: the cells were incubated for 1 h at RT with a 1:1 mixture of 2% osmium tetraoxide in distilled water and 3% potassium ferrocyanide in 0.2 M sodium cacodylate pH 7.4, and then rinsed six times with PBS and then with distilled water. The samples were then dehydrated: 3× 10 min in 50% ethanol; 3× 10 min in 70% ethanol; 3× 10 min in 90% ethanol; and 3× 10 min in 100% ethanol. The samples were subsequently incubated for 2 h in a 1:1 mixture of 100% ethanol and epoxy resin (EPON) at RT; the mixture was then removed with a pipette and finally samples were embedded for 2 h in epoxy resin at RT. The resin was polymerised for at least 10 h at 60 °C in an oven.

3.14 Post-embedding techniques

The name of these techniques arises because the labelling is performed after the sample embedding. The cryosectioning technique is the most important technique for post-embedding sub-cellular immunocytochemistry; indeed, cryosections have been used to immunolabel several different antigens and they have also been applied to other powerful techniques, such as *in-situ* hybridisation.

Cryosectioning offers three major advantages compared to pre-embedding techniques: (i) easier and faster sample preparation; (ii) both chemical and structural integrity of tissues are better preserved; (iii) possibility to perform double staining of the same specimen to precisely localise one antigen with respect to another.

In addition, it has been demonstrated that the cryosection technique appears to be the most sensitive detection method available for some antigens, and the only detection method available for other antigens, where antibodies do not label resin sections. Moreover, both the ease and rapidity of sample preparation for cryosectioning makes this a convenient way of performing routine immunocytochemistry localisation.

3.14.1 Materials

Multiwell™ (6 well) tissue culture plates were from Becton Dickinson (France). Acetylated BSA (BSA-c™) was from Aurion (Wageningen, The Netherlands). Protein A conjugated with 5, 10, and 15 nm gold particles was provided by J. Slot (Utrecht University, Utrecht, The Netherlands). Grids, paraformaldehyde and glutaraldehyde were from Electron Microscopy Sciences (USA). Uranyl acetate and glycine were from Fluka (Sigma, USA). Cold fish skin gelatin, BSA, and methyl cellulose were from Sigma (USA). Sucrose was from Carlo Erba (Italy). Whatman 50 filter papers were from Whatman (UK).

3.14.2 Ultrathin cryosectioning

The cells were fixed by adding to the culture medium the same volume of a mixture of 0.2 M PIPES–Hepes–EGTA–magnesium (PHEM) buffer, 4% paraformaldehyde, 2% glutaraldehyde for 2 h, and finally stored in storage solution O/N (0.1 M PHEM buffer, 0.5% paraformaldehyde, in distilled water). After washing with 0.15 M glycine buffer in PBS, the cells were scraped and pelleted by centrifugation, embedded in 10% gelatin, cooled on ice, and cut into 0.5-mm blocks in the cold room. The blocks were infused with 2.3 M sucrose, which acts as a cryo-protectant, and then placed onto small specimen pins. The pins were frozen by immersion in liquid nitrogen, and quickly transferred to a pre-cooled (–60 °C) cryo-chamber fitted onto a ultramicrotome (Leica ultracut R), for trimming to a suitable shape. The sections were cut at –120 °C using a dry diamond knife, and collected on the knife surface. The sections were retrieved from the knife by picking them up on a small drop of a 1:1 mixture of 2.3 M sucrose and 2% methyl cellulose, and transferring tem onto formvar-coated and carbon-coated specimen grids. The samples were processed for immuno-labelling as described in the following section. Ultrathin cryosections were cut by Claudia Puri (Telethon Institute of Genetics and Medicine, Via P. Castellino 111, Napoli, Italy).

3.14.3 Labelling of cryosections

During immuno-labelling, the grids were kept floating on drops of buffered saline solution with the section side in the liquid. The back of the grid was kept dry and the section side was kept hydrated at all times.

The grids were washed onto 100 µl droplets of PBS for 10 min and then additionally washed 3× 3 min with 0.02 M glycine in PBS, pH 7.4. The grids were incubated for 10 min in 0.5% BSA-c^{TM} in PBS, and then incubated on 10 µl droplets of diluted primary antibody for 1 h (as indicated in **Table 3.1**). The grids were washed six times with 0.1% BSA-c^{TM} in PBS, and then either directly incubated with Prot A-gold (10 nm) for 30 min, if the primary antibody was a polyclonal one, or with a rabbit anti-mouse immunoglobulin antibody (bridge antibody) and then with protein A golds, if the primary antibody was a monoclonal one. The grids were rinsed six times with 0.1% BSA-c^{TM} in PBS and post-fixed with 1% glutaraldehyde in 0.15 M Hepes for 5 min. In case of double immuno-labelling, the above described procedure was repeated with the incubating of the grids with Prot A-gold with different sizes (e.g., 5 nm). Finally, the grids were washed 5× 1 min in distilled water, and stained for 10 min in 1.8% methyl cellulose plus 0.4% uranyl acetate on ice. The grids were retrieved with a stainless steel loop, and placed onto a piece of a Whatman 50 filter paper at an angle of 45°. After air-drying, the grids were ready to be examined under the electron microscope.

3.15 Immuno-electron microscopy: data acquisition and quantitation

The samples were then examined under an iTEM transmission electron microscope (JEOL Ltd.). Random sampling for the Golgi stacks was performed, with the only criterion for selection being the presence of gold label on Golgi stacks that were sectioned perpendicularly to the plane of cisternae. The stacks were imaged at a magnification of 20,000 or 30,000 using a Morada CCD camera with the iTEM image acquisition software

(JEOL Ltd.). Some cells (~20% of the total) expressed high levels of MANI-FM and showed this construct at the PM. These cells were discarded. The cells selected for quantitation typically had 2-15 gold particles per stack. The images were analysed using the iTEM image analysis platform (Olympus). The polarity of the stacks was assigned based on compositional and morphological criteria. The former was based on immunogold staining with anti-GM130 antibodies, a *cis*-Golgi marker. The morphological criteria were based on the presence of clathrin buds or vesicles at the TGN side of the Golgi apparatus, and of typical fenestrated cisternae (*cis*-Golgi). The clathrin buds/ vesicles localised at the TGN at variable distances from the stack (from very close, to up to 500 nm from the last *trans*-cisterna). Only those stacks where the association of clathrin buds to the *trans* side was unambiguous were considered for quantification. The two criteria (morphological and compositional) were always in agreement. Several Golgi structures were evaluated. The number of cisternae varied from three to five. For quantification, we classified these as *cis*, medial, or *trans*. *Cis* indicated the *cis*-most cisterna in the case of a stack with three or four cisternae, and the two *cis*-most cisternae in the case of a stack with five cisternae (here, the linear density was the mean of the two). Trans was the last (trans) cisterna. Medial was the remaining one or two central cisternae. Vesicles were round profiles of 50 nm to 80 nm in diameter, present within 200 nm of the rims of the stack. Tubules were elongated profiles with length/width ratios greater than two. Of note, the analysis of thin sections precludes the discrimination of dissociated carriers and inter-cisternal tubular connections, and so quantification of tubules includes both of these. The cisternal rims were the most peripheral 100 nm of the cisternal profiles, and the rest of the cisterna was considered as the central cisternal part. All images were evaluated by three independent observers in a blind fashion. For surface density calculations, the number of gold particles associated with a structure was counted, and the membrane length was measured using the iTEM software. The linear density was then expressed as linear density (number of gold particles/μm).

When gold particles localised close to more than one structure, they were assigned to the closest structure. The number of Golgi stacks evaluated is specified in the legends.

3.16 Electron microscopy tomography

For EM tomography, the sample preparation and tomographic reconstruction were carried out essentially as described previously (Trucco, Polishchuk et al. 2004). In brief, HeLa cells were fixed with 2% gluteraldehyde for 2 h at room temperature, and the samples were then processed, stained, dehydrated, and Epon embedded. The samples were sectioned (200-nm sections), and gold particles were placed on the surfaces of the plastic sections and examined by EM (Tecnai-12; FEI). The Golgi profiles with well-preserved structures were identified and the images were acquired at tilt angles of +65° to -65° at 1° intervals, with a magnification of 26,500 using a Veletta CCD digital camera. The tomographic reconstruction was carried out using the Inspect 3D (FEI).

Table 3.1 List of antibodies used in the present study.

Antibody	Dilution	Type	Source
Anti-TGN46	1:800 (IF)	Sheep	AbD Serotec
Anti-GM130	1:1000 (IF) ; 1:50 (EM)	Mouse	BD
Anti-HA	1:1000 (IF) ; 1:300 (EM)	Mouse	Covance
Anti-β-COP	1:20 (EM)	Rabbit	Thermo Fisher Scientific
Anti-GALT	1:400 (IF)	Rabbit	Sigma-Aldrich
Anti-hMANI	1:100 (IF)	Rabbit	Sigma-Aldrich
Anti-VSVG	1:8000 (WB)	Rabbit	Bethyl Laboratories, Inc.
Alexa Fluor 488	1:400 (IF)	Donkey	Invitrogen
Alexa Fluor 568	1:400 (IF)	Donkey	Invitrogen
Alexa Fluor 633	1:400 (IF)	Donkey	Invitrogen
Dylight 405	1:100 (IF)	Donkey	Jackson Laboratories
Anti-GFP	1:400 (IF); 1:1000 (WB)	Rabbit	Abcam
Anti-GAPDH	1:10000 (WB)	Mouse	Santa Cruz Biotechnology
Anti-TNG38	1:500 (IF)	Rat	AbD Serotec

IF, immunofluorescence; EM, electron microscopy; WB, Western blotting.

CHAPTER 4.

Results

4.1 Engineering and characterisation of Golgi resident enzymes: localisation and reversible polymerisation properties

4.1.1 Engineering of the Golgi resident enzymes

The experimental approach that I used to reversibly manipulate the polymerisation state of the Golgi resident enzymes is based on the well-standardised system of a regulated secretion/aggregation kit from Ariad Pharmaceuticals (original reference Rivera, Wang et al. 2000; www.ariad.com).

Briefly, this uses a mutant FK506 binding protein (FKBP-Phe36Met) that is known as 'FM' that spontaneously dimerises. The dimer can be dissociated by using AP12998, which binds to the FK506 binding domain. Depending on the number of FM domains in the protein, the size of the polymer that is formed can be regulated.

To engineer a polymerisable Golgi resident enzyme, I fused the Golgi targeting portions (i.e., cytosolic tail, transmembrane domain, stem region) of mouse 1,2-MANI-B (Becker, Haggarty et al. 2000), which is a *cis*/medial-Golgi enzyme (Dunphy and Rothman 1983; Marra, Maffucci et al. 2001), with three tandem FM domains and with an HA tag for detection (MANI-FM; **Fig. 4.1.1a**). In addition, I prepared a similar construct using the targeting portions of the trans-Golgi enzyme GALT (GALT-FM; Cole, Smith et al. 1996). Once polymerised, those constructs can generate large two-dimensional submembrane networks (**Fig. 4.1.1b**).

MANI-FM was then expressed in HeLa cells, which were pulsed with radiolabelled ([^{35}S]) cysteine and methionine to confirm the expression of the protein, which appears to be at a level of two- to three-fold higher than that of the endogenous human α-1,2 Mannosidase IB (hMANI) (**Fig. 4.1.1c, d**).

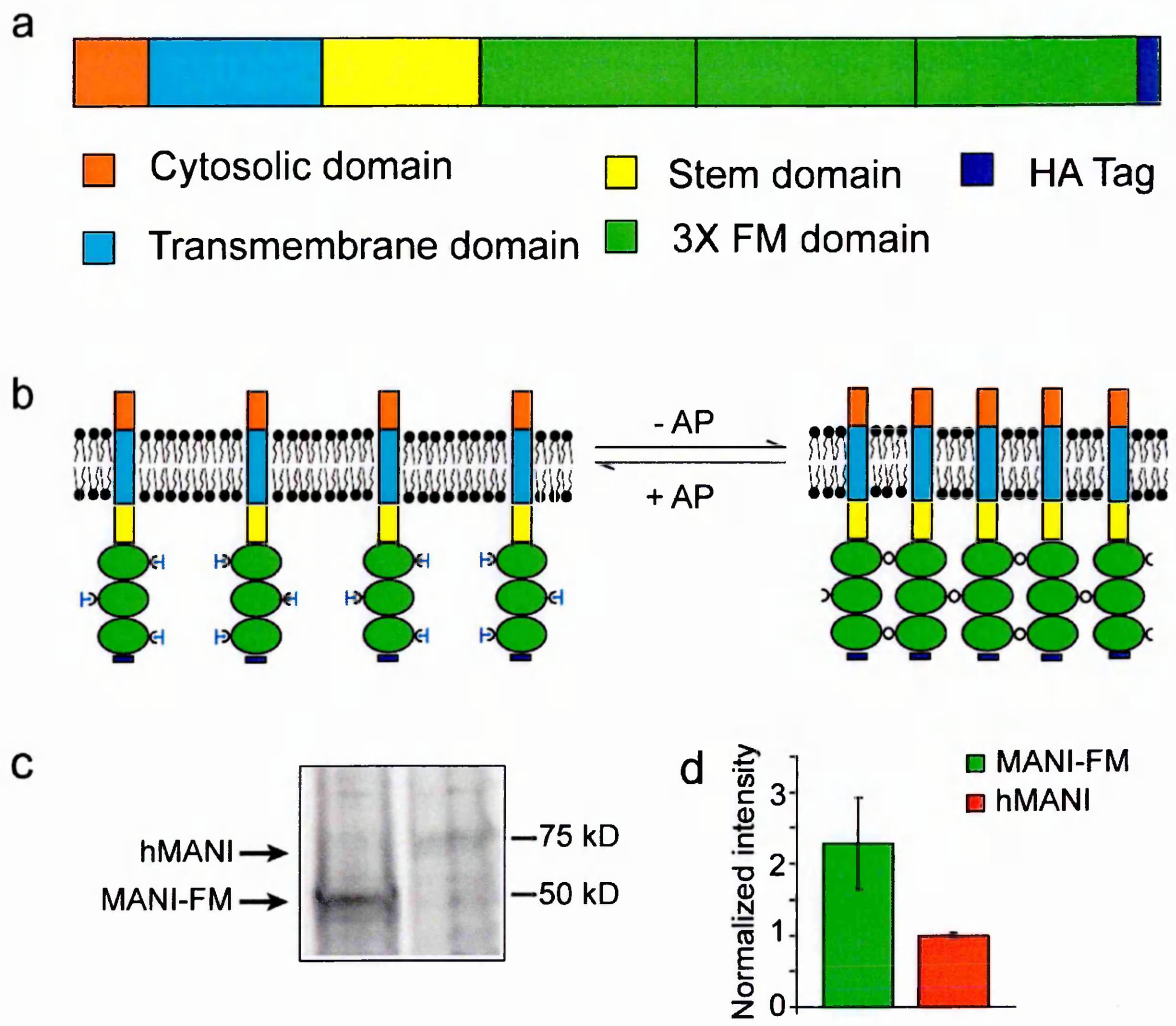

Figure 4.1.1 Domain composition of MANI-FM.

Three FM domains followed by an HA tag were fused to the C-terminal end of the Golgi-targeting portion (i.e. cytosolic, transmembrane, luminal stem domains) of mouse MANI. (**b**) Scheme of MANI-FM polymerisation and depolymerisation in the absence and presence, respectively, of AP12998. (**c**) To quantify the amount of MANI-FM present in the transfected cells relative to the endogenous enzyme (hMANI), transfected HeLa cells were pulsed with radiolabelled ([^{35}S]) cysteine and methionine for 24 h, and the endogenous and transfected proteins were immunoprecipitated (see Methods, Section **3.5**) and examined by autoradiography. Under the immunoprecipitation conditions, most of the target proteins were immunoprecipitated. (**d**) Quantitation of the levels of MANI-FM relative to that of the endogenous enzyme (hMANI).

4.1.2 Controlled aggregation/disaggregation state of MANI-FM

To study the polymerisation/depolymerisation kinetics of MANI-FM, I carried out a sedimentation assay on the basis that in the absence of AP12998, after detergent solubilisation of cells and low speed centrifugation, MANI-FM should be largely recovered in the insoluble pellet fraction, because its dimensions are bigger than its monomeric status. On the other hand, if the cells are incubated in the presence of AP12998, MANI-FM should move into the soluble detergent supernatant (Volchuk, Amherdt et al. 2000).

As expected, in the monomeric state (+AP12998), MANI-FM was in the supernatant whereas after AP12998 wash-out it shifted to the pellet, reflecting the formation of the large MANI-FM polymers (**Fig. 4.1.2a**). This shift started 5 min after AP12998 wash-out, and it was complete within 15 min. Sucrose gradient centrifugation confirmed that MANI-FM shifts from a monomeric to a polymeric state within 15 min of AP12998 removal (**Fig. 4.1.2c**). I then added AP12998 to polymeric MANI-FM (see **Fig. 4.1.2a**) to induce depolymerisation: MANI-FM shifted back to the supernatant rapidly (**Fig. 4.1.2b**).

Thus, MANI-FM polymerises upon AP12998 removal in ~10-12 min, and it depolymerises with AP12998 addition in <5 min.

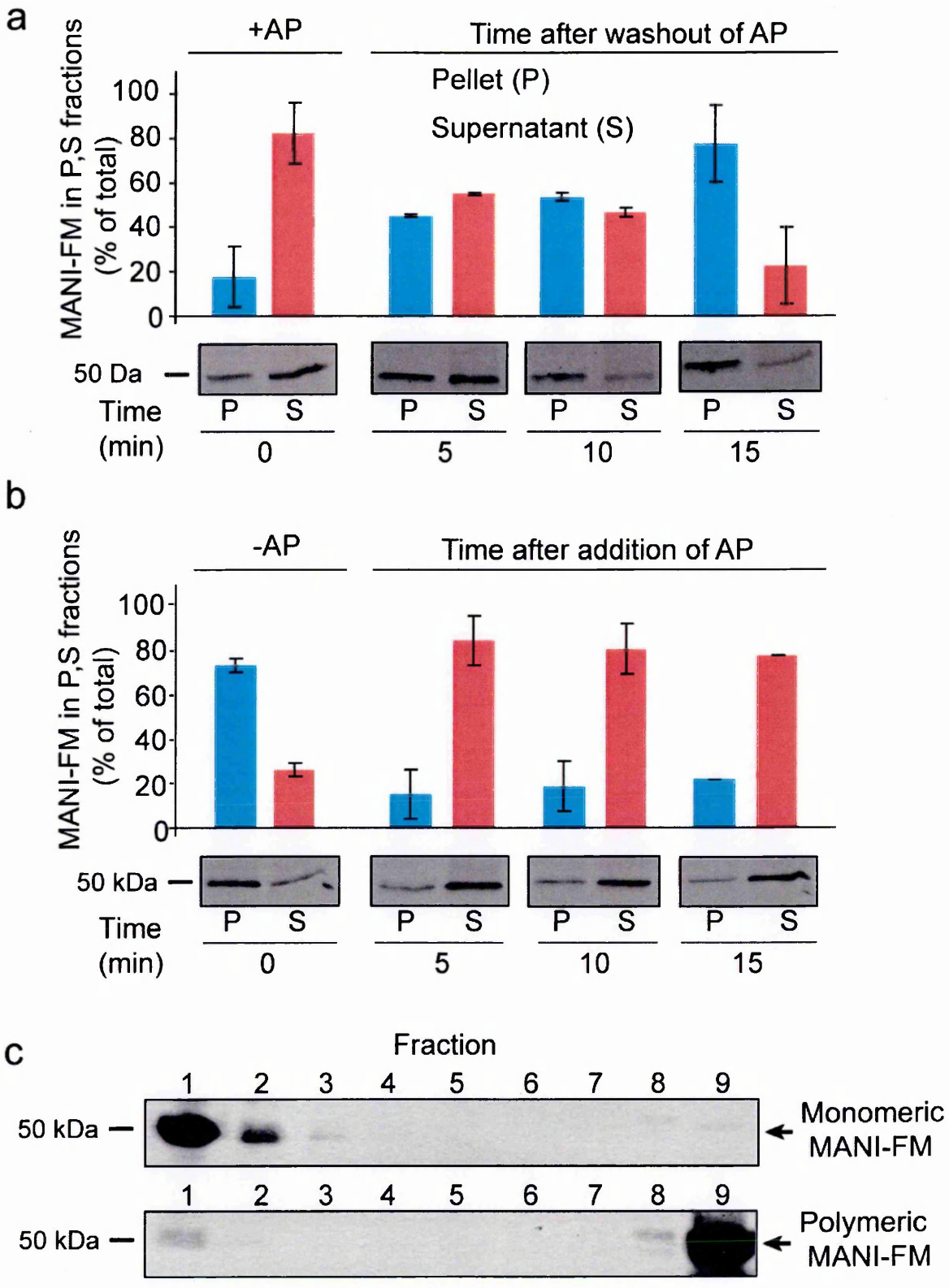

Figure 4.1.2 Reversible polymerisation of MANI-FM.

MANI-FM polymerisation as revealed using a sedimentation assay. (**a**) HeLa cells expressing MANI-FM were cultured in the presence of 1 μM AP12998 (+AP), and then

the AP12998 was washed out for the indicated times before cell lysis and low-speed centrifugation to separate the pellet and supernatant fractions. The MANI-FM in these fractions was then quantified by gel electrophoresis and Western blotting. MANI-FM shifts from the supernatant (S) to the pellet (P) in <15 min. (**b**) MANI-FM depolymerisation. HeLa cells expressing MANI-FM had the AP12998 washed out over 15 min (-AP; see panel **a**) and then 1 μM AP12998 was added again to the cells for the indicated times. MANI-FM shifts back to the supernatant in <5 min. (a, b) Data are means ±SEM, from three independent experiments. (**c**) Sucrose gradient centrifugation confirms that MANI-FM moves to the pellet after 15 min of AP12998 removal. The experiment was performed as in **a**, but after cell lysis the samples were processed for high-speed centrifugation in a sucrose gradient (20%-50% sucrose). Then, the different fractions were collected and precipitated with trichloroacetic acid. The proteins were analysed by SDS-PAGE and immunoblotting.

4.1.3 MANI-FM localises mainly to the Golgi apparatus, like the full-length protein

The MANI-FM construct contains only the targeting motifs of the mouse α-1,2 Mannosidase 1B (see **Fig. 4.1.1a**) without the catalytic domain. To determine whether the MANI-FM is targeted/retained in the Golgi like the full-length protein, I compared the efficiency of targeting/retention of MANI-FM with that of the full-length protein (mouse-α-1,2-Mannosidase IB fused to GFP; $MANI_{FL}$-GFP).

In cells expressing low-to-medium levels of MANI-FM and $MANI_{FL}$-GFP, these proteins localised only at the Golgi apparatus, whereas in highly expressing cells (~20% of the cell population), these two constructs were at both the Golgi and the PM (see **Fig. 4.1.3a-d**). Thus, the Golgi targeting and retention properties of MANI-FM do not appear to differ considerably from those of the transfected full-length $MANI_{FL}$-GFP. Similar observations have been reported for other Golgi enzymes (Berger 2002). In the localisation experiments described below, I included only cells expressing low-to-medium levels of MANI-FM.

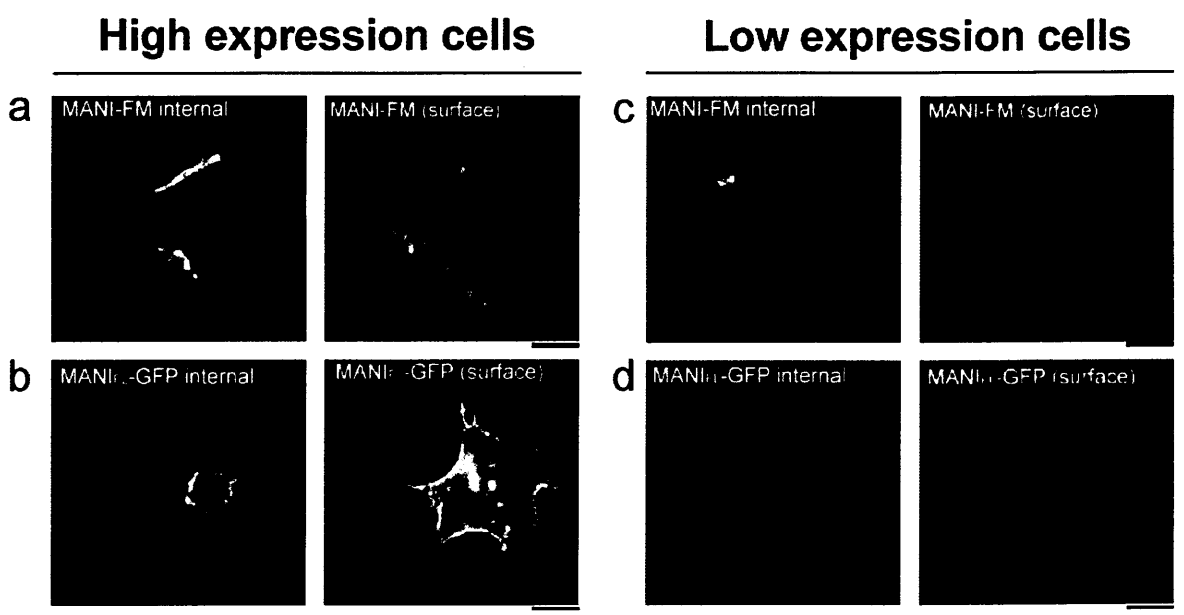

Figure 4.1.3 Monomeric MANI-FM is mainly retained in the Golgi apparatus

HeLa cells expressing high or low levels of MANI-FM (+AP12998; **a** and **c**) or $MANI_{FL}$-GFP (**b** and **d**) were fixed and labelled for surface-localised MANI-FM and $MANI_{FL}$-GFP using an anti-HA monoclonal antibody and anti-GFP antibodies, respectively, without permeabilisation (red). Later, the cells were permeabilised and labelled for the proteins present internally (green; anti-HA polyclonal antibody for MANI-FM; $MANI_{FL}$-GFP was not labelled). In cells expressing high levels of MANI-FM and $MANI_{FL}$-GFP, both are present at the PM. Bars: (**a**) 18 μm; (**b**) 16 μm; (**c** and **d**) 20 μm.

4.1.4 Characterisation of reversibly polymerisable Golgi resident enzymes

To define suitable conditions to examine the intra-Golgi localisation of MANI-FM in its monomeric or polymeric states (+AP12998), I first used nocodazole, which fragments the Golgi apparatus into separate but structurally and functionally "normal" stacks (ministacks; Cole, Sciaky et al. 1996; Trucco, Polishchuk et al. 2004). The advantages of the ministacks are that: (a) they provide good resolution between the *cis*-Golgi and *trans*-Golgi by immunofluorescence (Shima, Haldar et al. 1997); **Fig. 4.1.4.1a-d**); (b) they lack interstack tubular zones, which facilitates the analysis of peri-Golgi vesicles/tubules under EM (Trucco, Polishchuk et al. 2004); and (c) they are physically isolated from other stacks, which rules out the possibility of exchange of cargo through contacts with adjacent stacks, like in the Golgi ribbon (Trucco, Polishchuk et al. 2004; Pfeffer 2010). Secondly, I emptied the ER of MANI-FM by cycloheximide treatment for 30 min before starting the observations, to ensure that all of the MANI-FM that I examined was localised in the Golgi apparatus (see Materials and methods; Section **3.8**).

Using these conditions (see **Fig. 4.1.3**), I assessed the distribution of monomeric MANI-FM (+AP12998) in the Golgi cisternae and in peri-Golgi vesicles and tubules (as defined in Materials and methods; Section **3.15**) using immuno-EM and stereology. MANI-FM showed higher linear density in the *cis*- > medial > *trans*-cisternae, similar to the localisation reported for the endogenous MANI enzyme (Dunphy and Rothman 1983; Marra, Maffucci et al. 2001; **Fig. 4.1.4.1e**, **h**; and see also **Fig. 4.4.1.2a**). Moreover, MANI-FM was more concentrated at the rims than in the central parts of the cisternae (**Fig. 4.1.4.1f**, **g**, **i**), it was present in vesicles and tubules at concentrations 50% and 96%, respectively, of that found in the cisternae (tubules here included both dissociated carriers and inter-cisternal tubular connections; see Materials and methods, Section **3.15**; **Fig. 4.1.4.1j**), and it was practically absent from the ER and in regions outside of the Golgi stack area, including the PM.

By confocal microscopy, MANI-FM (again in cells expressing low-to-medium levels of the construct) localised between the CGN and the TGN (stained with the CGN and TGN markers GM130 and TGN46, respectively), in qualitative agreement with the EM data (**Fig. 4.1.4.1k, l**). This MANI-FM localisation was similar to that of full-length MANI, and it was also similar to that seen in the intact Golgi apparatus of NRK cells, where the *cis*-Golgi and *trans*-Golgi can be easily distinguished, even without nocodazole-mediated dissociation (**Fig. 4.1.4.2a-c**).

I also examined the localisation of the GALT-FM construct. As monomers, GALT-FM localised in the *trans*- >> medial > *cis*-cisternae, as visualised by EM (**Fig. 4.1.4.2d**). Again, this represented a distribution that was similar to that of the corresponding endogenous enzyme (Teasdale, D'Agostaro et al. 1992).

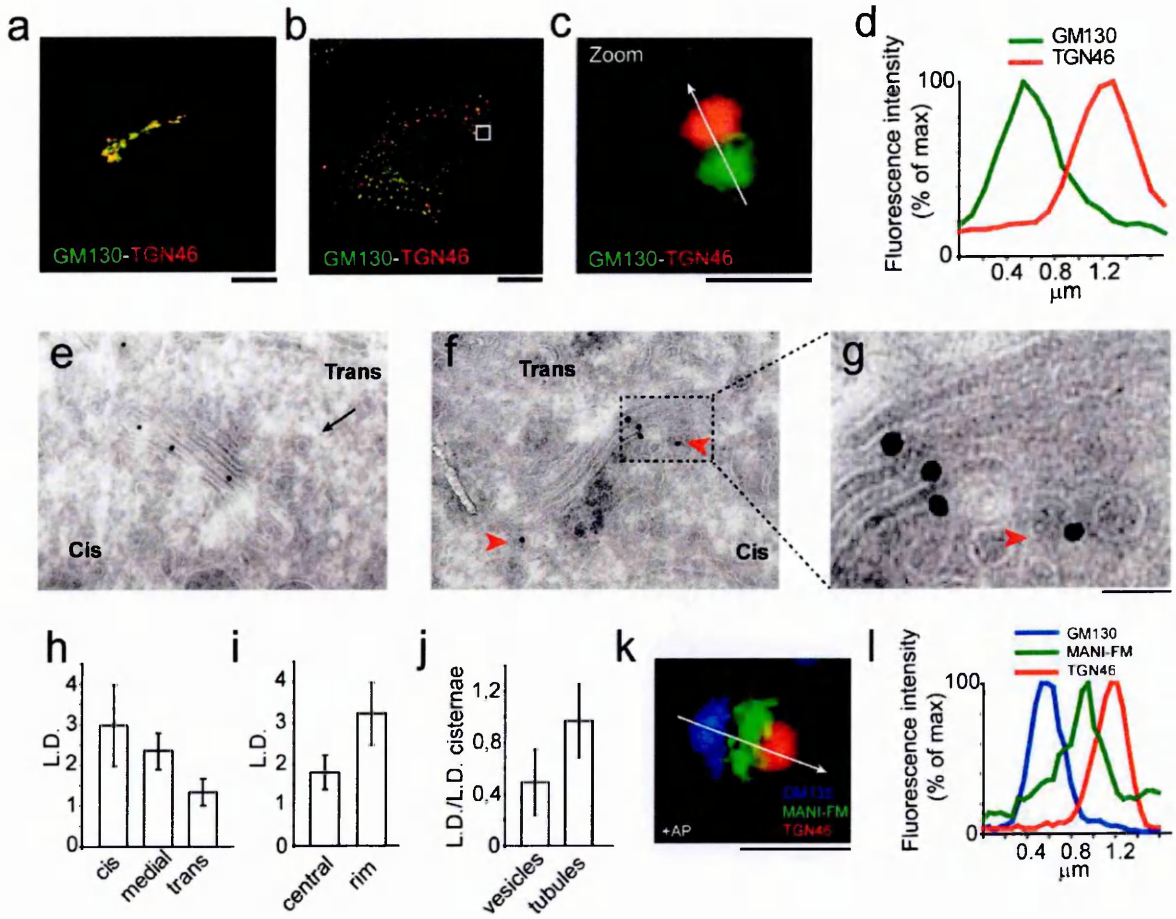

Figure 4.1.4.1 MANI-FM localises to a *cis*/medial position in the Golgi stack.

(**a**) Untreated HeLa cells show the typical ribbon-like structure of the Golgi apparatus. GM130 staining (green) and TGN46 (red) are shown. (**b**) Nocodazole treatment (33 µM for 3 h) fragments the intact Golgi ribbon into hundreds of ministacks spread throughout the cell. GM130 staining (green) and TGN46 (red) are shown. (**c**) Ministacks resulting from nocodazole treatment maintain their polarity, as seen by the clear separation of GM130 (green) and TGN46 (red). A magnified image of a single isolated stack from (**b**). The white arrow across the stack was used for the line-scan analyses. (**d**) Fluorescence intensity distribution of markers along the line scan (**c**, arrow). The fluorescence intensities were normalised to their respective peak values. The image shown is representative of more than three independent experiments, and for the data shown, n = 10. Bars: (**a, b**) 15 µm; (**c**) 1 µm. (**e-g**) HeLa cells expressing MANI-FM were cultured in the presence of

AP12998, and then fixed and processed for cryoimmuno-labelling with an anti-HA antibody (10-nm gold particles). (**e**) Localisation of MANI-FM in the *cis*-/medial cisternae, with a clathrin bud (arrow) marking the *trans* side. (**f**) An example of the preferential rim distribution of MANI-FM. (**g**) An enlargement of **f**, with MANI-FM in a peri-Golgi carrier (arrowhead). (**h-j**) Quantification of the distribution of MANI-FM across the Golgi stacks (**h**), in the central *versus* the rim sections of the cisternae (**i**), and in peri-Golgi vesicles and tubules (**j**). Data are means ±SEM, obtained from the analysis of 28 stack profiles. (**k**) Localisation of MANI-FM in a Golgi stack under confocal microscopy. MANI-FM (green) localises between GM130 (blue) and TGN46 (red). The white arrow across the stack was used for the line-scan analyses. The image is representative of >30 stacks analysed. (**l**) Fluorescence intensity distribution of markers along the line scan (arrow in **k**). The fluorescence intensities were normalised to their respective peak values. The image and the corresponding quantitation are representative of at least 30 Golgi ministacks from three independent experiments. For these data (**e-l**), $n = 30$. Bars: (**e**) 270 nm; (**f**) 240 nm; (**g**) 60 nm; (**k**) 1 μm.

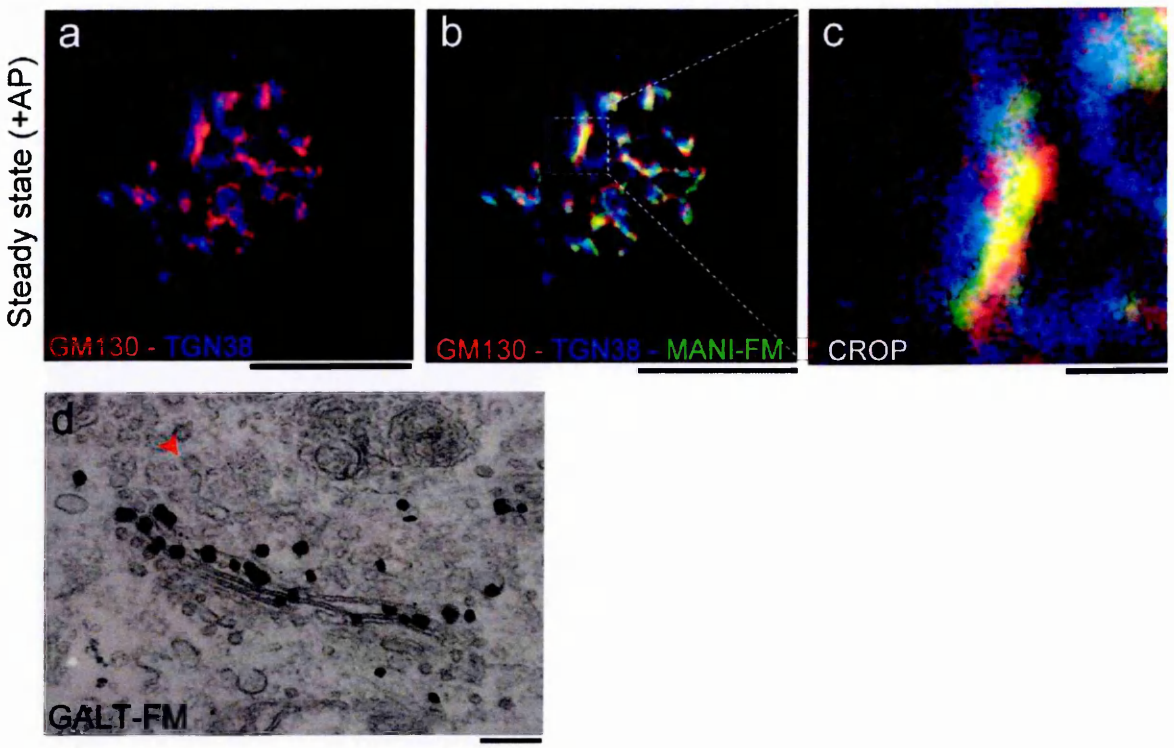

Figure 4.1.4.2 The FM fusion proteins show appropriate sub-Golgi localisations.

(**a-c**) Localisation of MANI-FM in an intact Golgi ribbon of NRK cells. NRK cells expressing MANI-FM were cultured in the presence of AP12998, fixed and stained for MANI-FM (green), GM130 (red), and TGN38 (blue). The enlargement in **c** (CROP) shows the co-localisation of MANI-FM with a *cis*-Golgi marker. The image is representative of >30 Golgi ribbon analysed. (**d**) HeLa cells transfected with GALT-FM in the presence of AP12998 were fixed and stained for GALT-FM (anti-HA) using immunonanogold. The *trans* side of the stack was identified by clathrin-coated structures (arrowhead). The labelling is mainly present in the *trans*-most cisterna of the stack. Bars: (**a**, **b**) 20 μm, (**c**) 3 μm (**d**) 150 nm.

4.2 Examination of the entry of the engineered Golgi resident enzymes into vesicular/tubular carriers under aggregation/disaggregation conditions

4.2.1 Polymerisation prevents entry of Golgi MANI-FM into peri-Golgi carriers

Based on the strategy that I decided to use to study the mechanisms of intra Golgi transport, an important aspect that needs to be explored is the possible entry of the MANI-FM polymer into Golgi vesicles/tubules. For this reason, I polymerised MANI-FM by removing AP12998 for 15 min, and examined by EM the entry of the polymer into Golgi dissociative carriers. When polymerised, the concentration (as linear density) of MANI-FM in vesicles and tubules dropped by ~90%, to barely detectable levels (**Fig. 4.2.1.1a, b**). Moreover, MANI-FM lost its concentration at the rims of the Golgi cisternae and was distributed randomly along the cisternal length (**Fig. 4.2.1.1c** and see also **Fig. 4.6.1c**). The Golgi morphology and the number of peri-Golgi vesicles and tubules did not change, except for a reduction in the surface area of the tubules (25%) (**Fig. 4.2.1.1d**). I also examined the entry of polymerised MANI-FM into Golgi tubules induced by the toxin brefeldin A (BFA; Lippincott-Schwartz, Donaldson et al. 1990). These tubules have a diameter of 40 nm to 80 nm (Lippincott-Schwartz, Donaldson et al. 1990), which is similar to that of Golgi carriers, and they contain Golgi-resident proteins (Lippincott-Schwartz, Donaldson et al. 1990). An 8-min treatment with BFA (6 μg/ml) induced the formation of numerous Golgi tubules that contained a *cis*-Golgi marker, the KDEL receptor (**Fig. 4.2.1.1e, f**). Polymeric MANI-FM did not enter these tubules, whereas MANI-FM monomers entered the tubules freely (**Fig. 4.2.1.1e, f**). Polymeric MANI-FM also reduced the number of BFA-induced tubules by 30% to 40%. However, this reduction did not prevent the redistribution of the Golgi resident enzymes, including MANI-FM into the ER after 30-min exposure to BFA (**Fig. 4.2.1.2a-d**). This is probably because of the peculiar mode of BFA-induced retrograde transport. As live-imaging experiments have shown

(Sciaky, Presley et al. 1997), the addition of BFA leads to the formation of numerous tubules that contain the Golgi residents. When these tubules fuse with the ER, they cause a sudden collapse of the Golgi into the ER in seconds ("blink out"), which is possibly caused by tension-driven membrane flow (Sciaky, Presley et al. 1997). This complete collapse can presumably bring back to the ER even those proteins that do not actually enter the tubules.

I also examined whether polymeric MANI-FM and GALT-FM can enter vesicular/ tubular carriers derived from the ER (Bannykh and Balch 1997; Antonny and Schekman 2001). Both MANI-FM and GALT-FM were retained in the ER when expressed in the absence of AP12998, whereas after depolymerisation (+AP) they left the ER and rapidly reached the Golgi complex (**Fig. 4.2.1.2e-h**).

In summary, polymerisation prevents MANI-FM from entering Golgi vesicles and tubules, including BFA-induced tubules and ER-derived vesicular/tubular carriers. This effect of polymerisation might be because: (a) the polymers are too large to enter the vesicles/tubules; (b) the polymers form a rigid platform that is incompatible with the curvature of the vesicles/tubules (Copic, Latham et al. 2012; or (c) the polymerisation hides the sorting signals that allow MANI-FM to enter into vesicles/tubules. The lack of entry of polymers into long BFA tubules and the concentration of polymers in the flat areas of the cisternae over the rims favour the second of these three possibilities (i.e., (b)).

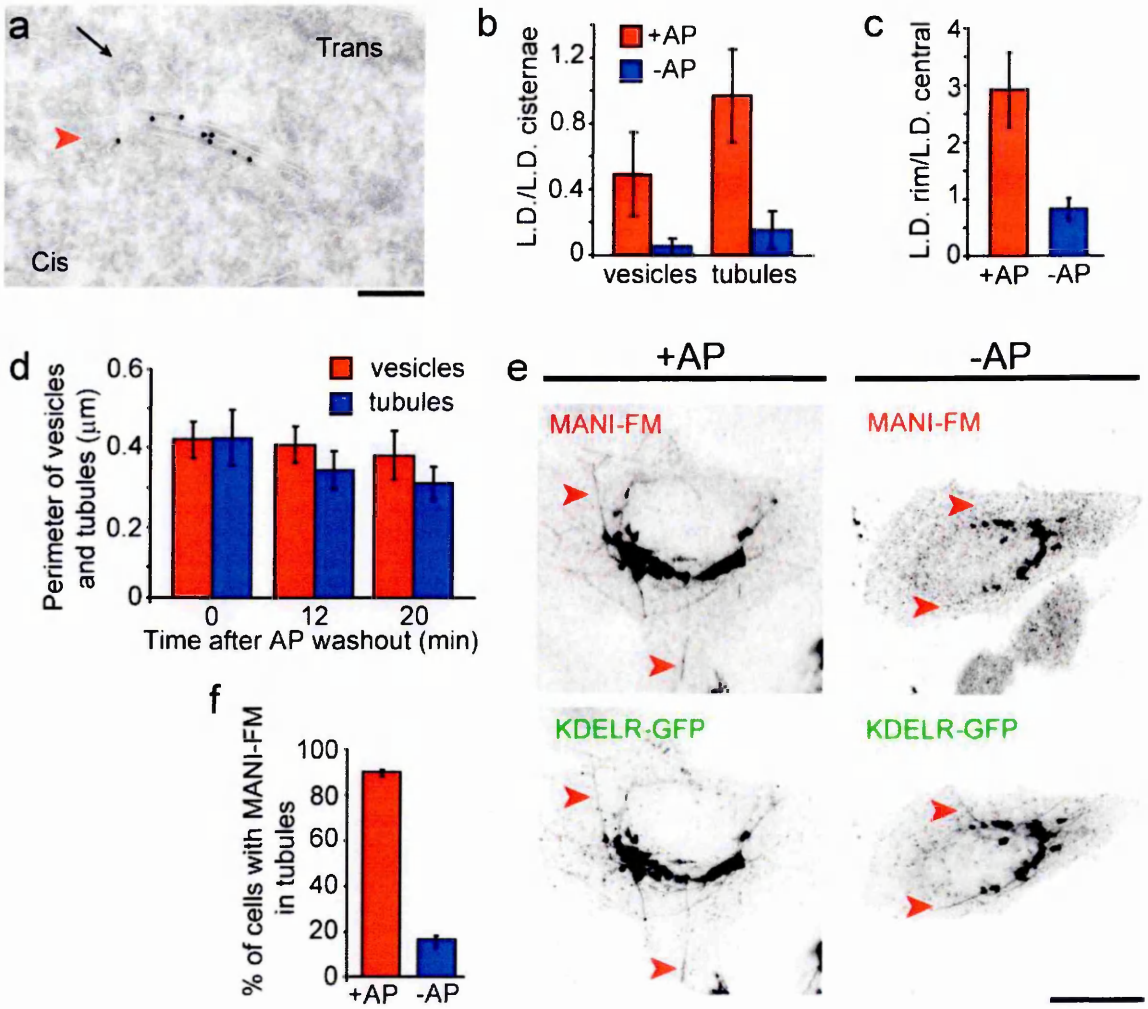

Figure 4.2.1.1 Polymerisation prevents MANI-FM entry into vesicles and tubules.

HeLa cells were transfected with MANI-FM in the presence of AP12998, and then AP12998 was removed for 15 min to induce polymerisation. (**a**) Polymeric MANI-FM (-AP for 15 min) is nearly absent in Golgi vesicles (arrowhead) and tubules. The *trans* side of the stack was identified by clathrin-coated buds (arrow). (**b**) Quantification of MANI-FM in vesicles and tubules. Polymeric MANI-FM (-AP) is strongly depleted in vesicles and tubules compared with the monomer (+AP). (**c**) MANI-FM distribution along the cisternal length, expressed as the ratio between the linear density (LD) in the rims *versus* the central part of the cisternae. MANI-FM shifts to a more central localisation after polymerisation. More than 20 stack profiles were analysed for each condition. (**d**) The membrane length of vesicles and tubules as a measure of the surface area, quantified and

expressed as the perimeter, was not appreciably changed after polymerisation of MANI-FM. The total surface area of the tubules decreased by ~25% after polymerisation of MANI-FM. (**e**) HeLa cells transfected with MANI-FM and KDEL receptor-GFP (KDELR-GFP) in the presence or absence of AP12998 (for 10 min) were treated with 6 μg/ml BFA for 8 min to induce tubules emanating from the Golgi apparatus, and then fixed and stained for MANI-FM. MANI-FM enters BFA-induced tubules in the presence of AP12998 (monomers), but not in the absence of AP12998 (polymers). (**f**) The number of BFA-induced tubules positive for MANI-FM was quantified. At least 10 cells per condition per experiment were analysed, and the data are from three independent experiments. Data are means ±SEM. Bars: (**a**) 250 nm; (**e**, +AP) 15 μm; (**e**, +AP) 18 μm.

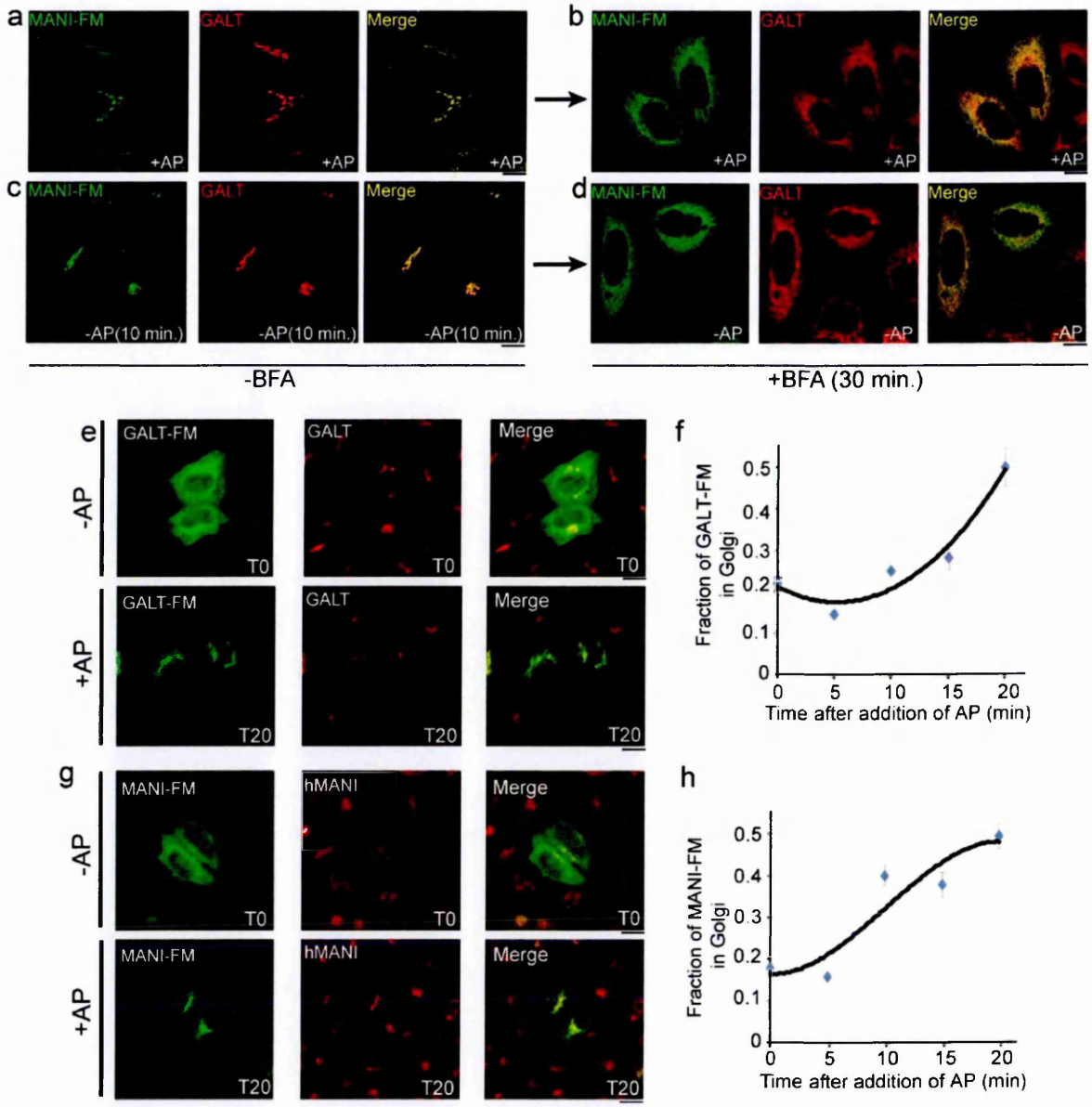

Figure 4.2.1.2 Polymerisation of FM fusion proteins does not prevent their BFA-induced retrograde transport to the ER, but prevents their exit out of the ER.

HeLa cells expressing MANI-FM cultured in the continued presence of AP12998 (**a, b**) or in the absence of AP12998 for 10 min (**c, d**) were incubated with BFA for 30 min (**b, d**) in the presence or absence of AP12998, respectively, and the localisation of the transfected proteins visualised by immunofluorescence. BFA treatment induces ER translocation of both monomeric and polymeric MANI-FM. (**e-h**) Polymerisation of FM fusion proteins prevents their exit out of the ER. (**e**) GALT-FM is retained in the ER in the absence of AP12998 (-AP) and is rapidly transported to the Golgi apparatus after addition of AP12998

(+AP). (**f**) Time kinetics of GALT-FM transport to the Golgi apparatus after addition of AP12998. The curve fitting was done using a third-order polynomial function. (**g**) Similar to (e), MANI-FM transport was monitored. (**h**) Similar to (f), time kinetics of MANI-FM transport to the Golgi apparatus. Antibodies against endogenous GALT (**e**) and MANI (**g**) were used to identify the Golgi apparatus. About 20-30 cells were analysed per time point. Values are means ±SEM. Bars: (**a-d**) 16 μm; (**e, g**) 18 μm.

4.3 Golgi function under polymerisation conditions of the Golgi resident enzymes

4.3.1 Polymerisation of MANI-FM does not affect the function of the Golgi apparatus

After confirming the reversible polymerisation of Golgi resident MANI-FM, I decided to determine whether MANI-FM polymerisation affects either the transport and glycosylation properties of the Golgi.

As a tool to study transport along the secretory pathway (ER-to-Golgi and Golgi-to-PM transport), I used the G-protein of the temperature-sensitive vesicular stomatitis virus (ts-045VSV) (see Methods; Section **3.11**). This version of VSVG is a temperature-sensitive mutant that accumulates in the ER at 39.5 °C due to incorrect folding (Rose and Bergmann 1983; Schnitzer, Dickson et al. 1979), but moves to the PM at the permissive temperature of 32 °C, providing a synchronised wave of movement of cargo along the secretory pathway.

Initially, to study the transport of VSVG into and out of the Golgi apparatus, HeLa cells were co-transfected with VSVG-GFP and MANI-FM, and incubated overnight at 40°C in the presence of AP12998, which resulted in the accumulation of VSVG-GFP in the ER and MANI-FM in the Golgi apparatus. Twenty-four h after transfection, the AP12998 was washed out in a subset of samples kept at 40°C, to induce the polymerisation of MANI-FM while retaining VSVG in the ER. The rest of the experiment was carried out in the absence of AP12998 for this subset, while the rest of the samples were maintained in the presence of AP12998. The rest of the cells were then either shifted to 32°C for the indicated time to study the ER-to-Golgi transport of VSVG (**Fig. 4.3.1.1**), or shifted from 40°C to 32°C for 20 min to accumulate VSVG-GFP in the Golgi apparatus, and then

shifted back to 40°C for the indicated times to monitor the transport of VSVG-GFP out of the Golgi (**Fig. 4.3.1.2 a-c**).

The observation that the transport of VSVG-GFP from the ER to the Golgi (**Fig. 4.3.1.1**) and its transport out of the Golgi (**Fig. 4.3.1.2 a-c**) were not affected under MANI-FM polymerisation conditions implies that the intra-Golgi transport of the viral protein, VSVG, should also be normal (see Results, Section **4.5.1**).

To study the glycosylation properties of the Golgi apparatus under polymerisation conditions of MANI-FM, I monitored the acquisition of endoH resistance of the VSVG (**Fig. 4.3.1.2 d**). Under these experimental conditions, this was also not affected (**Fig. 4.3.1.2 e;** see Methods **3.11**).

These observations indicated that the transport of VSVG into (**Fig. 4.3.1.1**) and out of the Golgi apparatus (**Fig. 4.3.1.2 a-c**) as well as the glycosylation of VSVG (**Fig. 4.3.1.2 d, e**) all occurred at normal rates, suggesting that MANI-FM polymerisation does not perturb Golgi function.

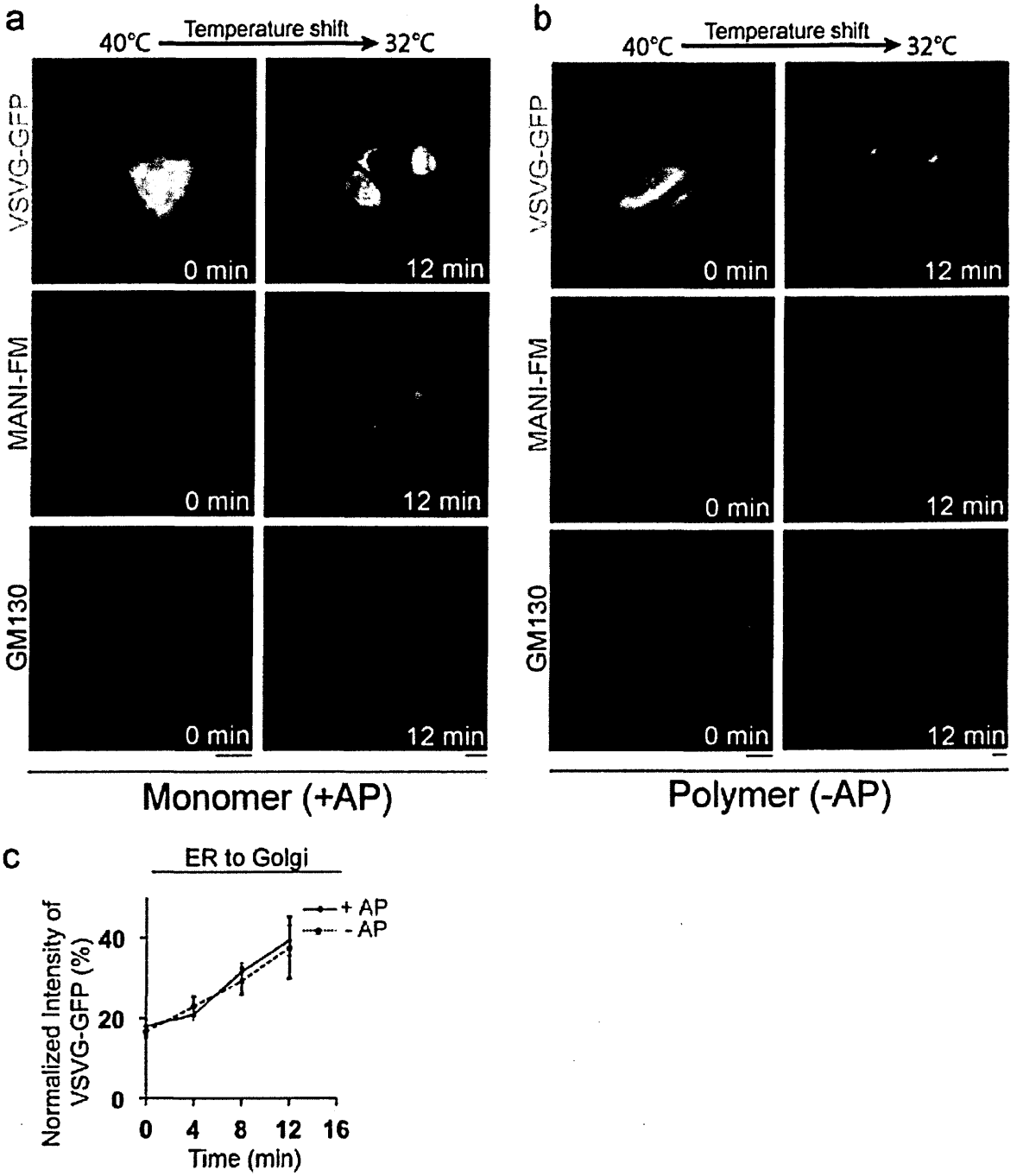

Figure 4.3.1.1 MANI-FM polymerisation does not affect the ER-to-Golgi transport of VSVG-GFP.

Transport of VSVG-GFP from the ER to the Golgi was quantified by measuring the fluorescence intensity of VSVG-GFP in the Golgi region, which was not affected by the polymeric state of MANI-FM (+AP, monomer; –AP, polymer) (**a**, **b**) HeLa cells were transfected with both MANI-FM and VSVG-GFP in the presence of AP12998, and then incubated at 40°C for 24 h. (**b**) The AP12998 was washed out at 40°C to polymerise the

MANI-FM in the Golgi apparatus and retain the VSVG-GFP in the ER, and after 10 min the cells were placed at the permissive temperature (32°C) for the indicated time to allow VSVG arrival at the Golgi. The same protocol in (**b**) was also applied in (**a**), but in presence of AP12998 for the entire duration of the experiment. (**c**) The quantification was carried out by measuring the fluorescence intensity of the VSVG-GFP at the Golgi apparatus, as normalised to its total intensity in the cell. The assay was carried out with the Golgi ribbon intact, with nocodazole not included in these experiments. At least 20 cells per time point per experiment were analysed, and the results are from three independent experiments. Data are means ±SEM. Bars: (**a, b**) 18 μm.

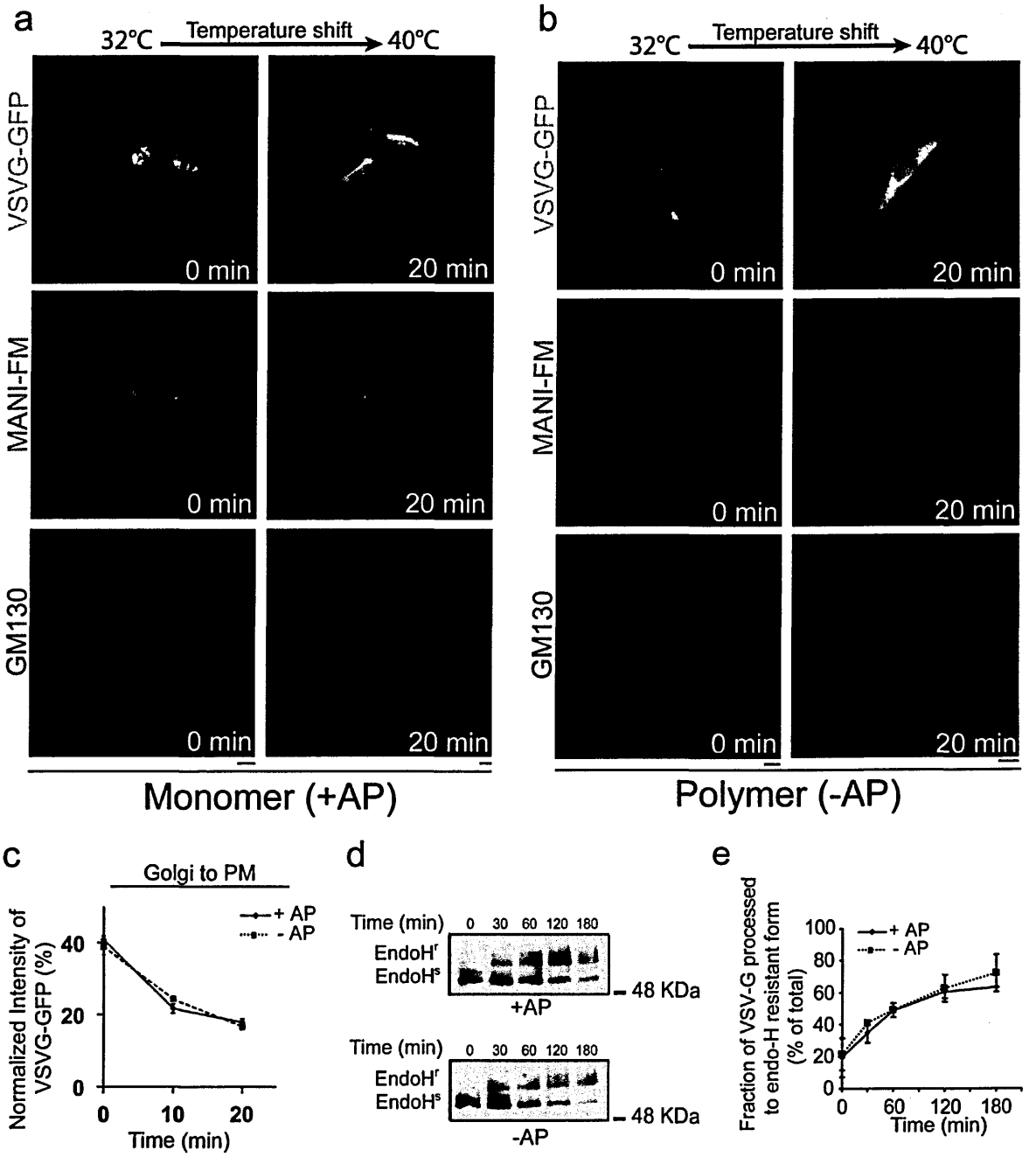

Figure 4.3.1.2 MANI-FM polymerisation does not affect the transport of VSVG-GFP out of the Golgi as well as its processing.

The transport of VSVG-GFP out of the Golgi (quantified as in Fig. 4.4.1.1) was not affected by the polymeric state of MANI-FM (+AP, monomer; –AP, polymer). (**a**, **b**) HeLa cells were transfected with both MANI-FM and VSVG-GFP in the presence of AP12998, and then incubated at 40°C for 24 h. (**b**) The AP12998 was washed out at 40°C to polymerise the MANI-FM in the Golgi apparatus and to retain the VSVG-GFP in the ER,

and after 10 min the cells were placed at the permissive temperature (32°C) for 20 min to accumulate VSVG-GFP in the Golgi (Time 0). The same protocol in (**b**) was also applied in (**a**), but in the presence of AP12998. The cells were then shifted back to 40°C in the absence (**b**) and presence (**a**) of AP12998, to prevent further entry of VSVG-GFP into the Golgi, and to monitor the exit of the VSVG-GFP that was present in the Golgi apparatus. The exit of VSVG-GFP from the Golgi was quantified by measuring the intensity of the VSVG-GFP fluorescence at the Golgi, normalised to the total VSVG-GFP fluorescence of the cell over time, as shown in (**c**). At least 20 cells per time point per experiment were analysed, and the results are from three independent experiments. Data are means ±SEM. Bars: (**a, b**) 18 μm. (**d**) VSVG glycosylation as measured by acquisition of resistance to endoH ($EndoH^r$, endoH resistant; $EndoH^s$, endoH sensitive) was not affected by the polymeric state of MANI-FM (+AP, monomer; –AP, polymer). The assays were carried out using intact Golgi ribbon in the absence of nocodazole. (**e**) Quantification of the acquisition of endoH resistance represented as the fraction of VSVG that was resistant to digestion by endoglycosidase H. Data are means ±SEM, from three different experiments.

4.4 Fate of a *cis*-Golgi resident after its polymerisation in the Golgi

4.4.1 Polymerisation causes MANI-FM to move forward in the Golgi stack

Finally, I sought to determine whether upon shifting from a monomeric to polymeric state, MANI-FM remains in its *cis* position, as would be predicted by the stable cisternae models, or if it moves from the *cis*- to *trans*-cisternae, as would be predicted by cisternal maturation.

After AP12998 removal (0 min), the MANI-FM peak shifted from the *cis*- to the medial cisternae (at 12 min), and then to the *trans*-cisterna (at 20 min; **Fig. 4.4.1.1a-e**; and see also **Fig. 4.4.1.2**). Considering that polymerisation lags behind by 10 min to 12 min after AP12998 washout (**Fig. 4.1.2a**), the intra-Golgi transport rate of polymeric MANI-FM was similar to that reported for procollagen and VSVG (Mironov, Beznoussenko et al. 2001), both of which have been proposed to move by cisternal maturation.

A difficulty in the interpretation of these data (**Fig. 4.4.1.1d**) is that according to the cisternal-maturation model, 12 min after AP12998 removal (MANI-FM polymerisation), the *cis*-cisterna should be empty of MANI-FM, yet it appears to still contain measurable levels of this construct. This apparent discrepancy is most likely because the polymerisation of MANI-FM is not instantaneous, but rather takes several minutes to reach completion after AP12998 removal (**Fig. 4.1.2a**). Hence, during this time interval, the residual monomeric MANI-FM fraction can recycle backwards into the *cis*-cisterna. By light microscopy, the MANI-FM peak shifted away from GM130 (*cis*) and towards TGN46 (*trans*) within 20 min of AP12998 removal, in agreement with the EM data (**Fig. 4.4.1.3a-d**; and see also **Fig. 4.4.1.4**). Later, MANI-FM moved from the Golgi apparatus to assume a diffuse/punctuate distribution (**Fig. 4.4.1.5b**) and began to be degraded, presumably in the lysosomes (**Fig. 4.4.1.5c**), whereas monomeric MANI-FM was as stable as the endogenous MANI enzyme (**Fig. 4.4.1.5d, e**).

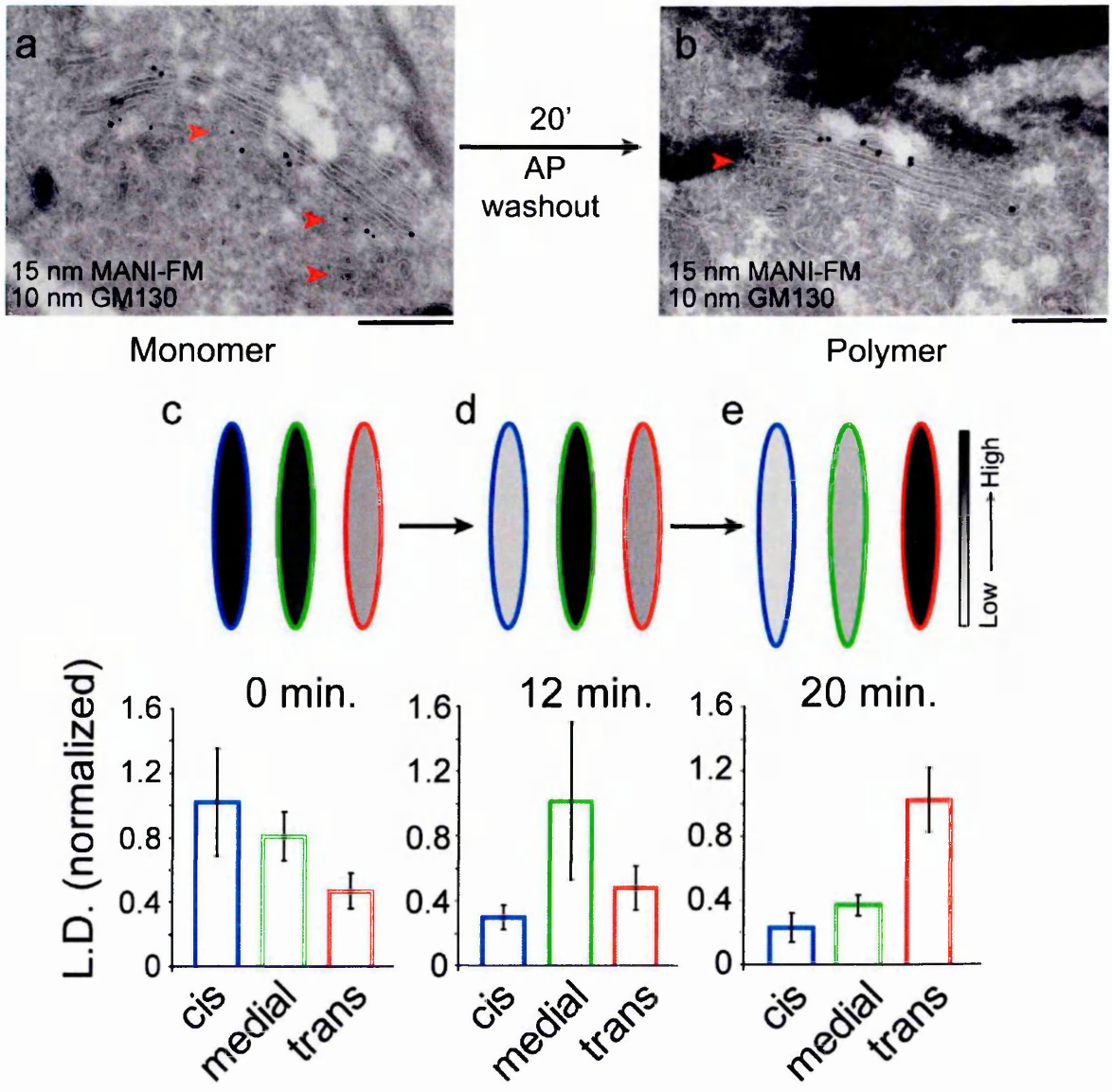

Figure 4.4.1.1 Polymerised MANI-FM shifts from *cis*-/medial to *trans*-Golgi cisternae (by EM)

(**a, b**) HeLa cells were transfected with MANI-FM in the presence of AP12998 (**a**), and then AP12998 was removed for 20 min (**b**) to induce polymerisation of MANI-FM. The MANI-FM (15-nm gold) shifted from the *cis*-cisternae (labelled with the *cis* marker GM130; 10-nm gold; arrowheads) to the *trans*-cisternae after AP12998 washout. (**c-e**) The distribution of MANI-FM across the stack at time 0 (**c**), 12 min (**d**), and 20 min (**e**) after AP12998 washout, quantified and expressed as the linear density (L.D.) normalised to that of the maximum. The normalised linear density in the *cis*-cisternae is indicated in blue, in

the medial, in green, and in the *trans*, in red. The schemes above the graphs depict the shift of the MANI-FM peak from the *cis*/medial to the *trans* side of the Golgi stack. The intensities of the fill colours correspond to the normalised linear density of MANI-FM in the corresponding graphs (intensity scale on right). At least 20 stacks were analysed for each time point. Data are means ±SEM. Bars: (**a, b**) 220 nm.

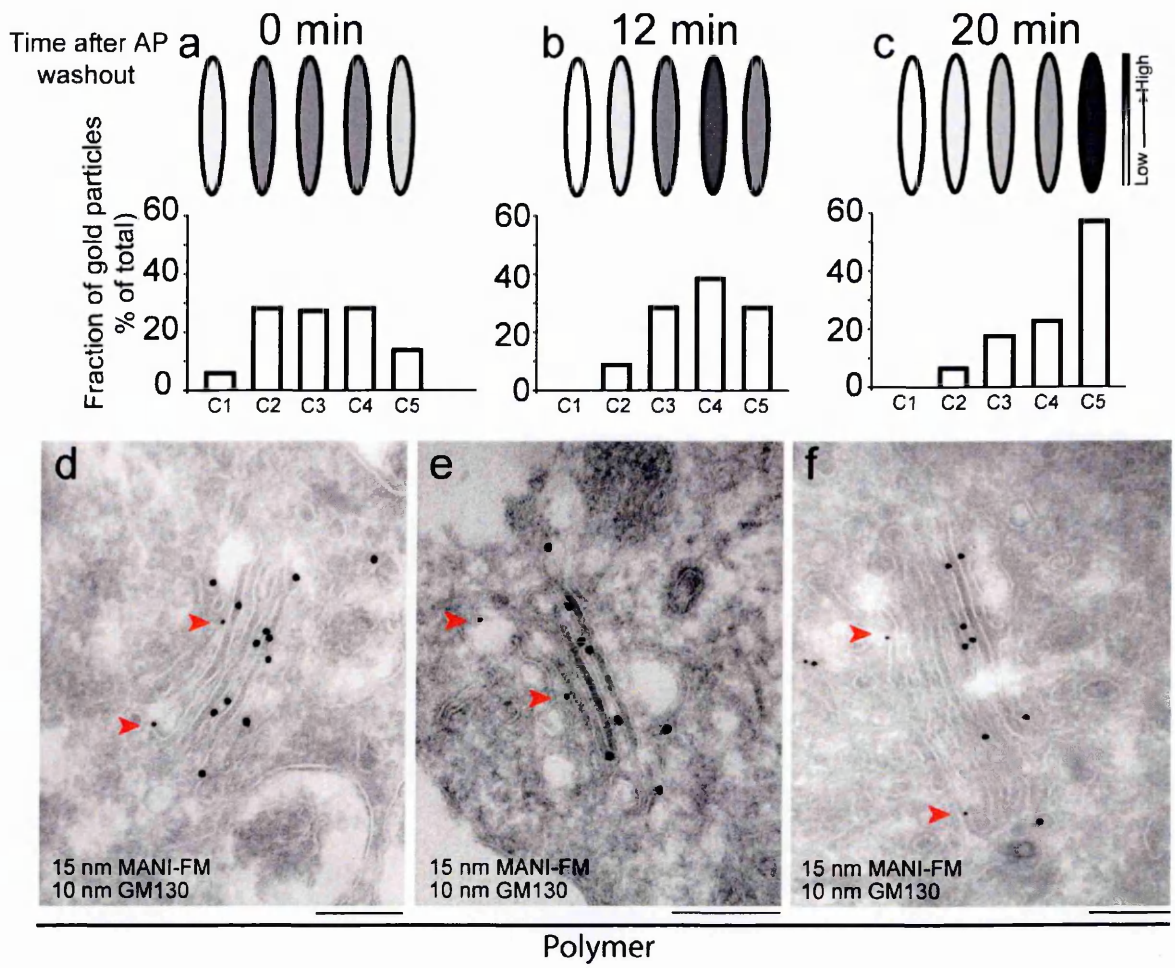

Figure 4.4.1.2 Frequency distribution analysis and double immune-labelling with GM130 as a *cis* marker confirms that polymerisation of MANI-FM induces its shift from the *cis* to *trans* side of the Golgi apparatus.

HeLa cells expressing MANI-FM were cultured in the presence of AP12998 (**a**) or after AP12998 wash-out for 12 min (**b**) or 20 min (**c**) were fixed and processed for cryoimmunogold labelling. The *trans*-most cisterna (*trans* side identified by the presence of clathrin coats) was named as C5, and the rest of the cisterna assigned accordingly, with C1 being the fifth *cis*-most cisterna. The frequency distribution of the gold particles across the cisternae was quantified and is represented as the fractions of gold particles present in each cisterna. Notably, 40% of the stacks had three cisternae, 50% had four cisternae, and only 10% of the stacks had five cisternae. Given the procedure used for the calculations, this accounts for the low values of gold particles in cisternae C1 and C2. Nevertheless, the

shift of the MANI-FM peak from the *cis*/medial to the *trans* side of the stack remains evident, as shown in the schemes above the graphs. The intensity of the filling colour corresponds to the number of gold particles of MANI-FM (see intensity scale on the right). At least 20 Golgi profiles per time point were used for quantitation, and >100 gold particles per time point were counted from two independent experiments. For this experiment, n >20 for each time point. (**d-f**) HeLa cells expressing MANI-FM were cultured in the presence of AP12998 and then AP12998 was washed out for 20 min before fixing and processing for cryoimmunogold labelling. The *cis* side of the stack was identified by GM130 (arrowheads; 10-nm gold). Polymerisation leads to the translocation of the MANI-FM (15-nm gold) to the *trans* side. Bars, (**d-f**) 180 nm.

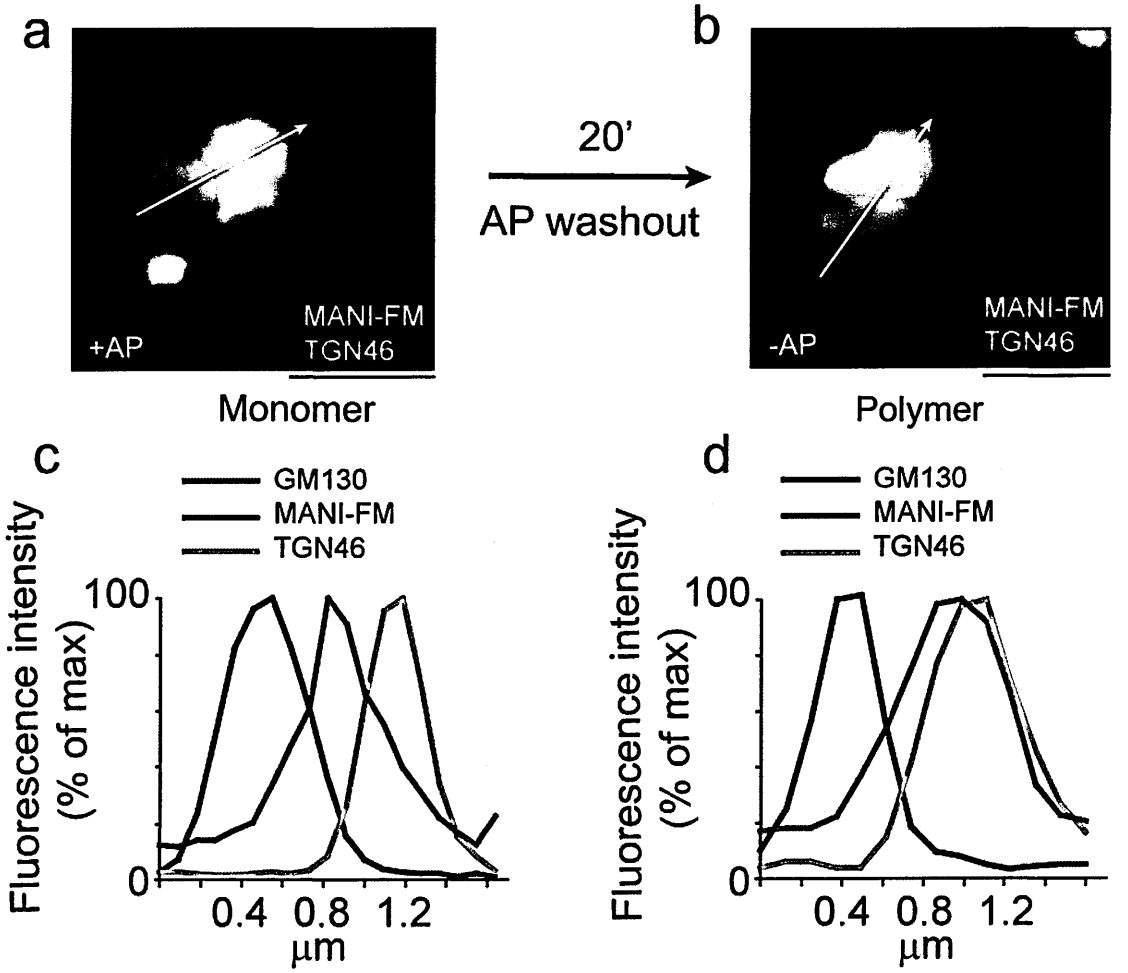

Figure 4.4.1.3 Visualisation of the shift of MANI-FM from the *cis*-/medial to the *trans*-Golgi, by confocal microscopy.

(**a**, **b**) HeLa cells were transfected with MANI-FM in the presence of AP12998 (**a**), and AP12998 was removed for 20 min (**b**), and then the cells were fixed and stained for MANI-FM (green), GM130 (blue), and TGN46 (red). The white arrow across the stacks was used for the line-scan analyses. The images are representative of >30 stacks analysed for each condition. (**c**, **d**) Fluorescence intensity distribution of markers along the line scan (arrow in **a**, **b**). The fluorescent intensities were normalised to their respective peak values. The image and the corresponding quantitation are representative of at least 30 Golgi ministacks from three independent experiments. For this experiment, $n = 30$. Bars: (**a**, **b**) 1 µm.

a

Monomer (+AP)

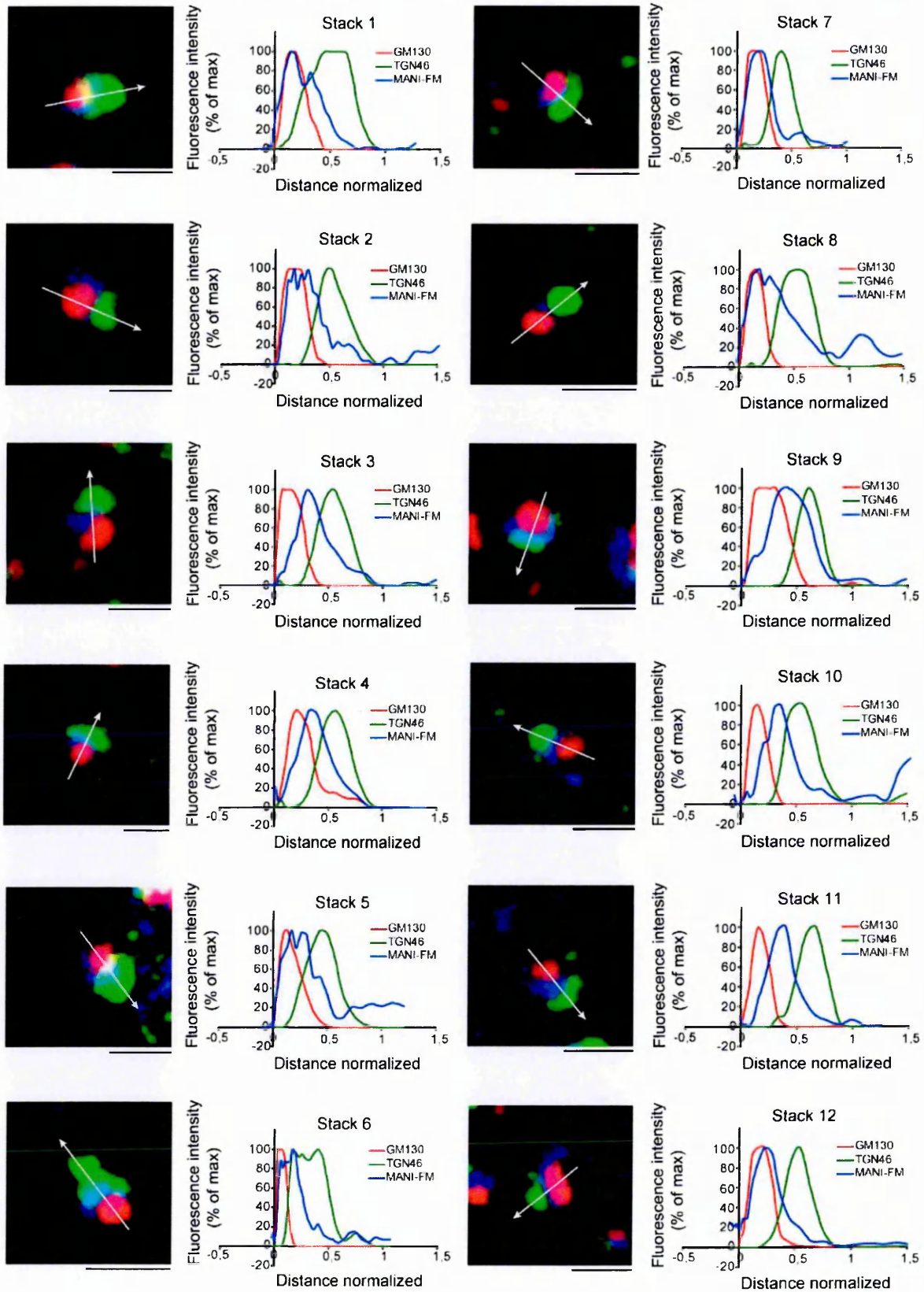
Stack 1
Stack 7
Stack 2
Stack 8
Stack 3
Stack 9
Stack 4
Stack 10
Stack 5
Stack 11
Stack 6
Stack 12
GM130
TGN46
MANI-FM
Fluorescence intensity (% of max)
Distance normalized

b

Polymer (-AP)

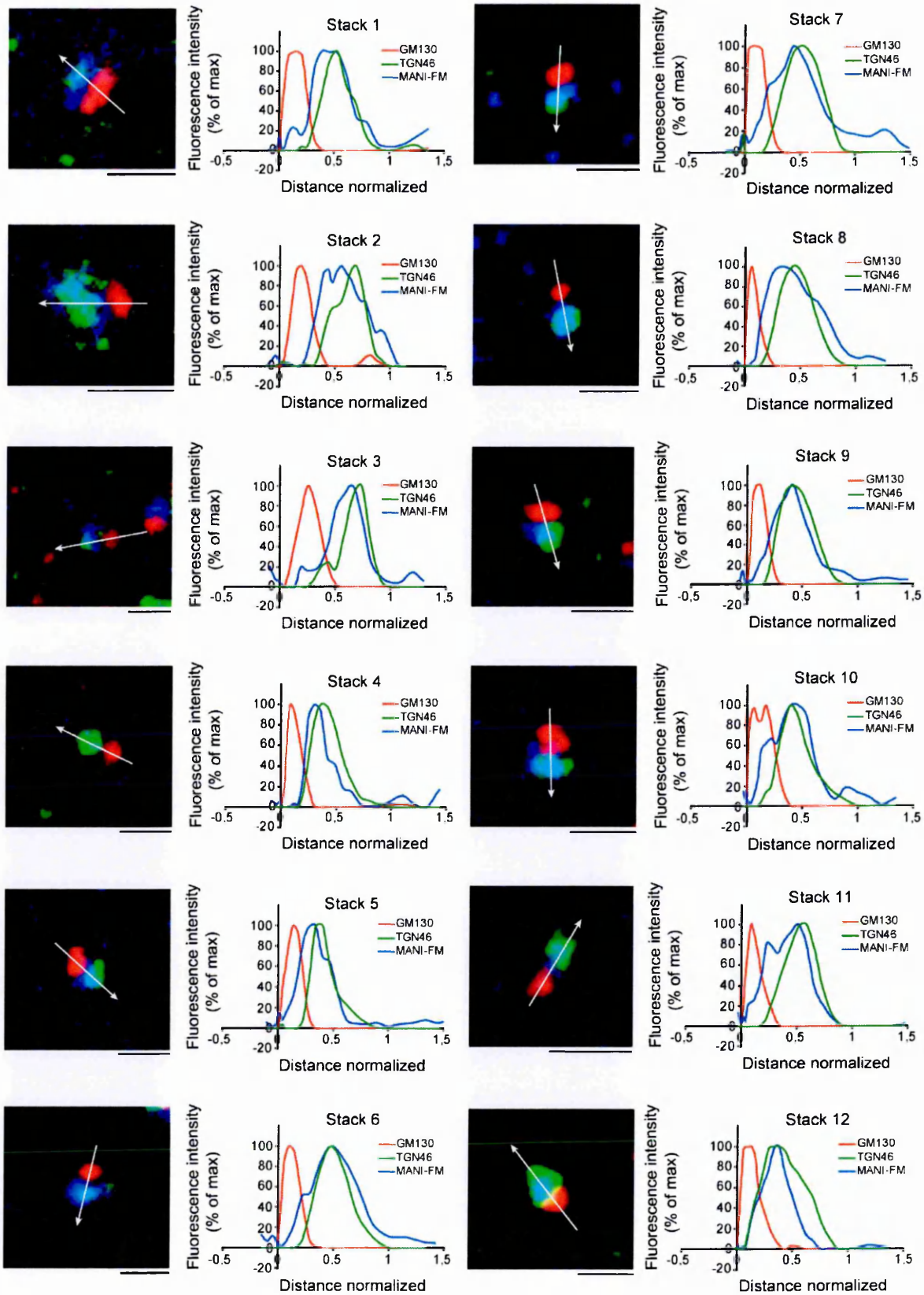
Stack 1
Stack 2
Stack 3
Stack 4
Stack 5
Stack 6
Stack 7
Stack 8
Stack 9
Stack 10
Stack 11
Stack 12
GM130
TGN46
MANI-FM
Fluorescence intensity (% of max)
Distance normalized

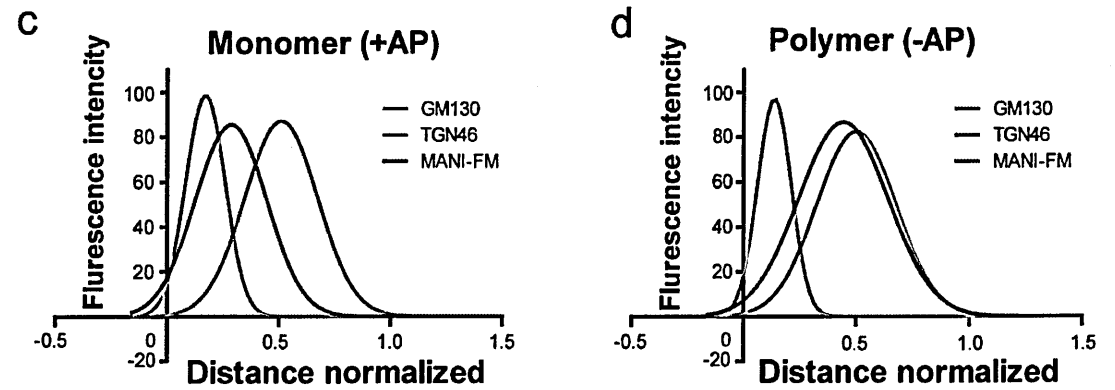

e

Monomer (+AP)

	GM130	TGN46	MANI-FM
Gaussian			
Best-fit values			
Amplitude	98,47	87,07	85,44
Mean	0,1705	0,5106	0,2860
SD	0,08846	0,1637	0,1599
Std. Error			
Amplitude	3,020	2,892	2,760
Mean	0,003120	0,006297	0,005881
SD	0,002833	0,006047	0,005468
95% Confidence Intervals			
Amplitude	92.55 to 104.4	81.40 to 92.73	80.04 to 90.85
Mean	0.1643 to 0.1766	0.4983 to 0.5230	0.2745 to 0.2975
SD	0.08291 to 0.09401	0.1519 to 0.1756	0.1492 to 0.1706
Goodness of Fit			
Degrees of Freedom	351	351	351
R square	0,7509	0,7197	0,6455
Absolute Sum of Squares	113798	109618	132419
Sy.x	18,01	17,67	19,42
Constraints			
SD	SD > 0.0	SD > 0.0	SD > 0.0
Number of points			
Analyzed	354	354	354

f

Polymer (-AP)

	GM130	TGN46	MAN1-FM
Gaussian			
Best-fit values			
Amplitude	96,77	82,33	86,61
Mean	0,1386	0,5025	0,4446
SD	0,07518	0,1755	0,1986
Std. Error			
Amplitude	3,068	2,706	2,520
Mean	0,002723	0,006675	0,006683
SD	0,002470	0,006368	0,006088
95% Confidence Intervals			
Amplitude	90.75 to 102.8	77.02 to 87.63	81.67 to 91.55
Mean	0.1332 to 0.1439	0.4894 to 0.5156	0.4315 to 0.4577
SD	0.07034 to 0.08002	0.1830 to 0.1880	0.1867 to 0.2105
Goodness of Fit			
Degrees of Freedom	322	322	322
R square	0,7681	0,7419	0,7344
Absolute Sum of Squares	82667	84112	89134
Sy.x	16,02	16,16	16,64
Constraints			
SD	SD > 0.0	SD > 0.0	SD > 0.0
Number of points			
Analyzed	325	325	325

Figure 4.4.1.4 Computational coalescence of the line scans of 12 Golgi stacks.

HeLa cells expressing MANI-FM were cultured in the presence of AP12998 (**a**) or with AP12998 washed out for 20 min (**b**), and fixed and processed for immunofluorescence labelling. The white arrows across the stacks were used for line-scan analyses. Representative stacks from the same pool of images from which **Fig. 4.4.1.3 (a, b)** was selected are shown. (**c-f**) Computational coalescence of the 12 graphs shown in **a, b** are shown in **c, d**, respectively, with the associated parameters used for curve fitting in **e, f**. This is a representative experiment out of three independent experiments. For this experiment, $n = 12$. Bars, (**a, b**) 1 μm.

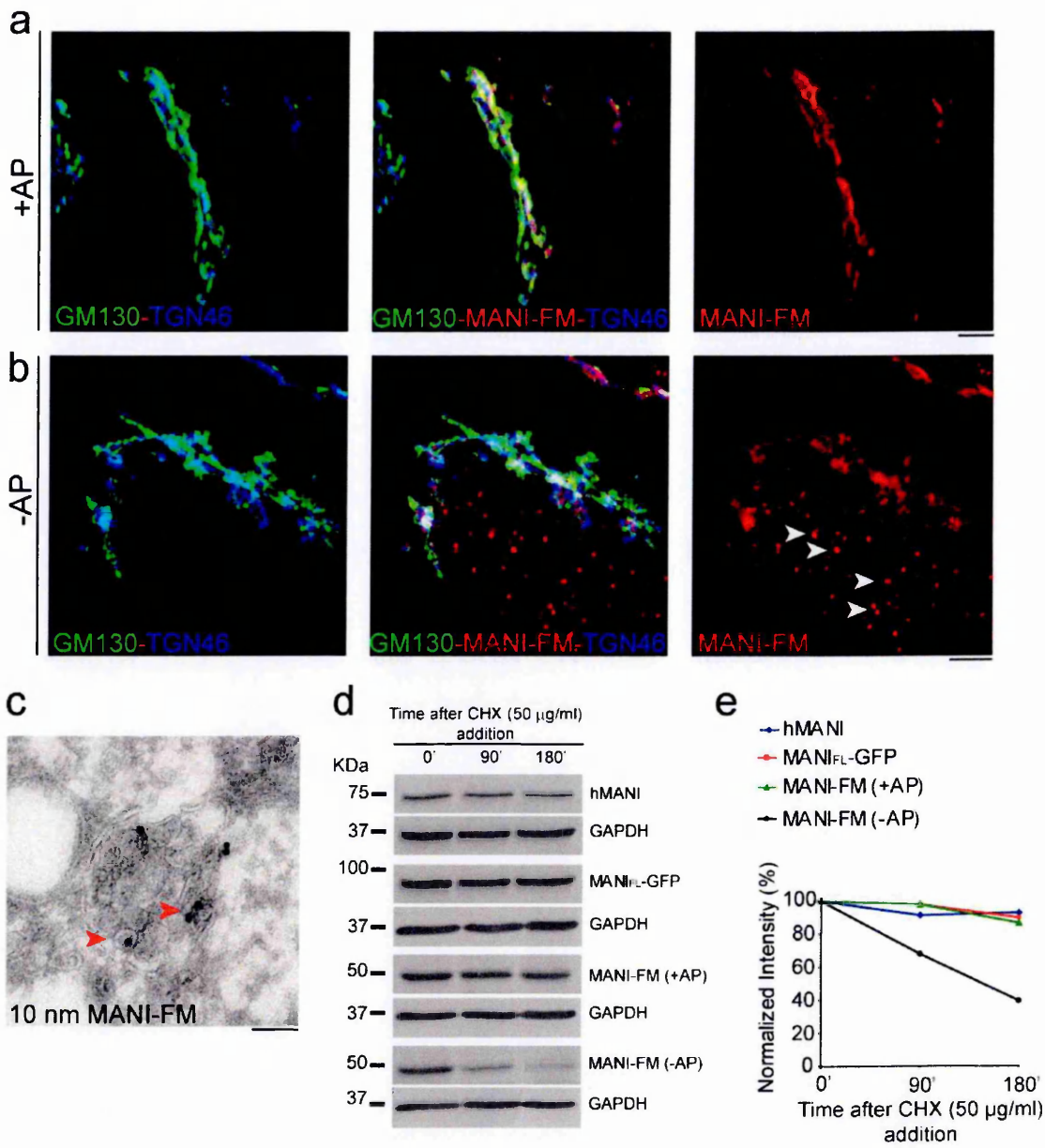

Figure 4.4.1.5 Degradation of MANI-FM after prolonged polymerisation in the Golgi. (**a**,**b**) HeLa cells were transfected with MANI-FM in the presence of AP12998 (**a**), and AP12998 was removed for 1 h (**b**), and then the cells were fixed and stained for MANI-FM (red), GM130 (green), and TGN46 (blue). The experiment was carried out in the absence of nocodazole to maintain the intact Golgi ribbon. The white arrowheads in **b** show the diffuse/ punctuate distribution of MANI-FM after prolonged Golgi polymerisation. (**c**) An example of MANI-FM in lysosomal-like structures after 1 h of AP12998 wash-out. HeLa cells were treated as in (**b**) and then fixed and processed for cryoimmuno-labelling with an

anti-HA antibody (10-nm gold particles). (**d**) HeLa cells expressing MANI-FM or $MANI_{FL}$-GFP were cultured in the presence and absence of AP12998, and treated with cycloheximide for the indicated times, and the amounts of the MANI and GAPDH (loading control) proteins were analysed by lysis of the cells followed by Western blotting. The quantification of the blots in panel (**d**) is shown in (**e**). Whereas the polymeric MANI-FM (-AP) is degraded, the monomeric MANI-FM (+AP) is stable, like $MANI_{FL}$-GFP and endogenous MANI. The results are typical of two independent experiments. Bars: (**a, b**) 5 μm; (**c**) 100 nm.

4.5 Intra-Golgi transport as well as Golgi morphology and the intra-Golgi localisation of endogenous MANI are not affected under MANI-FM polymerisation

4.5.1 Polymerised MANI-FM parallels the transport of VSVG-GFP within the Golgi

Once I had shown that the polymerised MANI-FM can move from the early to the late Golgi cisternae in the same time window as most of the cargo known so far, I decided to determine whether this movement parallels the transport of VSVG, and at the same time, to determine whether the intra-Golgi transport of VSVG-GFP occurred at normal rates.

To test this hypothesis, HeLa cells were transfected for both VSVG-GFP and MANI-FM in the presence of AP12998. After 24 h of incubation at 40°C to accumulate VSVG-GFP in ER (see Methods; Section **3.11**), the temperature was shifted to 15°C for 1 h to concentrate the VSVG-GFP in the VTCs (or ERGIC). Then the cells were placed at 40°C again to prevent the export of newly synthesised VSVG-GFP from the ER in order to follow the transport of only the VSVG-GFP that had already accumulated in the ERGIC. In a subset of samples, AP12998 was washed out 5 min before the temperature shift from 15°C to 40°C, to induce the polymerisation of MANI-FM in the Golgi apparatus (see protocol in **Fig. 4.5.1.3g**). The cells were then fixed at different times after the shift and labelled for both *cis*- and *trans*-Golgi markers to monitor the intra-Golgi localisation of VSVG-GFP and MANI-FM at the same time (**Fig. 4.5.1.3a-f, h**). Of note, to facilitate the line-scan quantification, the cells were pretreated for 3 h with nocodazole before the start of the experiment and the nocodazole was maintained throughout these experiments.

As can be seen from **Fig. 4.5.1.3h,** the VSVG-GFP was transported across the Golgi apparatus with identical kinetics under both polymerisation and non-polymerisation conditions for MANI-FM, suggesting that the polymerisation of MANI-FM does not affect

the anterograde transport properties of the Golgi apparatus. Moreover, the kinetics of forward movement of the polymerised MANI-FM paralleled the transport of VSVG-GFP, again indicating that the forward movement of the MANI-FM upon polymerisation probably occurs by the same mechanism by which anterograde cargo is transported.

Polymerisation of MANI-FM did not modify the morphology and the surface area of the Golgi apparatus, either in the presence or absence of nocodazole (**Fig. 4.5.1.4c, d**); and the localisation of endogenous MANI was not affected by MANI-FM polymerisation (**Fig. 4.5.1.4a, b**).

Thus, polymeric MANI-FM progresses from the *cis*- to the *trans*-Golgi without entering the carriers (vesicles/ tubules) at rates that are similar to those reported for procollagen and VSVG (Mironov, Beznoussenko et al. 2001), and without perturbing the function (see also Results; Section **4.3**) and structure of the Golgi apparatus.

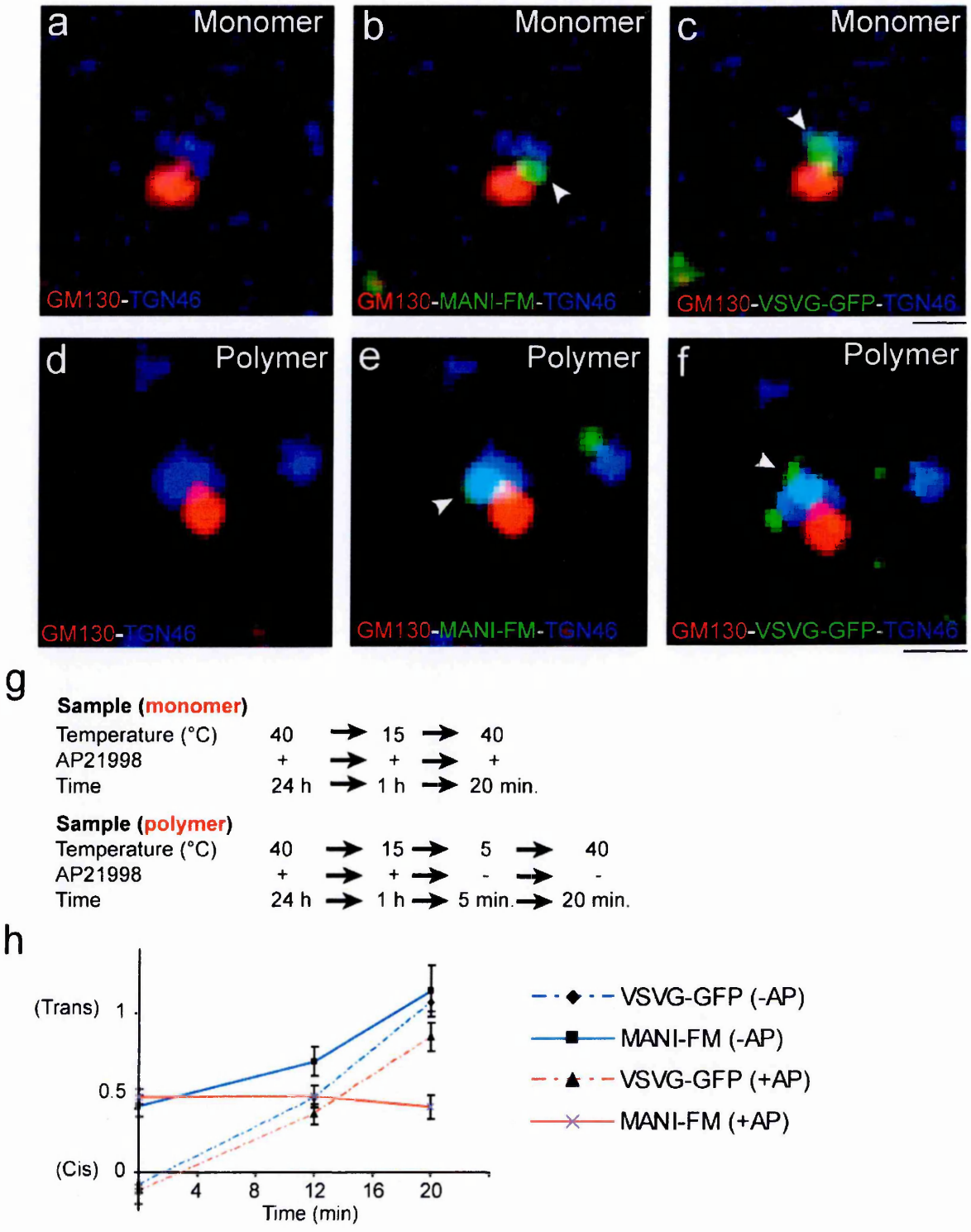

Figure 4.5.1.3 MANI-FM polymerisation does not affect intra-Golgi transport of VSVG.

(**a-f, h**) VSVG-GFP parallels the transport of the MANI-FM polymer in the Golgi apparatus. HeLa cells co-expressing MANI-FM with VSVG-GFP were incubated overnight at 40°C in the presence of AP12998, prior to shifting the temperature to 15°C for

1 h in the presence of AP12998. Immediately after the 15 °C block (time 0 in **h**), the temperature was shifted back to 40°C in the presence (**a-c**) or in the absence (**d-f**) of AP12998. The cells were fixed for the indicated time (see **h**) and processed for immunofluorescence. The good separation between the *cis*-Golgi marker (GM130) and *trans*-Golgi marker (TGN46) is shown in (**a, d**). After 20 min of the temperature shift from 15°C to 40°C, the MANI-FM monomer (**b**) is in the *cis*-medial Golgi (white arrowhead) whereas VSVG-GFP is localised in the *trans*-Golgi (**c,** see white arrowhead). In the absence of AP12998 (-AP), both the MANI-FM polymer (**e**) and VSVG-GFP (**f**) move to the *trans*-Golgi (white arrowhead). The synchronisation protocol in (**g**) refers to images (**a-f**). (**h**) Quantification was carried out by normalised line-scan analysis (normalisation of distances was done by considering the middle of the GM130 peak as 0, and the middle of the TGN peak as 1). At least 30 stacks per time point per experiment were analysed, and the data are from two independent experiments. Data are means ±SEM. Bars: (**a-f**) 1 μm.

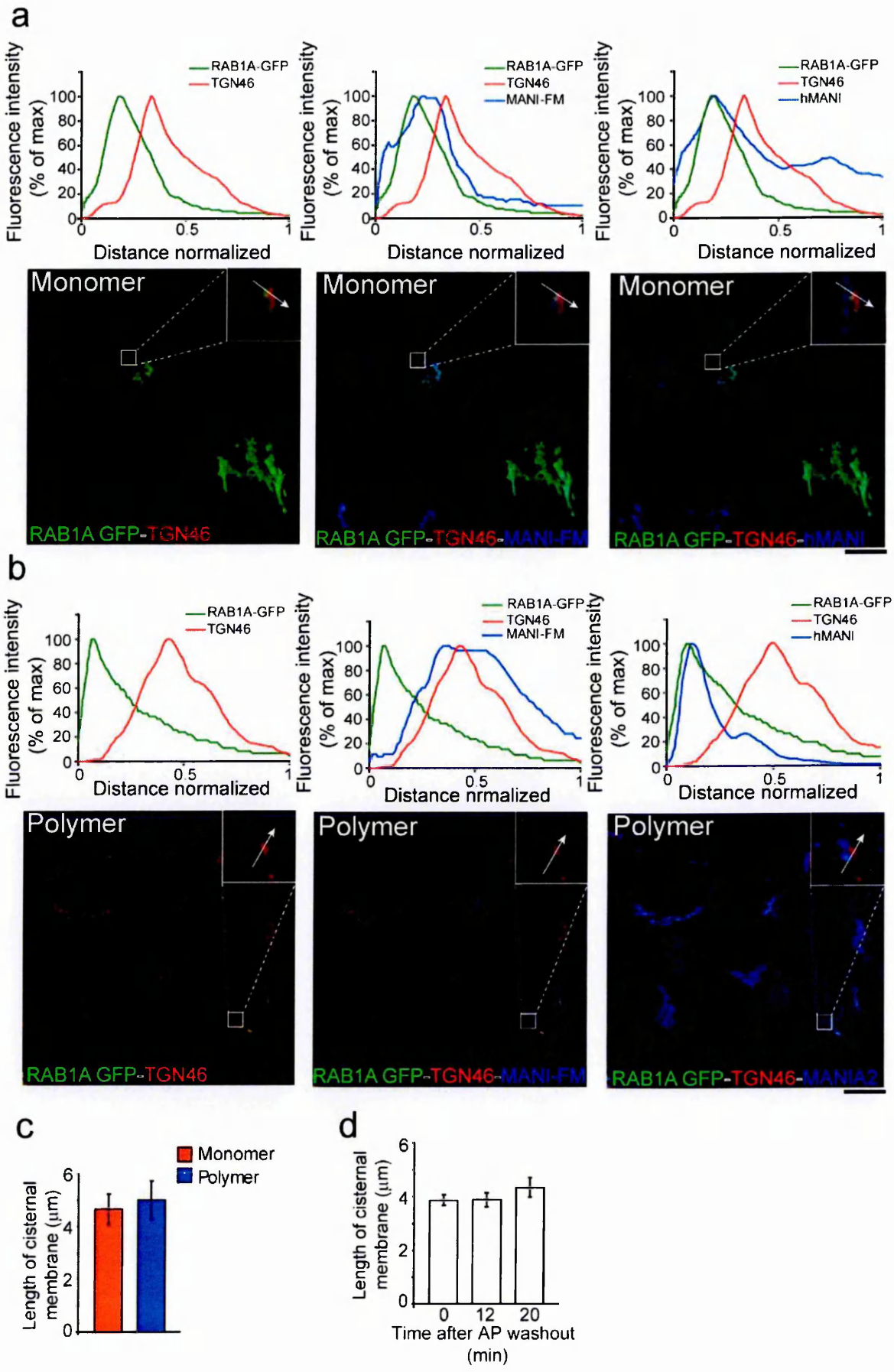
a
Fluorescence intensity (% of max)
RAB1A-GFP
TGN46
MANI-FM
hMANI
Distance normalized
Monomer
RAB1A GFP-TGN46
RAB1A GFP-TGN46-MANI-FM
RAB1A GFP-TGN46-hMANI
b
Polymer
RAB1A GFP-TGN46
RAB1A GFP-TGN46-MANI-FM
RAB1A GFP-TGN46-MANIA2
c
Monomer
Polymer
Length of cisternal membrane (μm)
d
Length of cisternal membrane (μm)
Time after AP washout (min)

Figure 4.5.1.4 Polymerisation of MANI-FM does not modify the Golgi structure and the localisation of endogenous MANI.

(a, b) MANI-FM polymerisation does not change the localisation of endogenous MANI. HeLa cells co-transfected with MANI-FM and Rab1A-GFP were cultured in the presence of AP12998 (**a**) and AP12998 was washed out for 20 min (**b**) before fixing and processing for immunofluorescence labelling. The experiment was carried out in the absence of nocodazole to maintain the Golgi ribbon intact. The white arrow across the ribbon was used for the line-scan analyses shown above the images. The fluorescent intensities were normalised to their respective peak values. The images shown are representative of at least 10 Golgi profiles examined for each condition from two independent experiments. For the experiment shown, $n = 10$. The polymerisation shifts MANI-FM (blue) from the *cis* (Rab1-GFP, green) to *trans* side (TGN46, red) of the Golgi, whereas the endogenous MANI (MANI endo, blue) maintains its *cis*/medial position. **(c, d)** Morphology of the Golgi stacks is not affected by MANI-FM polymerisation. HeLa cells expressing MANI-FM cultured in the presence of AP12998 (+AP) or with AP12998 washed out for 20 min (-AP), in the absence (**c**) or presence (**d**) of nocodasole, were fixed and processed by EM imaging. The length of the Golgi cisternal membranes were measured and expressed in μm. The cisternal membrane length (as a measure of surface area) did not change appreciably after MANI-FM polymerisation. Bars: **(a, b)** 20 μm.

4.6 Depolymerisation of the Golgi resident enzyme restores its entry into peri-Golgi carriers and its intra-Golgi localisation

The observation that MANI-FM moves forwards in the stack when it is polymerised and is excluded from vesicular or tubular transport intermediates implies that monomeric MANI-FM normally recycles through these intermediates to maintain its *cis*-medial position. So far, however, direct evidence for the recycling of Golgi resident enzymes through the Golgi stack in synchrony with transport in the mammalian Golgi has been missing (Hoe, Slusarewicz et al. 1995; Malsam, Satoh et al. 2005).

I considered that if the MANI-FM polymers were depolymerised in the *trans*-cisterna, the resulting monomers should regain their entry into carriers, and could then recycle synchronously from the *trans* to the more proximal cisternae. To investigate this hypothesis, I first polymerised MANI-FM for 20 min to let the polymer reach the *trans*-cisterna (**Fig. 4.4.1.1e**), and then I depolymerised the MANI-FM by adding back AP12998. At 20 min after AP12998 wash-out, as expected, polymeric MANI-FM was homogeneously distributed in the *trans*-cisterna (**Fig. 4.6.1a**; and see also **Fig. 4.4.1.1b**). Upon depolymerisation, MANI-FM rapidly (in 1.5-3.0 min) underwent the following distribution changes:

a) it became concentrated at the cisternal rims (**Fig. 4.6.1c**);

b) it increased greatly in peri-Golgi vesicles/tubules (the number of which also increased two- to three-fold; **Fig. 4.6.1b, d, e**);

c) it started to return back to the *cis*/medial localisation, which is typical of the MANI-FM monomers (**Fig. 4.6.1f, Fig. 4.6.2a-f**). Throughout this redistribution process, the total levels of MANI-FM did not change detectably in the Golgi ministacks or in the Golgi ribbon. Notably, more than 50% of the MANI-FM–containing vesicles and tubules stained for COPI (**Fig. 4.6.3g**). Thus, the depolymerisation of MANI-FM in the *trans*-cisterna appears to result in a burst of recycling mediated via COPI-dependent vesicles and tubules,

and in the rapid redistribution of MANI-FM to the proximal cisternae. Even though the amount of overexpressed MANI-FM was only two- to three-fold that of the endogenous enzyme (**Fig. 4.1.1c**), the sudden appearance of all of the *cis*/medial resident MANI-FM in the *trans*-cisterna can presumably be sensed and compensated for by mechanisms that actively respond to variable demands on the recycling process.

I also examined the structure of the Golgi carriers and of the Golgi stack by tomography. All of the reconstructions indicated that the morphology of the carriers (**Fig. 4.6.3a-f**) and the structure and size of the Golgi stack were similar under all experimental conditions (**Fig. 4.5.1.4c, d**). Moreover, tomography confirmed that most round, 50-nm to 80-nm structures were indeed vesicles (**Fig. 4.6.3a-f**), and that the relative frequency of vesicles and tubules was similar to that seen in thin sections.

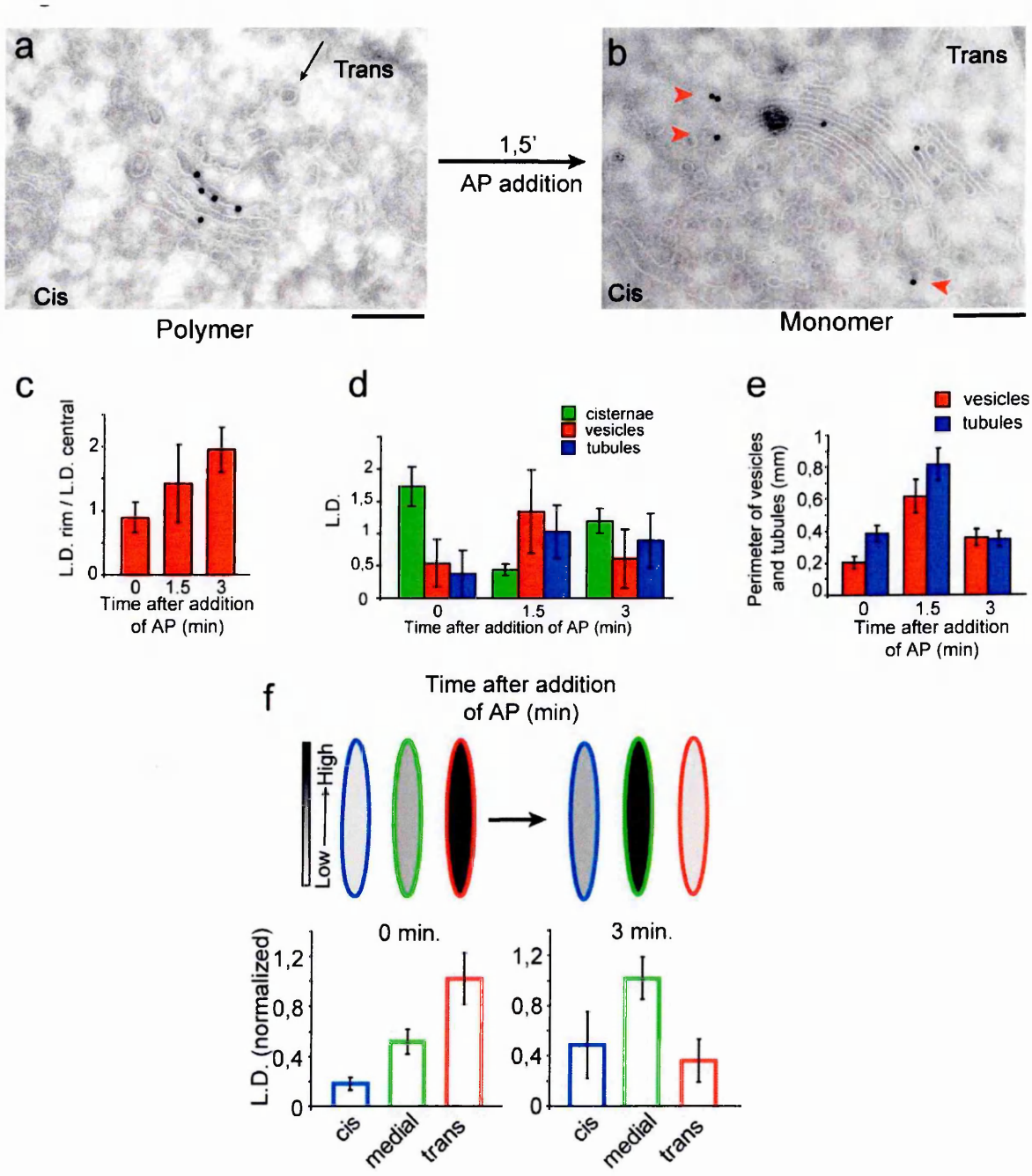

Figure 4.6.1 MANI-FM recycles from the *trans*- to the *cis*-/medial Golgi after depolymerisation in the *trans*-Golgi

(**a, b**) HeLa cells were transfected with MANI-FM in the presence of AP12998, and then the AP12998 was removed for 20 min to induce MANI-FM polymerisation and the transfer of MANI-FM to the *trans*-cisterna (**a**); finally, AP12998 was added for 1.5 min (**b**). Arrowheads in (**b**) indicate the peri-Golgi carriers seen after AP12998 addition. (**c, d**) The lateral distribution of MANI-FM along the cisternal length (**c**) and the distribution of

MANI-FM in peri-Golgi carriers (**d**), expressed as the linear density. (**e**) The membrane length of vesicles and tubules as a measure of the surface area was quantified and is expressed as the perimeter (in μm). (**f**) Co-localisation of COPI and MANI-FM in vesicles and tubules (arrowheads) in cells fixed 1.5 min after addition of AP12998, to depolymerise MANI-FM. (**g**) The change in the distribution of MANI-FM from the *trans*- to the *cis*-/medial Golgi after addition of AP12998 is expressed as the linear density (L.D.) normalised to that of the maximum (see **Fig. 4.4.1.1** for description). Around 10-20 Golgi stack profiles were examined for each time point. Data are means ±SEM. Bars: (**a, b**) 220 nm

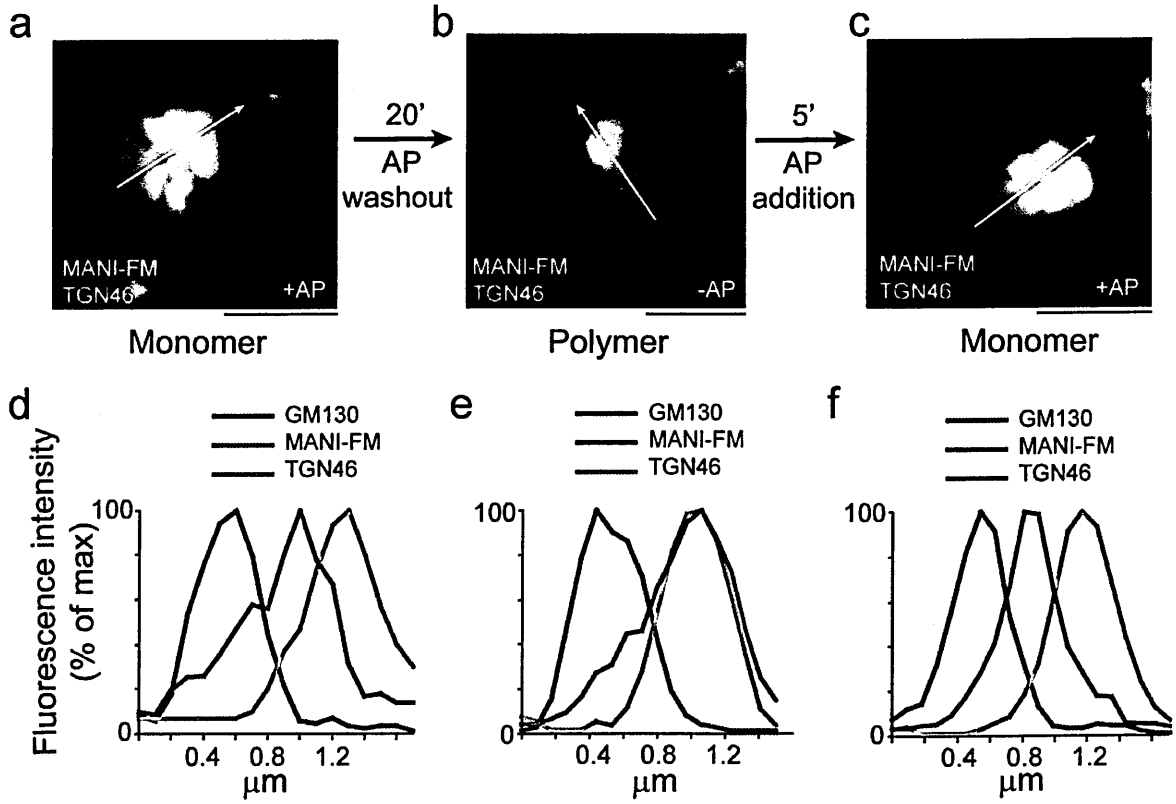

Figure 4.6.2 MANI-FM recycling visualised by confocal microscopy.

(**a-f**) HeLa cells were fixed in the presence of AP12998 (**a, d**), after 20 min of AP12998 wash-out (**b, e**), and 5 min after readdition of AP12998 (**c, f**). The cells were then stained for MANI-FM (green), GM130 (blue), and TGN46 (red). The white arrows across the stacks were used for the line-scan analyses. The fluorescence intensity distribution of markers along the line scan (**a-c**, arrow), normalised to their respective peak values, is shown in (**d-f**). The images are representative of >30 stacks analysed for each condition from three independent experiments. For this experiment, $n = 30$. Bars: (**a-c**) 1 μm.

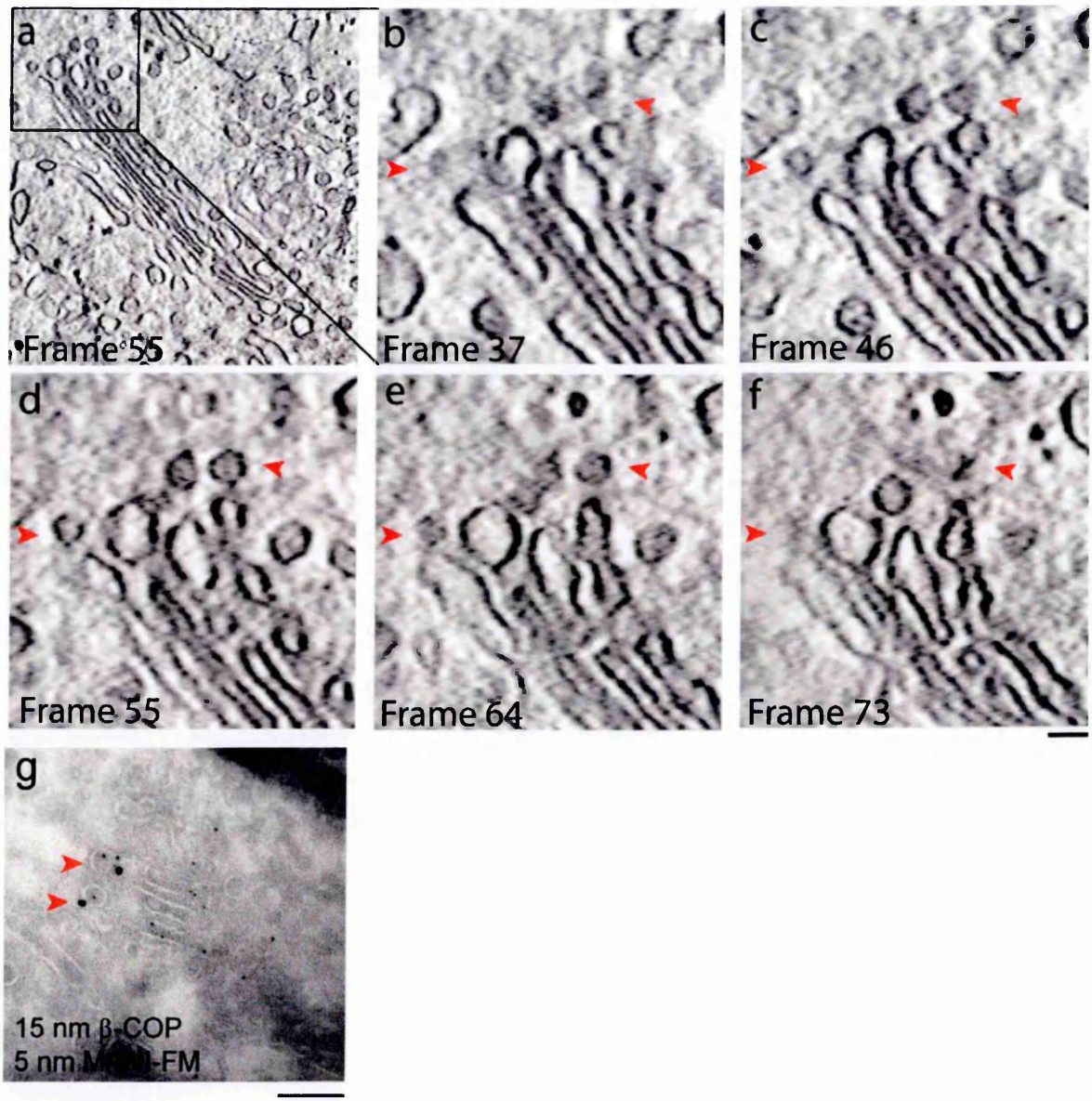

Figure 4.6.3 Round profiles seen in thin sections are actual vesicles and they are COPI coated.

(**a**) HeLa cells expressing MANI-FM were cultured in the presence of AP12998 and then AP12998 was washed out for 20 min before adding it back again for 1.5 min. The cells were then fixed and processed for tomography and cryoimmunogold labelling. (**a-f**) A single frame from the tomographic reconstruction of a Golgi stack (**a**). The boxed area containing round profiles is enlarged in (**b-f**). Frames are shown from the tomographic reconstruction where two round profiles (arrowheads) were followed, to validate them as isolated vesicles. (**g**) The cells were processed as in (**a**) and then fixed and processed for

cryoimmunogold labelling with anti–β-COP antibodies (15-nm gold) and anti-HA antibodies (5-nm gold; MANI-FM). The COPI-coated structures contain MANI-FM (arrowheads). (**g**) Co-localisation of COPI and MANI-FM in vesicles and tubules (arrowheads) in cells fixed 1.5 min after addition of AP12998 to depolymerise MANI-FM. Bars: (**a**) 180 nm; (**b-f**) 60 nm, (**g**) 120 nm.

CHAPTER 5.

Discussion

A peculiar characteristic of the eukaryotic cell is the presence of organelles that are membrane-bound structures that allow the spatial restriction of specific enzymatic reaction, thus improving certain cellular functions. This compartmentalization, at the same time, prevents potential damage that dangerous molecules could cause if they could freely roam within the cell. Obviously, cellular organelles need to exchange specific molecules between each other and, in other cases, molecules have to be secreted out of the cell. To insure the correct delivery of molecules to the right place, eukaryotic cells have developed different transport strategies such as compartmental fusion, transport mediated by coated vesicles or large pleiomorphic carriers as well as direct tubular continuities between distinct compartments (see review by De Matteis and Luini, 2011).

A common factor of all of these transport strategies is represented by three different processes that include budding, fission and fusion, a series of events that can promote different mechanisms of transport according to their sequence of action.

An important and still unresolved question in cell biology concerns the mechanisms of intra-Golgi transport. Two classes of mechanisms have been proposed: one is based on stable cisternae that contain resident proteins while cargo-laden carriers move across these cisternae, and the other is based on progressing and 'maturing' cisternae that carry cargo forward while residents are recycled through the stack. Thus a key difference between the two concerns the behaviour of Golgi-resident glycosylation enzymes. In this work I have engineered Golgi-enzyme constructs that can be polymerized at will to prevent their recycling via Golgi carriers.

This study reports that: (a) monomeric MANI-FM localises to *cis*/medial Golgi cisternae and is present in peri-Golgi vesicles and tubules (**Fig. 5.1a**); and (b) upon shifting to a polymeric state, MANI-FM moves from the rims to the centre of the cisternae, cannot enter peri-Golgi carriers (**Fig. 5.1b**), and shifts from the *cis* to the *trans*-Golgi, while remaining within the cisternae (**Fig. 5.1c**). This movement occurs at the same rate as supramolecular secretory cargo that have been proposed to move by cisternal progression (Bonfanti, Mironov et al. 1998). Moreover, when MANI-FM is depolymerised in the *trans*-cisterna, it rapidly re-enters the cisternal rims and vesicles/tubules, and shifts back towards its *cis*-Golgi location (**Fig. 5.1d**). These findings are consistent with the cisternal-progression/maturation mechanism, and are inconsistent with stable cisterna schemes (Rizzo, Parashuraman et al. 2013).

A more detailed analysis is necessary to compare the experimental observations made in this study with all of the intra-Golgi transport models that have been proposed over the years. This should mainly focus on two fundamental aspects for a critical and comparative analysis: the anterograde movement of cargoes and the mechanisms of recycling of Golgi resident enzymes that is predicted by each model.

As noted, cisternal maturation predicts that MANI-FM polymers that cannot enter transport carriers will move forward within the advancing cisternae. Instead, stable cisterna models predict that MANI-FM will be retained within the cisternae irrespective of its polymerisation status. Here, it can be hypothesised that polymerisation might somehow induce MANI-FM to move across stable cisternae. However, MANI-FM can do so only by entering anterograde transport carriers, which is just the opposite of what is observed experimentally: polymerisation induces a nearly complete decrease of MANI-FM in all types of peri-Golgi carriers and a shift of this construct from the rims to the centre of the cisternae, a location that is not suitable for export. Finally, while maturation models require efficient and adaptable enzyme recycling mechanisms, stable cisterna models do not. A

possible complexity might be that under the stable cisterna models the Golgi resident enzymes might 'leak' forward and be recycled back by carriers. However, this would not predict forward transport of the resident enzymes upon polymerisation with kinetics similar to the intra-Golgi transport of cargoes.

The rapid-partitioning model suggests that the *cis*-to-*trans* movement of cargoes is observed only after low-temperature-induced synchronisation, while at physiological temperatures both newly arrived and pre-existing cargoes in the Golgi apparatus have an equal probability of exiting i.e., the cargo can exit even from the *cis*-side of the Golgi apparatus where an exit domain can be formed due to the non-homogenous lipid distribution (Patterson, Hirschberg et al. 2008). Our observations of the *cis*-to-*trans* movement of cargoes upon polymerisation directly contradicts this prediction of the model. Finally, the rapid-partitioning model proposes that the polarised distribution of the Golgi resident enzymes is due to the affinity of their transmembrane domains for the differential lipid distribution across the Golgi apparatus. As we have not studied the lipid affinities of MANI-FM during its monomeric or polymeric state, this prediction cannot be tested at the moment.

According to the cisternal-progenitor model (see also the kiss-and-run model; Mironov and Beznoussenko 2012), the anterograde movement of cargo is the result of segregation of Rabs within the Golgi cisternae, which would lead to homotypic fusion of compartments enriched in the same Rabs via the generation of intercisternal connections (see model in **Fig. 1.4, 3**). As an example of such an intermediate, I have chosen a published EM micrograph showing the Golgi apparatus of a guinea pig exocrine pancreas cell (**Fig 5.2a**; Pfeffer 2010; see original Figure in Farquhar and Palade 1981; **Fig. 5.2b**), where a discontinuity in the Golgi cisternae was presented as an example of this process. The discontinuous cisternae seen in the transverse section of the Golgi apparatus (**Fig. 5.2a, b**; (Pfeffer 2010; Farquhar and Palade 1981) could be the result of two very different

situations that can be settled only by observation of tangential sections of the cisternae (see cartoon in **Fig. 5.2d-f**). The presence of two distinct pieces of cisternae that are not connected (**Fig. 5.2d**) or are connected by tubules (**Fig. 5.2f**), or the presence of a hole inside the cisternae (**Fig. 5.2e**), could generate the discontinuities seen in the cross-section of the Golgi apparatus (**Fig. 5.2a, b**). While this last option is known to exist and is well documented, as well as in the Golgi stack (**Fig. 5.2c**; Ladinsky, Mastronarde et al. 1999; Rambourg and Clermont 1990), the former situation (**Fig. 5.2f**) has never been observed. This consideration indicates a weakness in the cisternal-progenitor model. Regarding the anterograde movement of large cargoes through the Golgi apparatus, the progenitor model proposes an "alternative homotypic fusion process", which implies that a homotypic fusion event between two neighbouring cisternae from adjacent Golgi stacks promotes the forward movement of cargo. As the experiments reported here were carried out in the presence of nocodazole (see Material and Methods; Section **3.8**), which separates the Golgi ribbon into individual stacks, and thus prevents inter-stack exchange although it still allows forwards movement of cargoes, these observations directly contradict the cisternal-progenitor model. Although this model does not exclude the possibility that other types of Golgi dissociative carriers, like megavesicles, might be involved in anterograde transport of "large aggregates", such membranous structures were never observed in my samples; nevertheless, it is important to note that the fission and fusion process of these carriers might be very fast events, thus preventing their routine detection.

Along the same lines, considering that the cisternal-progenitor model is based on a mechanism of Rab conversion, a segregation of polymeric MANI-FM is also needed for its incorporation in megavesicles. At steady-state, MANI-FM appears to be more concentrated at the rims than in the central parts of the Golgi cisternae, but upon polymerisation the MANI-FM is distributed randomly along the cisternal length, making it difficult to reconcile these observations with the predictions of this model.

A recent publication from the laboratory of Rothman described the trafficking of a modified CD8 transmembrane cargo through the Golgi complex, using the same FM strategy that I applied in this study. The experimental approach was the same, and consists of the aggregation of a synchronised transmembrane cargo on the *cis* side of the Golgi apparatus to discriminate between static *versus* mobile Golgi cisternae (see also objective; Chapter **2**). When modified, the CD8 protein was allowed to polymerise in the ER in a *trans* configuration, where it forms membrane constrictions that was named by Lavieu et al. (2013) as "staples". Through the manipulation of the temperature and the aggregation status of the artificial protein, the Rothman team was able to localise the protein to the *cis*-Golgi and then to induce the formation of staples there, and finally to follow the fate of the aggregates. They showed that cargoes remained where they had been 'stapled', but without stapling, they moved to the cell surface (Lavieu, Zheng et al. 2013). Under conditions in which staples were allowed to form in the Golgi apparatus, the transport of VSVG, collagen, and a soluble aggregate of growth hormone (hGH), were not affected. These observations fit with the idea of a static Golgi compartment, which is opposite to what I have found in my study.

The only weakness of the study of Rothman and colleagues is that there were no quantifications related to the microscopy observations, so it is hard to say whether the phenotype is rare and representative of a subset of Golgi stacks. Lavieu et al. (2013) also did not determine the size of the polymerised CD8; indeed, it is highly possible that the polymerisation can induce the formation of aggregates with different sizes, and not all of the polymerised CD8 can form staples. In support of this hypothesis, the EM micrograph used by Lavieu et al. (2013) to highlight the staples in the ER (**Fig. 5.2g**) clearly shows that pieces of the ER are completely swollen, which indicates that a massive amount of protein resides in that region. Therefore, it is possible that only a few Golgi stacks have these staples, and their presence inside the cisternae might affect the functionality of these

ministacks. The observation that different cargoes, including VSVG, can cross the Golgi normally under aggregation conditions of CD8 might be the result of the cargo bypass of these inactive Golgi ministacks. Obviously this is speculation, but these possibilities can be tested simply by breaking the Golgi ribbon with nocodazole and then applying the same polymerisation protocol of CD8-FM. If this hypothesis is correct, the non-functional Golgi ministacks with the staples should not allow the transport of VSVG or other cargo proteins, or they might be empty of cargoes. This model proposes the existence of a stable cisternal centre and a "maturing" rim that progresses forwards, thereby transporting large cargoes from the *cis* to the *trans* side of the Golgi. Nevertheless, the observations presented in my study show that upon polymerisation, MANI-FM shifts from the cisternal rims to a random distribution, but nevertheless "progresses" from *cis* to *trans*, which suggests that the observed progression involves the complete cisternae rather than the rims alone.

Thus, my experimental observations can be only partially explained by the models mentioned so far. The simplest interpretation of the data reported in this study is that monomeric MANI-FM normally recycles backwards in the stack in step with the progression of the cisternae (and of the cargoes) via retrograde transport intermediates, to maintain its *cis* location, and that when its recycling is inhibited by polymerisation it progresses through the stack along with the cisternal flow. The findings in my study are therefore consistent with the cisternal-progression/maturation mechanism, and not with stable cisternae models.

A further line of evidence in favour of cisternal maturation is that when MANI-FM is depolymerised in the *trans*-cisterna, it rapidly re-enters the cisternal rims as well as vesicles/tubules and shifts back toward its *cis*-Golgi location. These data represent evidence for the rapid recycling of Golgi resident enzymes through the stack in mammals. Notably, a Golgi enzyme, GAlNacT2, has been reported recently to cycle rapidly between the Golgi apparatus and the intermediate compartment in mammals (Jarvela and Linstedt

2012). This finding does not relate to the progression/maturation of the cisternae through the stack; rather it reflects the formation of new *cis*-cisternae from the intermediate compartment (Jarvela and Linstedt 2012).

Regarding the mechanism of recycling, the MANI-FM–containing carriers that proliferate upon MANI-FM depolymerisation appear to be COP-I–coated tubules and vesicles. Discordant conclusions have been proposed in the past regarding the question of whether vesicles or tubules (which might be dissociated or connected with adjacent cisternae) are involved in recycling (Orci, Amherdt et al. 2000; Lanoix, Ouwendijk et al. 2001; Martinez-Menarguez, Prekeris et al. 2001; Kweon, Beznoussenko et al. 2004; Trucco, Polishchuk et al. 2004). The data from my study, and the recent proposal that Golgi vesicles and tubules are strongly mechanistically related (Yang, Valente et al. 2011), might explain the previous discrepancies.

These findings do not show that cisternal maturation is the only mode of intra-Golgi transport; indeed, these transport mechanisms are not mutually exclusive (Emr, Glick et al. 2009). Thus, although my data provide evidence for cisternal maturation, they do not exclude that other transport principles might coexist with the maturation process in the Golgi complex, such as vesicular trafficking (Rothman and Wieland 1996; Malsam, Satoh et al. 2005) or diffusional trafficking via continuities (Trucco, Polishchuk et al. 2004). Here, the prevailing mechanism perhaps depends on the type of cargo being transported, the pathophysiological conditions, the cell type, and/or the trafficking step being examined. Examples of the eclectic nature of the transport apparatus have been provided by studies of the endocytic pathway, where different transport principles have been shown to coexist (Pryor and Luzio 2009; De Matteis and Luini 2011). Membrane trafficking has central roles in many cellular processes (Mellman and Warren 2000; De Matteis and Luini 2011), thus a better understanding of the full repertoire of eukaryotic

trafficking principles will provide valuable insights into key aspects of cell physiology and pathology.

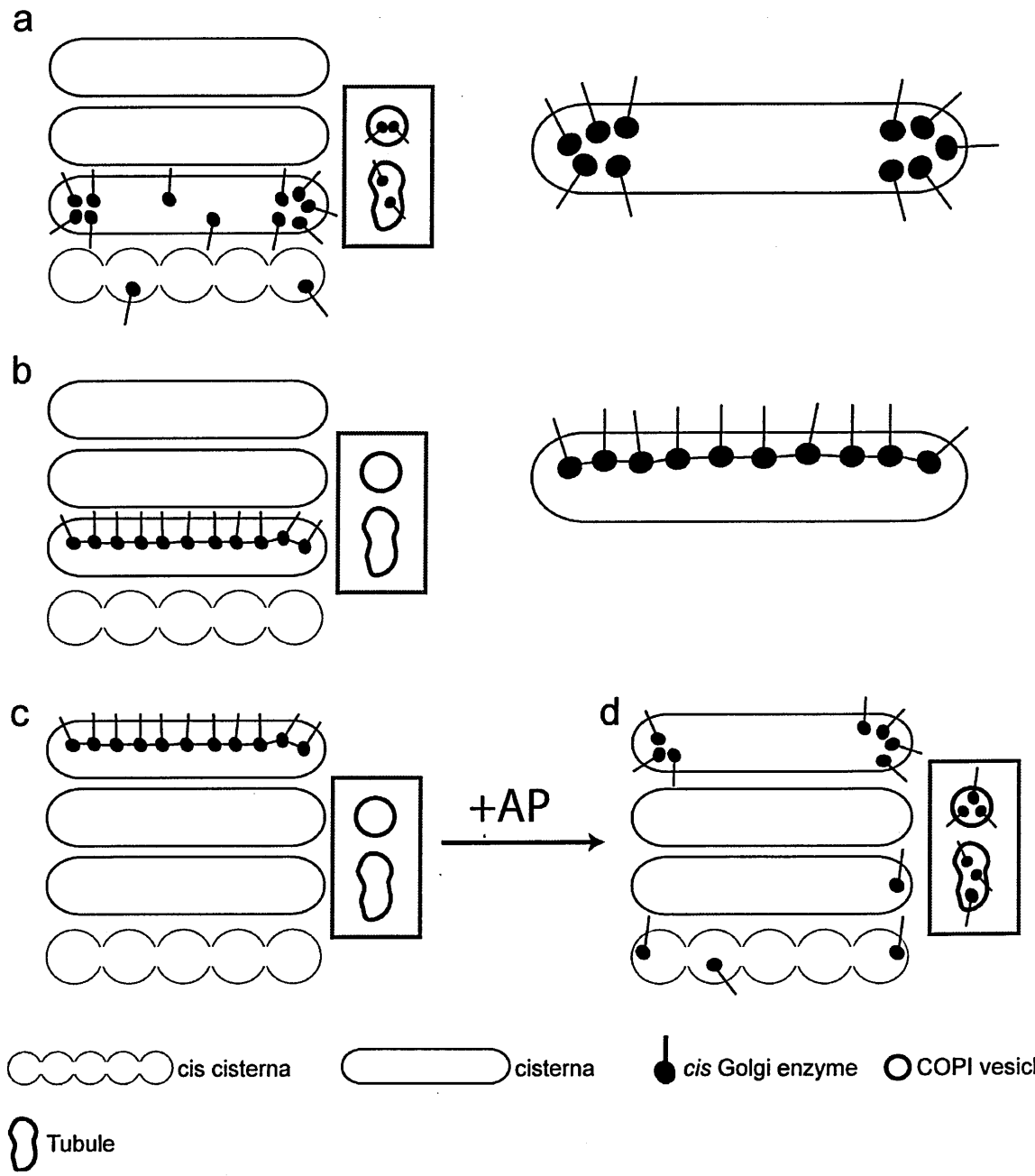

Fig. 5.1 Working model.

(a-d) The dynamics of a *cis*-Golgi resident enzyme support the cisternal-maturation model. (a) Steady-state distribution of MANI-FM. (b) After polymerisation, MANI-FM disappears from vesicles/ tubules and appears randomly distributed in the cisternae. (c) The MANI-FM polymer can shift from the *cis*-medial to the *trans* Golgi stack. (d) Depolymerisation of MANI-FM in the *trans*-Golgi induces its fast re-distribution into the cisternal rims and vesicles/ tubules, and shifts it back towards its *cis*-Golgi location.

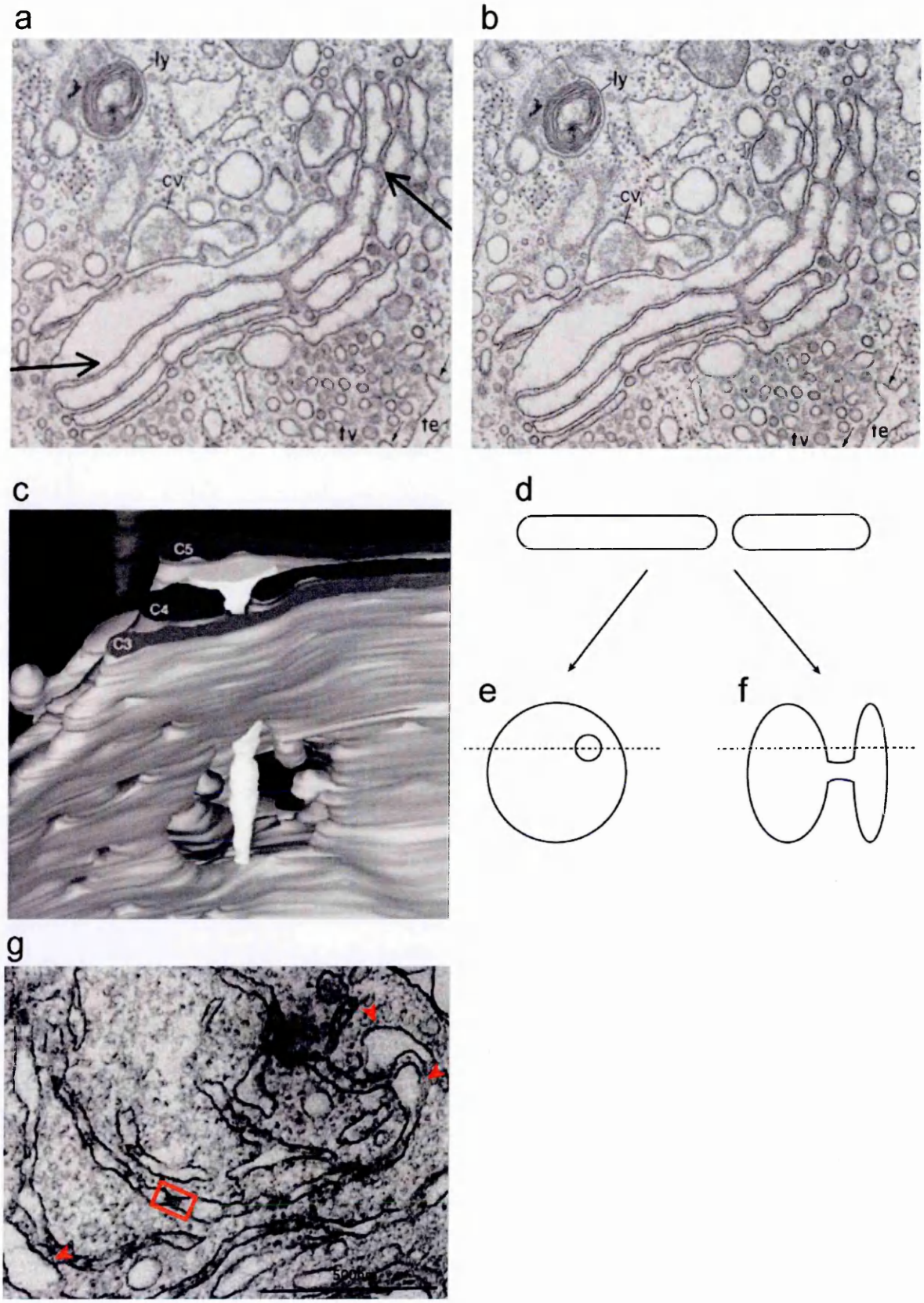

Fig. 5.2 Arguments against competing models.

(**a, b**) Electron micrographs of the Golgi apparatus of a guinea-pig exocrine pancreas cell (Farquhar and Palade 1981; Pfeffer 2010). (**a**) Adapted electron micrograph of **b**, chosen by (Pfeffer 2010) to emphasise the discontinuity of the cisternae, to describe the progenitor model. (**b**) Original electron micrograph of the Golgi (Farquhar and Palade 1981). (**c**) Stereo images of three Golgi cisternae (from C3 to C5) showing wells (image from Ladinsky, Mastronarde et al. 1999). (**d**) Schematic representation of a discontinuous Golgi cisterna in transverse section. (**e**) Schematic representation of a Golgi cisterna with a well, in tangential section. (**f**) Schematic representation of a Golgi cisterna composed of two pieces connected to each other by a tubule, in tangential section. (**g**) Adapted electron micrograph from (Lavieu, Zheng et al. 2013) showing CD8 staples in the ER (red box) of HeLa cells. Red arrowheads, pieces of swollen ER.

References

Abe, M., Y. Noda, et al. (2004). "Localization of GDP-mannose transporter in the Golgi requires retrieval to the endoplasmic reticulum depending on its cytoplasmic tail and coatomer." J Cell Sci **117**(Pt 23): 5687-5696.

Ali, B. R., C. Wasmeier, et al. (2004). "Multiple regions contribute to membrane targeting of Rab GTPases." J Cell Sci **117**(Pt 26): 6401-6412.

Ali, M. F., V. B. Chachadi, et al. (2012). "Golgi phosphoprotein 3 determines cell binding properties under dynamic flow by controlling Golgi localization of core 2 N-acetylglucosaminyltransferase 1." J Biol Chem **287**(47): 39564-39577.

Anelli, T., S. Ceppi, et al. (2007). "Sequential steps and checkpoints in the early exocytic compartment during secretory IgM biogenesis." EMBO J **26**(19): 4177-4188.

Antonny, B. and R. Schekman (2001). "ER export: public transportation by the COPII coach." Curr Opin Cell Biol **13**(4): 438-443.

Banfield, D. K. (2011). "Mechanisms of protein retention in the Golgi." Cold Spring Harb Perspect Biol **3**(8): a005264.

Bannykh, S. I. and W. E. Balch (1997). "Membrane dynamics at the endoplasmic reticulum-Golgi interface." J Cell Biol **138**(1): 1-4.

Bannykh, S. I., N. Nishimura, et al. (1998). "Getting into the Golgi." Trends Cell Biol **8**(1): 21-25.

Bannykh, S. I., T. Rowe, et al. (1996). "The organization of endoplasmic reticulum export complexes." J Cell Biol **135**(1): 19-35.

Barlowe, C. (2003). "Signals for COPII-dependent export from the ER: what's the ticket out?" Trends Cell Biol **13**(6): 295-300.

Barlowe, C., L. Orci, et al. (1994). "COPII: a membrane coat formed by Sec proteins that drive vesicle budding from the endoplasmic reticulum." Cell **77**(6): 895-907.

Barr, F. A. (2009). "Rab GTPase function in Golgi trafficking." Semin Cell Dev Biol **20**(7): 780-783.

Becker, B., B. Bolinger, et al. (1995). "Anterograde transport of algal scales through the Golgi complex is not mediated by vesicles." Trends Cell Biol **5**(8): 305-307.

Becker, B., A. Haggarty, et al. (2000). "The transmembrane domain of murine alpha-mannosidase IB is a major determinant of Golgi localization." Eur J Cell Biol **79**(12): 986-992.

Berger, E. G. (2002). "Ectopic localizations of Golgi glycosyltransferases." Glycobiology **12**(2): 29R-36R.

Bergmann, J. E. (1989). "Using temperature-sensitive mutants of VSV to study membrane protein biogenesis." Methods Cell Biol **32**: 85-110.

Block, M. R., B. S. Glick, et al. (1988). "Purification of an N-ethylmaleimide-sensitive protein catalyzing vesicular transport." Proc Natl Acad Sci U S A **85**(21): 7852-7856.

Bonfanti, L., A. A. Mironov, Jr., et al. (1998). "Procollagen traverses the Golgi stack without leaving the lumen of cisternae: evidence for cisternal maturation." Cell **95**(7): 993-1003.

Bonifacino, J. S. (2001). "Metabolic labeling with amino acids." Curr Protoc Mol Biol **Chapter 10**: Unit 10 18.

Bonifacino, J. S. and B. S. Glick (2004). "The mechanisms of vesicle budding and fusion." Cell **116**(2): 153-166.

Bos, J. L., H. Rehmann, et al. (2007). "GEFs and GAPs: critical elements in the control of small G proteins." Cell **129**(5): 865-877.

Bretscher, M. S. and S. Munro (1993). "Cholesterol and the Golgi apparatus." Science **261**(5126): 1280-1281.

Breuza, L., R. Halbeisen, et al. (2004). "Proteomics of endoplasmic reticulum-Golgi intermediate compartment (ERGIC) membranes from brefeldin A-treated HepG2 cells identifies ERGIC-32, a new cycling protein that interacts with human Erv46." J Biol Chem **279**(45): 47242-47253.

Chang, W. L., C. W. Chang, et al. (2013). "The Drosophila GOLPH3 homolog regulates the biosynthesis of heparan sulfate proteoglycans by modulating the retrograde trafficking of exostosins." Development **140**(13): 2798-2807.

Clermont, Y., A. Rambourg, et al. (1995). "Trans-Golgi network (TGN) of different cell types: three-dimensional structural characteristics and variability." Anat Rec **242**(3): 289-301.

Clermont, Y., L. Xia, et al. (1993). "Transport of casein submicelles and formation of secretion granules in the Golgi apparatus of epithelial cells of the lactating mammary gland of the rat." Anat Rec **235**(3): 363-373.

Cluett, E. B. and W. J. Brown (1992). "Adhesion of Golgi cisternae by proteinaceous interactions: intercisternal bridges as putative adhesive structures." J Cell Sci **103 (Pt 3)**: 773-784.

Cole, N. B., N. Sciaky, et al. (1996). "Golgi dispersal during microtubule disruption: regeneration of Golgi stacks at peripheral endoplasmic reticulum exit sites." Mol Biol Cell **7**(4): 631-650.

Cole, N. B., C. L. Smith, et al. (1996). "Diffusional mobility of Golgi proteins in membranes of living cells." Science **273**(5276): 797-801.

Copic, A., C. F. Latham, et al. (2012). "ER cargo properties specify a requirement for COPII coat rigidity mediated by Sec13p." Science **335**(6074): 1359-1362.

Cottam, N. P. and D. Ungar (2012). "Retrograde vesicle transport in the Golgi." Protoplasma **249**(4): 943-955.

Dahan, S., J. P. Ahluwalia, et al. (1994). "Concentration of intracellular hepatic apolipoprotein E in Golgi apparatus saccular distensions and endosomes." J Cell Biol **127**(6 Pt 2): 1859-1869.

Dalton, A. J. and M. D. Felix (1954). "Cytologic and cytochemical characteristics of the Golgi substance of epithelial cells of the epididymis in situ, in homogenates and after isolation." Am J Anat **94**(2): 171-207.

Davidson, H. W. and W. E. Balch (1993). "Differential inhibition of multiple vesicular transport steps between the endoplasmic reticulum and trans Golgi network." J Biol Chem **268**(6): 4216-4226.

de Graffenried, C. L. and C. R. Bertozzi (2004). "The roles of enzyme localisation and complex formation in glycan assembly within the Golgi apparatus." Curr Opin Cell Biol **16**(4): 356-363.

De Matteis, M. A. and A. Luini (2008). "Exiting the Golgi complex." Nat Rev Mol Cell Biol **9**(4): 273-284.

De Matteis, M. A. and A. Luini (2011). "Mendelian disorders of membrane trafficking." N Engl J Med **365**(10): 927-938.

Dejgaard, S. Y., A. Murshid, et al. (2007). "Confocal microscopy-based linescan methodologies for intra-Golgi localization of proteins." J Histochem Cytochem **55**(7): 709-719.

Dejgaard, S. Y., A. Murshid, et al. (2008). "Rab18 and Rab43 have key roles in ER-Golgi trafficking." J Cell Sci **121**(Pt 16): 2768-2781.

Donaldson, J. G., D. Cassel, et al. (1992). "ADP-ribosylation factor, a small GTP-binding protein, is required for binding of the coatomer protein beta-COP to Golgi membranes." Proc Natl Acad Sci U S A **89**(14): 6408-6412.

Dunphy, W. G. and J. E. Rothman (1983). "Compartmentation of asparagine-linked oligosaccharide processing in the Golgi apparatus." J Cell Biol **97**(1): 270-275.

Dunphy, W. G. and J. E. Rothman (1985). "Compartmental organization of the Golgi stack." Cell **42**(1): 13-21.

Emr, S., B. S. Glick, et al. (2009). "Journeys through the Golgi--taking stock in a new era." J Cell Biol **187**(4): 449-453.

Farquhar, M. G. and G. E. Palade (1981). "The Golgi apparatus (complex)-(1954-1981)-from artifact to center stage." J Cell Biol **91**(3 Pt 2): 77s-103s.

Farquhar, M. G. and J. F. Rinehart (1954). "Cytologic alterations in the anterior pituitary gland following thyroidectomy: an electron microscope study." Endocrinology **65**(6): 857-876.

Fenteany, F. H. and K. J. Colley (2005). "Multiple signals are required for alpha2,6-sialyltransferase (ST6Gal I) oligomerization and Golgi localization." J Biol Chem **280**(7): 5423-5429.

Franke, W. W., J. Kartenbeck, et al. (1972). "Inter- and intracisternal elements of the Golgi apparatus. A system of membrane-to-membrane cross-links." Z Zellforsch Mikrosk Anat **132**(3): 365-380.

Freeze, H. H. (2013). "Understanding human glycosylation disorders: biochemistry leads the charge." J Biol Chem **288**(10): 6936-6945.

Fujiwara, T., K. Oda, et al. (1988). "Brefeldin A causes disassembly of the Golgi complex and accumulation of secretory proteins in the endoplasmic reticulum." J Biol Chem **263**(34): 18545-18552.

Geuze, H. J. and D. J. Morre (1991). "Trans-Golgi reticulum." J Electron Microsc Tech **17**(1): 24-34.

Gilchrist, A., C. E. Au, et al. (2006). "Quantitative proteomics analysis of the secretory pathway." Cell **127**(6): 1265-1281.

Giraudo, C. G., J. L. Daniotti, et al. (2001). "Physical and functional association of glycolipid N-acetyl-galactosaminyl and galactosyl transferases in the Golgi apparatus." Proc Natl Acad Sci U S A **98**(4): 1625-1630.

Glick, B. S. and A. Luini (2011). "Models for Golgi traffic: a critical assessment." Cold Spring Harb Perspect Biol **3**(11): a005215.

Glick, B. S. and A. Nakano (2009). "Membrane traffic within the Golgi apparatus." Annu Rev Cell Dev Biol **25**: 113-132.

Golgi, C. (1989). "On the structure of the nerve cells of the spinal ganglia. 1898." J Microsc **155**(Pt 1): 9-14.

Griffiths, G., S. D. Fuller, et al. (1989). "The dynamic nature of the Golgi complex." J Cell Biol **108**(2): 277-297.

Griffiths, G., S. Pfeiffer, et al. (1985). "Exit of newly synthesized membrane proteins from the trans cisterna of the Golgi complex to the plasma membrane." J Cell Biol **101**(3): 949-964.

Hand, A. R. and C. Oliver (1984). "Effects of secretory stimulation on the Golgi apparatus and GERL of rat parotid acinar cells." J Histochem Cytochem **32**(4): 403-412.

Harris, S. L. and M. G. Waters (1996). "Localization of a yeast early Golgi mannosyltransferase, Och1p, involves retrograde transport." J Cell Biol **132**(6): 985-998.

Hauri, H. P., F. Kappeler, et al. (2000). "ERGIC-53 and traffic in the secretory pathway." J Cell Sci **113 (Pt 4)**: 587-596.

Hoe, M. H., P. Slusarewicz, et al. (1995). "Evidence for recycling of the resident medial/trans Golgi enzyme, N-acetylglucosaminyltransferase I, in ldlD cells." J Biol Chem **270**(42): 25057-25063.

Hu, H., K. Eggers, et al. (2011). "ST3GAL3 mutations impair the development of higher cognitive functions." Am J Hum Genet **89**(3): 407-414.

Jackson, C. L. (2009). "Mechanisms of transport through the Golgi complex." J Cell Sci **122**(Pt 4): 443-452.

Jahn, R. and R. H. Scheller (2006). "SNAREs--engines for membrane fusion." Nat Rev Mol Cell Biol **7**(9): 631-643.

Jarvela, T. and A. D. Linstedt (2012). "Irradiation-induced protein inactivation reveals Golgi enzyme cycling to cell periphery." J Cell Sci **125**(Pt 4): 973-980.

Jiang, S. and B. Storrie (2005). "Cisternal rab proteins regulate Golgi apparatus redistribution in response to hypotonic stress." Mol Biol Cell **16**(5): 2586-2596.

Kingsley, D. M., K. F. Kozarsky, et al. (1986). "Three types of low density lipoprotein receptor-deficient mutant have pleiotropic defects in the synthesis of N-linked, O-linked, and lipid-linked carbohydrate chains." J Cell Biol **102**(5): 1576-1585.

Klumperman, J. (2011). "Architecture of the mammalian Golgi." Cold Spring Harb Perspect Biol **3**(7).

Kornfeld, R. and S. Kornfeld (1985). "Assembly of asparagine-linked oligosaccharides." Annu Rev Biochem **54**: 631-664.

Krijnse-Locker, J., M. Ericsson, et al. (1994). "Characterization of the budding compartment of mouse hepatitis virus: evidence that transport from the RER to the Golgi complex requires only one vesicular transport step." J Cell Biol **124**(1-2): 55-70.

Kweon, H. S., G. V. Beznoussenko, et al. (2004). "Golgi enzymes are enriched in perforated zones of golgi cisternae but are depleted in COPI vesicles." Mol Biol Cell **15**(10): 4710-4724.

Ladinsky, M. S., D. N. Mastronarde, et al. (1999). "Golgi structure in three dimensions: functional insights from the normal rat kidney cell." J Cell Biol **144**(6): 1135-1149.

Ladinsky, M. S., C. C. Wu, et al. (2002). "Structure of the Golgi and distribution of reporter molecules at 20 degrees C reveals the complexity of the exit compartments." Mol Biol Cell **13**(8): 2810-2825.

Lanoix, J., J. Ouwendijk, et al. (2001). "Sorting of Golgi resident proteins into different subpopulations of COPI vesicles: a role for ArfGAP1." J Cell Biol **155**(7): 1199-1212.

Lavieu, G., H. Zheng, et al. (2013). "Stapled Golgi cisternae remain in place as cargo passes through the stack." Elife **2**: e00558.

Letourneur, F., E. C. Gaynor, et al. (1994). "Coatomer is essential for retrieval of dilysine-tagged proteins to the endoplasmic reticulum." Cell **79**(7): 1199-1207.

Lewis, M. J. and H. R. Pelham (1990). "A human homologue of the yeast HDEL receptor." Nature **348**(6297): 162-163.

Lippincott-Schwartz, J., J. G. Donaldson, et al. (1990). "Microtubule-dependent retrograde transport of proteins into the ER in the presence of brefeldin A suggests an ER recycling pathway." Cell **60**(5): 821-836.

Lippincott-Schwartz, J., L. Yuan, et al. (1991). "Brefeldin A's effects on endosomes, lysosomes, and the TGN suggest a general mechanism for regulating organelle structure and membrane traffic." Cell **67**(3): 601-616.

Losev, E., C. A. Reinke, et al. (2006). "Golgi maturation visualized in living yeast." Nature **441**(7096): 1002-1006.

Malsam, J., S. Kreye, et al. (2008). "Membrane fusion: SNAREs and regulation." Cell Mol Life Sci **65**(18): 2814-2832.

Malsam, J., A. Satoh, et al. (2005). "Golgin tethers define subpopulations of COPI vesicles." Science **307**(5712): 1095-1098.

Marra, P., T. Maffucci, et al. (2001). "The GM130 and GRASP65 Golgi proteins cycle through and define a subdomain of the intermediate compartment." Nat Cell Biol **3**(12): 1101-1113.

Marsh, B. J., N. Volkmann, et al. (2004). "Direct continuities between cisternae at different levels of the Golgi complex in glucose-stimulated mouse islet beta cells." Proc Natl Acad Sci U S A **101**(15): 5565-5570.

Martinez-Menarguez, J. A., H. J. Geuze, et al. (1999). "Vesicular tubular clusters between the ER and Golgi mediate concentration of soluble secretory proteins by exclusion from COPI-coated vesicles." Cell **98**(1): 81-90.

Martinez-Menarguez, J. A., R. Prekeris, et al. (2001). "Peri-Golgi vesicles contain retrograde but not anterograde proteins consistent with the cisternal progression model of intra-Golgi transport." J Cell Biol **155**(7): 1213-1224.

Martinez, O., A. Schmidt, et al. (1994). "The small GTP-binding protein rab6 functions in intra-Golgi transport." J Cell Biol **127**(6 Pt 1): 1575-1588.

Matsuura-Tokita, K., M. Takeuchi, et al. (2006). "Live imaging of yeast Golgi cisternal maturation." Nature **441**(7096): 1007-1010.

Mayer, A., W. Wickner, et al. (1996). "Sec18p (NSF)-driven release of Sec17p (alpha-SNAP) can precede docking and fusion of yeast vacuoles." Cell **85**(1): 83-94.

McCormick, C., G. Duncan, et al. (2000). "The putative tumor suppressors EXT1 and EXT2 form a stable complex that accumulates in the Golgi apparatus and catalyzes the synthesis of heparan sulfate." Proc Natl Acad Sci U S A **97**(2): 668-673.

McNew, J. A., F. Parlati, et al. (2000). "Compartmental specificity of cellular membrane fusion encoded in SNARE proteins." Nature **407**(6801): 153-159.

Melia, T. J., T. Weber, et al. (2002). "Regulation of membrane fusion by the membrane-proximal coil of the t-SNARE during zippering of SNAREpins." J Cell Biol **158**(5): 929-940.

Mellman, I. and K. Simons (1992). "The Golgi complex: in vitro veritas?" Cell **68**(5): 829-840.

Mellman, I. and G. Warren (2000). "The road taken: past and future foundations of membrane traffic." Cell **100**(1): 99-112.

Miller, V. J. and D. Ungar (2012). "Re'COG'nition at the Golgi." Traffic **13**(7): 891-897.

Mironov, A. A. and G. V. Beznoussenko (2012). "The Kiss-and-Run Model of Intra-Golgi Transport." Int J Mol Sci **13**(6): 6800-6819.

Mironov, A. A., G. V. Beznoussenko, et al. (2001). "Small cargo proteins and large aggregates can traverse the Golgi by a common mechanism without leaving the lumen of cisternae." J Cell Biol **155**(7): 1225-1238.

Mogelsvang, S., B. J. Marsh, et al. (2004). "Predicting function from structure: 3D structure studies of the mammalian Golgi complex." Traffic **5**(5): 338-345.

Munro, S. (1998). "Localization of proteins to the Golgi apparatus." Trends Cell Biol **8**(1): 11-15.

Munro, S. (2011). "The golgin coiled-coil proteins of the Golgi apparatus." Cold Spring Harb Perspect Biol **3**(6).

Nakano, A. and A. Luini (2010). "Passage through the Golgi." Curr Opin Cell Biol **22**(4): 471-478.

Nilsson, T., C. E. Au, et al. (2009). "Sorting out glycosylation enzymes in the Golgi apparatus." FEBS Lett **583**(23): 3764-3769.

Nilsson, T., M. H. Hoe, et al. (1994). "Kin recognition between medial Golgi enzymes in HeLa cells." EMBO J **13**(3): 562-574.

Nilsson, T., C. Rabouille, et al. (1996). "The role of the membrane-spanning domain and stalk region of N-acetylglucosaminyltransferase I in retention, kin recognition and structural maintenance of the Golgi apparatus in HeLa cells." J Cell Sci **109 (Pt 7)**: 1975-1989.

Novikoff, A. B. (1976). "The endoplasmic reticulum: a cytochemist's view (a review)." Proc Natl Acad Sci U S A **73**(8): 2781-2787.

Oka, T., D. Ungar, et al. (2004). "The COG and COPI complexes interact to control the abundance of GEARs, a subset of Golgi integral membrane proteins." Mol Biol Cell **15**(5): 2423-2435.

Opat, A. S., F. Houghton, et al. (2000). "Medial Golgi but not late Golgi glycosyltransferases exist as high molecular weight complexes. Role of luminal domain in complex formation and localization." J Biol Chem **275**(16): 11836-11845.

Orci, L., M. Amherdt, et al. (2000). "Exclusion of golgi residents from transport vesicles budding from Golgi cisternae in intact cells." J Cell Biol **150**(6): 1263-1270.

Orci, L., R. Montesano, et al. (1981). "Heterogeneous distribution of filipin--cholesterol complexes across the cisternae of the Golgi apparatus." Proc Natl Acad Sci U S A **78**(1): 293-297.

Orci, L., M. Stamnes, et al. (1997). "Bidirectional transport by distinct populations of COPI-coated vesicles." Cell **90**(2): 335-349.

Ortiz, D. and P. J. Novick (2006). "Ypt32p regulates the translocation of Chs3p from an internal pool to the plasma membrane." Eur J Cell Biol **85**(2): 107-116.

Ostermann, J., L. Orci, et al. (1993). "Stepwise assembly of functionally active transport vesicles." Cell **75**(5): 1015-1025.

Palade, G. (1975). "Intracellular aspects of the process of protein synthesis." Science **189**(4200): 347-358.

Patterson, G. H., K. Hirschberg, et al. (2008). "Transport through the Golgi apparatus by rapid partitioning within a two-phase membrane system." Cell **133**(6): 1055-1067.

Pearse, B. M. and M. S. Robinson (1990). "Clathrin, adaptors, and sorting." Annu Rev Cell Biol **6**: 151-171.

Peden, A. A., V. Oorschot, et al. (2004). "Localization of the AP-3 adaptor complex defines a novel endosomal exit site for lysosomal membrane proteins." J Cell Biol **164**(7): 1065-1076.

Pfeffer, S. R. (2007). "Unsolved mysteries in membrane traffic." Annu Rev Biochem **76**: 629-645.

Pfeffer, S. R. (2010). "How the Golgi works: a cisternal progenitor model." Proc Natl Acad Sci U S A **107**(46): 19614-19618.

Pobbati, A. V., A. Stein, et al. (2006). "N- to C-terminal SNARE complex assembly promotes rapid membrane fusion." Science **313**(5787): 673-676.

Polishchuk, R. S. and A. A. Mironov (2004). "Structural aspects of Golgi function." Cell Mol Life Sci **61**(2): 146-158.

Polishchuk, R. S., E. V. Polishchuk, et al. (2000). "Correlative light-electron microscopy reveals the tubular-saccular ultrastructure of carriers operating between Golgi apparatus and plasma membrane." J Cell Biol **148**(1): 45-58.

Pryor, P. R. and J. P. Luzio (2009). "Delivery of endocytosed membrane proteins to the lysosome." Biochim Biophys Acta **1793**(4): 615-624.

Qian, R., C. Chen, et al. (2001). "Location and mechanism of alpha 2,6-sialyltransferase dimer formation. Role of cysteine residues in enzyme dimerization, localization, activity, and processing." J Biol Chem **276**(31): 28641-28649.

Rabouille, C., T. Misteli, et al. (1995). "Reassembly of Golgi stacks from mitotic Golgi fragments in a cell-free system." J Cell Biol **129**(3): 605-618.

Rambourg, A. and Y. Clermont (1990). "Three-dimensional electron microscopy: structure of the Golgi apparatus." Eur J Cell Biol **51**(2): 189-200.

Ramirez, I. B. and M. Lowe (2009). "Golgins and GRASPs: holding the Golgi together." Semin Cell Dev Biol **20**(7): 770-779.

Reynders, E., F. Foulquier, et al. (2011). "How Golgi glycosylation meets and needs trafficking: the case of the COG complex." Glycobiology **21**(7): 853-863.

Rink, J., E. Ghigo, et al. (2005). "Rab conversion as a mechanism of progression from early to late endosomes." Cell **122**(5): 735-749.

Rivera, V. M., X. Wang, et al. (2000). "Regulation of protein secretion through controlled aggregation in the endoplasmic reticulum." Science **287**(5454): 826-830.

Rizzo, R., S. Parashuraman, et al. (2013). "The dynamics of engineered resident proteins in the mammalian Golgi complex relies on cisternal maturation." J Cell Biol **201**(7): 1027-1036.

Rose, J. K. and J. E. Bergmann (1983). "Altered cytoplasmic domains affect intracellular transport of the vesicular stomatitis virus glycoprotein." Cell **34**(2): 513-524.

Roth, J., D. J. Taatjes, et al. (1985). "Demonstration of an extensive trans-tubular network continuous with the Golgi apparatus stack that may function in glycosylation." Cell **43**(1): 287-295.

Rothman, J. E. (1987). "Transport of the vesicular stomatitis glycoprotein to trans Golgi membranes in a cell-free system." J Biol Chem **262**(26): 12502-12510.

Rothman, J. E. and F. T. Wieland (1996). "Protein sorting by transport vesicles." Science **272**(5259): 227-234.

Saint-Jore-Dupas, C., V. Gomord, et al. (2004). "Protein localization in the plant Golgi apparatus and the trans-Golgi network." Cell Mol Life Sci **61**(2): 159-171.

San Pietro, E., M. Capestrano, et al. (2009). "Group IV phospholipase A(2)alpha controls the formation of inter-cisternal continuities involved in intra-Golgi transport." PLoS Biol **7**(9): e1000194.

Sato, K., M. Sato, et al. (2001). "Rer1p, a retrieval receptor for endoplasmic reticulum membrane proteins, is dynamically localized to the Golgi apparatus by coatomer." J Cell Biol **152**(5): 935-944.

Schnitzer, T. J., C. Dickson, et al. (1979). "Morphological and biochemical characterization of viral particles produced by the tsO45 mutant of vesicular stomatitis virus at restrictive temperature." J Virol **29**(1): 185-195.

Sciaky, N., J. Presley, et al. (1997). "Golgi tubule traffic and the effects of brefeldin A visualized in living cells." J Cell Biol **139**(5): 1137-1155.

Serafini, T., L. Orci, et al. (1991). "ADP-ribosylation factor is a subunit of the coat of Golgi-derived COP-coated vesicles: a novel role for a GTP-binding protein." Cell **67**(2): 239-253.

Sesso, A., F. P. de Faria, et al. (1994). "A three-dimensional reconstruction study of the rough ER-Golgi interface in serial thin sections of the pancreatic acinar cell of the rat." J Cell Sci **107 (Pt 3)**: 517-528.

Sharpe, H. J., T. J. Stevens, et al. (2010). "A comprehensive comparison of transmembrane domains reveals organelle-specific properties." Cell **142**(1): 158-169.

Shima, D. T., K. Haldar, et al. (1997). "Partitioning of the Golgi apparatus during mitosis in living HeLa cells." J Cell Biol **137**(6): 1211-1228.

Sinka, R., A. K. Gillingham, et al. (2008). "Golgi coiled-coil proteins contain multiple binding sites for Rab family G proteins." J Cell Biol **183**(4): 607-615.

Sjostrand, F. S. and V. Hanzon (1954). "Ultrastructure of Golgi apparatus of exocrine cells of mouse pancreas." Exp Cell Res **7**(2): 415-429.

Slusarewicz, P., T. Nilsson, et al. (1994). "Isolation of a matrix that binds medial Golgi enzymes." J Cell Biol **124**(4): 405-413.

Sohda, M., Y. Misumi, et al. (2010). "Interaction of Golgin-84 with the COG complex mediates the intra-Golgi retrograde transport." Traffic **11**(12): 1552-1566.

Sohda, M., Y. Misumi, et al. (2007). "The interaction of two tethering factors, p115 and COG complex, is required for Golgi integrity." Traffic **8**(3): 270-284.

Sollner, T., M. K. Bennett, et al. (1993). "A protein assembly-disassembly pathway in vitro that may correspond to sequential steps of synaptic vesicle docking, activation, and fusion." Cell **75**(3): 409-418.

Sollner, T., S. W. Whiteheart, et al. (1993). "SNAP receptors implicated in vesicle targeting and fusion." Nature **362**(6418): 318-324.

Starr, T., Y. Sun, et al. (2010). "Rab33b and Rab6 are functionally overlapping regulators of Golgi homeostasis and trafficking." Traffic **11**(5): 626-636.

Stenmark, H., A. Valencia, et al. (1994). "Distinct structural elements of rab5 define its functional specificity." EMBO J **13**(3): 575-583.

Storrie, B., J. White, et al. (1998). "Recycling of golgi-resident glycosyltransferases through the ER reveals a novel pathway and provides an explanation for nocodazole-induced Golgi scattering." J Cell Biol **143**(6): 1505-1521.

Suvorova, E. S., R. Duden, et al. (2002). "The Sec34/Sec35p complex, a Ypt1p effector required for retrograde intra-Golgi trafficking, interacts with Golgi SNAREs and COPI vesicle coat proteins." J Cell Biol **157**(4): 631-643.

Tanigawa, G., L. Orci, et al. (1993). "Hydrolysis of bound GTP by ARF protein triggers uncoating of Golgi-derived COP-coated vesicles." J Cell Biol **123**(6 Pt 1): 1365-1371.

Teasdale, R. D., G. D'Agostaro, et al. (1992). "The signal for Golgi retention of bovine beta 1,4-galactosyltransferase is in the transmembrane domain." J Biol Chem **267**(6): 4084-4096.

Thorne-Tjomsland, G., M. Dumontier, et al. (1998). "3D topography of noncompact zone Golgi tubules in rat spermatids: a computer-assisted serial section reconstruction study." Anat Rec **250**(4): 381-396.

Thyberg, J. and S. Moskalewski (1985). "Microtubules and the organization of the Golgi complex." Exp Cell Res **159**(1): 1-16.

Tisdale, E. J., J. R. Bourne, et al. (1992). "GTP-binding mutants of rab1 and rab2 are potent inhibitors of vesicular transport from the endoplasmic reticulum to the Golgi complex." J Cell Biol **119**(4): 749-761.

Todorow, Z., A. Spang, et al. (2000). "Active recycling of yeast Golgi mannosyltransferase complexes through the endoplasmic reticulum." Proc Natl Acad Sci U S A **97**(25): 13643-13648.

Trucco, A., R. S. Polishchuk, et al. (2004). "Secretory traffic triggers the formation of tubular continuities across Golgi sub-compartments." Nat Cell Biol **6**(11): 1071-1081.

Tu, L. and D. K. Banfield (2010). "Localization of Golgi-resident glycosyltransferases." Cell Mol Life Sci **67**(1): 29-41.

Tu, L., W. C. Tai, et al. (2008). "Signal-mediated dynamic retention of glycosyltransferases in the Golgi." Science **321**(5887): 404-407.

Ungar, D., T. Oka, et al. (2002). "Characterization of a mammalian Golgi-localized protein complex, COG, that is required for normal Golgi morphology and function." J Cell Biol **157**(3): 405-415.

Valsdottir, R., H. Hashimoto, et al. (2001). "Identification of rabaptin-5, rabex-5, and GM130 as putative effectors of rab33b, a regulator of retrograde traffic between the Golgi apparatus and ER." FEBS Lett **508**(2): 201-209.

van Meer, G. (1998). "Lipids of the Golgi membrane." Trends Cell Biol **8**(1): 29-33.

Varki, A. (1998). "Factors controlling the glycosylation potential of the Golgi apparatus." Trends Cell Biol **8**(1): 34-40.

Vivero-Salmeron, G., J. Ballesta, et al. (2008). "Heterotypic tubular connections at the endoplasmic reticulum-Golgi complex interface." Histochem Cell Biol **130**(4): 709-717.

Volchuk, A., M. Amherdt, et al. (2000). "Megavesicles implicated in the rapid transport of intracisternal aggregates across the Golgi stack." Cell **102**(3): 335-348.

Volchuk, A., M. Ravazzola, et al. (2004). "Countercurrent distribution of two distinct SNARE complexes mediating transport within the Golgi stack." Mol Biol Cell **15**(4): 1506-1518.

Weisz, O. A., A. M. Swift, et al. (1993). "Oligomerization of a membrane protein correlates with its retention in the Golgi complex." J Cell Biol **122**(6): 1185-1196.

White, J., L. Johannes, et al. (1999). "Rab6 coordinates a novel Golgi to ER retrograde transport pathway in live cells." J Cell Biol **147**(4): 743-760.

Whiteheart, S. W., I. C. Griff, et al. (1993). "SNAP family of NSF attachment proteins includes a brain-specific isoform." Nature **362**(6418): 353-355.

Whyte, J. R. and S. Munro (2001). "The Sec34/35 Golgi transport complex is related to the exocyst, defining a family of complexes involved in multiple steps of membrane traffic." Dev Cell **1**(4): 527-537.

Wieland, F. T., M. L. Gleason, et al. (1987). "The rate of bulk flow from the endoplasmic reticulum to the cell surface." Cell **50**(2): 289-300.

Yang, J. S., C. Valente, et al. (2011). "COPI acts in both vesicular and tubular transport." Nat Cell Biol **13**(8): 996-1003.

Zolov, S. N. and V. V. Lupashin (2005). "Cog3p depletion blocks vesicle-mediated Golgi retrograde trafficking in HeLa cells." J Cell Biol **168**(5): 747-759.

Zuber, C., J. Y. Fan, et al. (2001). "Immunolocalization of UDP-glucose:glycoprotein glucosyltransferase indicates involvement of pre-Golgi intermediates in protein quality control." Proc Natl Acad Sci U S A **98**(19): 10710-10715.